

# Barometric Pressure Sensing Using the Effect of Fluid Structure Interaction in Cantilever-based Structure

(カンチレバー構造における流体構造連成を利用した気圧計測)

グエン ミン ジューン

**Table of Contents****Chapter 1 Introduction - - - - - 4**

1.1 Conventional barometric pressure measurement. . . . .	4
1.1.1 Piezo-resistive pressure sensors . . . . .	6
1.1.2 Capacitive and optical pressure sensors . . . . .	7
1.2 Observed issues in conventional sensing methods . . . . .	7
1.3 Cantilever-based barometric pressure sensing . . . . .	8
1.4 Objective and significance. . . . .	10
1.5 Dissertation Structure . . . . .	11

**Chapter 2 Sensing Theory and Experiment Preparation - - - - - 13**

2.1 Physical properties of a cantilever. . . . .	13
2.1.1 Parameter definition . . . . .	15
2.1.2 Material mechanics of a simple cantilever beam . . . . .	15
2.1.3 Piezo-resistive effect . . . . .	15
2.1.4 Fractional resistance change of a piezo-resistive cantilever . . . . .	17
2.1.5 Reynolds number in gap area . . . . .	19
2.2 Design of a piezo-resistive cantilever . . . . .	19
2.2.1 Cantilever deformation and the fractional resistance change. . . . .	19
2.2.2 Calculation the amount of air leak and Reynolds number . . . . .	21
2.3 Theory on cantilever-based barometric pressure measurement . . . . .	21
2.4 Fabrication of a piezo-resistive cantilever and the sensor device . . . . .	23
2.5 Preparation for evaluation experiments. . . . .	25
2.5.1 Voltage divider circuit . . . . .	26
2.5.2 Wheatstone bridge circuit. . . . .	27
2.5.3 Setup for measuring cantilever's frequency characteristic . . . . .	28
2.5.4 Setup for evaluating the sensor characteristic at low frequency . . . . .	29
2.5.5 Relationship between barometric pressure and absolute altitude. . . . .	30

**Chapter 3 Fluid structure interaction simulation- - - - - 33**

3.1 Cantilever deformation . . . . .	33
3.2 Pressure decay and dependence on gap size . . . . .	35
3.3 Simulations of fluid structure interaction . . . . .	40
3.3.1 Gap size variation. . . . .	40
3.3.2 Cavity volume variation. . . . .	45
3.3.3 Applied pressure variation . . . . .	46
3.4 Summary of simulation results . . . . .	48
 <b>Chapter 4 Evaluation experiments - - - - -</b>	<b>49</b>
4.1 Static characteristics of a piezo-resistive cantilever . . . . .	49
4.1.1 Cantilever deformation. . . . .	49
4.1.2 Cantilever's sensitivity toward applied pressure . . . . .	51
4.2 Frequency characteristics of a piezo-resistive cantilever . . . . .	53
4.3 Barometric pressure measurement. . . . .	56
4.3.1 Characteristics toward static applied pressure . . . . .	56
4.3.2 Effect of gap size on differential pressure decay . . . . .	59
4.3.3 Effect of cavity volume on differential pressure decay . . . . .	61
4.3.4 Measurement at high frequency range . . . . .	63
4.3.5 Measurement at low frequency range . . . . .	64
4.4 Noise evaluation . . . . .	72
4.5 Demonstration . . . . .	77
 <b>Chapter 5 Conclusion- - - - -</b>	<b>79</b>
5.1 Conclusion . . . . .	79
5.2 Future works . . . . .	82
 <b>Reference - - - - -</b>	<b>83</b>
 <b>Appendix - - - - -</b>	<b>88</b>
Appendix A : Application of the fluid structure interaction in cantilever structure . .	88
Appendix B : Theoretical calculation for barometric pressure measurement . . . . .	96
Appendix C : Electrical apparatus using in experimental setups . . . . .	99
Appendix D : Fabrication process of a piezo-resistive cantilever . . . . .	102

Appendix E : Devices and chemicals used in MEMS processes. . . . .	106
Appendix F : Mask design of a piezo-resistive cantilever. . . . .	108
<b>Publication - - - - -</b>	<b>-109</b>
<b>Acknowledgement - - - - -</b>	<b>-112</b>



---

# Chapter 1 Introduction

“Is it a surprise that into the vessel, in which the mercury has no inclination and no repugnance, not even the slightest, to being there, it should enter and should rise in a column high enough to make equilibrium with the weight of the external air which forces it up”

Evangelista Torricelli

## 1.1 Conventional barometric pressure measurement

---

The first experiment on measuring the barometric pressure was done by the Italian scientist and inventor Evangelista Torricelli <sup>[4]</sup>. The start of the experiment was that he wanted to solve the problem of why water could not be pumped from a mine or a well more than 32 feet deep. Torricelli verified the idea by filling a 3 foot long (approximately 90 cm) long glass tube with mercury, and hermetically sealed it at one end with the open end in a basin of mercury. Note that mercury is a liquid fourteen times more dense than water. He found that with each repeat of the experiment the height of the mercury column fell to about 76 cm while leaving an empty space above it. Torricelli supposed that the empty space was a vacuum and the weight of the column was balanced by the weight of the atmosphere. Furthermore, he discovered that the changes of atmospheric pressure cause different height of the mercury. Thus Torricelli gave the first description of a barometer in 1644, which is the basis of the science of meteorology.

The accomplishment of barometer gives the answer to a question of : “Does the air have weight ?”. By the experiment with mercury, Torricelli did overturn the traditional thinking at his time of that the air

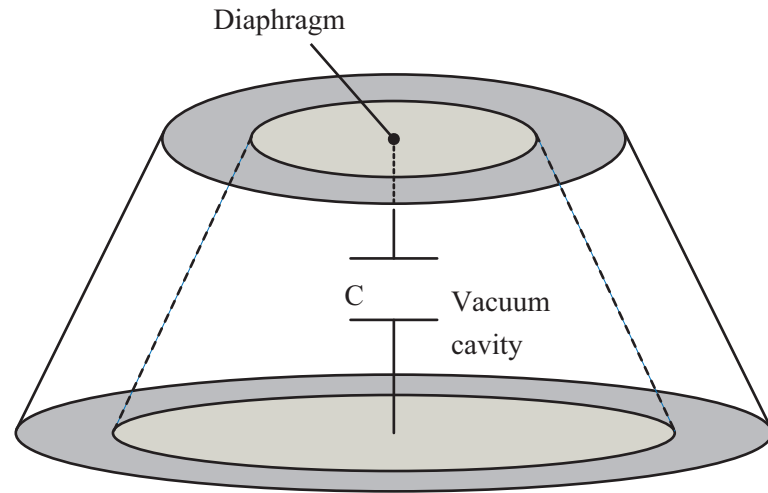


Fig. 1. 1 Image of conventional MEMS capacitive pressure sensor

did not have weight. The air contains certain weight since the air is composed of molecules of gases such as nitrogen, oxygen, carbon dioxide. These gases have mass and this is the reason why air is forced in by the gravity. The weight of the air applying on every unit of surface area of the earth is called atmospheric pressure (or barometric pressure), which is the pressure measured by a barometer.

Sensing performance (sensitivity, measurement resolution) and size are the issues in barometric pressure measurement<sup>[5] [6]</sup> that using traditional pressure sensors. The advent of Micro Electro Mechanical System (MEMS) technology has given the solution toward these issues. Indeed, MEMS has received a great deal of attention recently as a key of developments and solutions for various fields such as environment monitoring, transportation and health care systems. Indeed, MEMS devices, which typically have dimensions from hundred nanometers to hundred micrometers, have a potential to be applied in every fields. The most significant advantage of MEMS is the ability to integrate electrical elements, such as sensors and actuators, on the same semiconductor substrate. This ability leads to other advantages of small footprint, low power consumption and high performance.

The sensing principle of most traditional MEMS pressure sensors is to convert the applied pressure to the deformation of a mechanical element, which can be read as electrical signals. Conventional MEMS pressure sensors were based on diaphragms (see **Fig. 1. 1**). In these sensors, the applied pressure is

measured by the diaphragm deflection. The reference pressure is the internal pressure of a vacuum-sealed cavity such that absolute or gauge pressures can be obtained, respectively. For circular diaphragm, the deflection is calculated by the following equation providing that the deflection is small enough.

$$y(x) = \frac{PR^4}{64F} \left[ 1 - \left( \frac{x}{R} \right)^2 \right] \quad (1.1)$$

Here  $y$ ,  $P$ , and  $R$  are the deflection, the applied pressure and the radius of the diaphragm, respectively.  $x$  is the radial distance.  $F$  is defined as the flexural rigidity, which is expressed as follows.

$$F = \frac{Et^3}{12(1 - \nu^2)} \quad (1.2)$$

where  $E$  is Young's modulus,  $t$  is the thickness, and  $\nu$  is Poisson's ratio, respectively, of the corresponding diaphragm. According to the above equations, we can see a proportional relationship between displacement of the diaphragm and the applied pressure. However, this linearity would not be correct in the case of relatively large applied pressure.

Three common types of conventional MEMS pressure sensor have been developed so far are piezo-resistive type, capacitive type and optical type<sup>[7]</sup>.

### 1.1.1 Piezo-resistive pressure sensors

The piezo-resistive effect of silicon was firstly discovered by Smith in 1954<sup>[8]</sup>. Up to now, various piezo-resistive pressure sensors have been developed based on this effect<sup>[9][10][11][12]</sup>. In these sensors, piezo-resistive layer is fabricated on a diaphragm such that the resistance change of the piezo-resistive layer is linear with the applied pressure on the diaphragm. Indeed, most of MEMS pressure sensors have been fabricated on a silicon wafer since silicon obeys Hooke's law up to 1% strain, which is much better than the conventional metallic materials<sup>[9]</sup>. Additionally, silicon has gauge factors much more higher than those of metallic materials<sup>[8]</sup>. And silicon is also superior considering tensile strength, which is three times higher than stainless steel<sup>[13]</sup>.

### 1.1.2 Capacitive and optical pressure sensors

Capacitive sensors are based on parallel plate capacitors<sup>[14][15][16][17][18][19]</sup>. **Fig. 1. 1** shows a skeptical diagram of a typical capacitive pressure sensor. The capacitance is calculated as follows.

$$C = \frac{\epsilon S}{d} \quad (1.3)$$

Here  $\epsilon$ ,  $S$  and  $d$  are defined as the air permittivity, the plate area, and the distance between the two parallel plates, respectively. Capacitive pressure sensor has advantages in high pressure sensitivity and the independence in the temperature<sup>[20][21][22][23][24]</sup>. However, the parasitic capacitance is an inherent and serious disadvantage for this type of sensor<sup>[30-61]</sup>.

Optical pressure sensors are generally developed based on interferometry method<sup>[57][58][59][60]</sup>. However, the systems with optical sensing is relatively complicated and has high cost. Moreover the system is not compact so that this type of sensor is not used in applications.

## 1.2 Observed issues in conventional sensing methods

---

(In this section, I have been allowed to reused some sentences and expressions from my previous paper, which is the reference<sup>[1]</sup> with the Copyright 2011 IEEE)

As shown in previous sections, conventional barometric pressure sensors consist of a diaphragm, which is usually piezo-resistive or capacitive or optical type, and a vacuum-sealed cavity underneath. In these researches, pressure sensing normally based on diaphragm deformation, but for small pressure, the deformation is too small to be detectable. To make the diaphragm thinner may solve the above issue to some extent, but the fabrication is rather complicated. In addition, thinner diaphragm becomes fragile and easy to be damaged by high pressure change. Particularly, for capacitive type, the sensors have an inherent problem caused by parasitic capacitance. To reduce that noise, the sensors have been integrated with circuits on a chip to partly eliminate useless parasitic capacitance. Nevertheless, for these conventional sensors, the vacuum sealing process of the cavity beneath diaphragm is also an issue, since it is complicated and has been affected by leakage and gas permeation. Optical sensors are considered to have good accuracy. However, these type of sensors have inherent issues of temperature dependent sensitivity<sup>[61]</sup>. Furthermore, the systems of optical sensors is quite expensive.

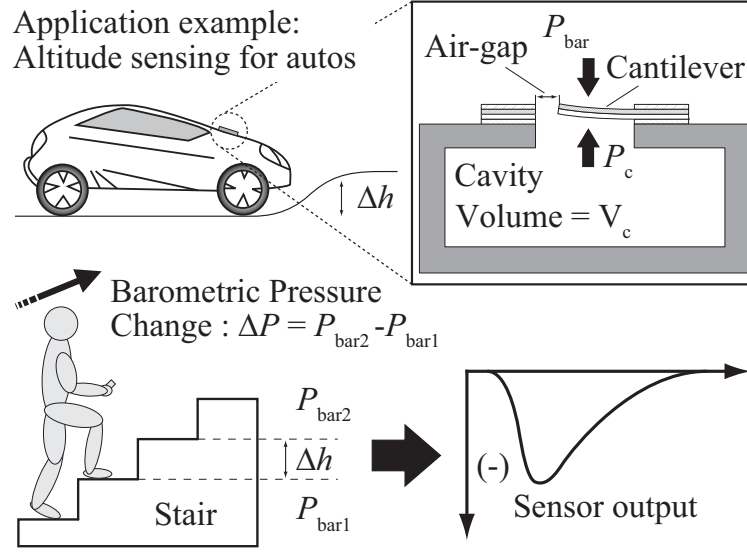


Fig. 1. 2 Image of the cantilever-based barometric pressure sensor and its applications.

### 1.3 Cantilever-based barometric pressure sensing

(In this section, I have been allowed to reused some sentences and expressions from my previous paper, which is the reference <sup>[1]</sup> with the Copyright 2011 IEEE)

As mentioned in previous sections, conventional MEMS pressure sensors generally based on a diaphragm. So come to a question: “Why don’t we use a microcantilever instead of a diaphragm?”. A microcantilever has the shape of a diving board, and it can act as a physical, chemical or biological sensor by detecting the deflection and frequency shift. Theoretical calculation of mechanical properties of a microcantilever will be briefly presented in chapter 2. The deflection of a microcantilever under a applied pressure  $P$  is expressed as follows.

$$w = \frac{3PL^4}{2Eh^3} \quad (1.4)$$

where  $E$  is Young’s modulus,  $L$  is length,  $h$  is thickness, respectively of the microcantilever. According to **Eq. 1.1** and **Eq. 1.4**, we can calculate that the deflection of a silicon-based microcantilever is at least 100 times bigger than a silicon-based diaphragm consider the same dimensions.

In this study, I propose a different approach to achieve a highly sensitive barometric pressure sensor,

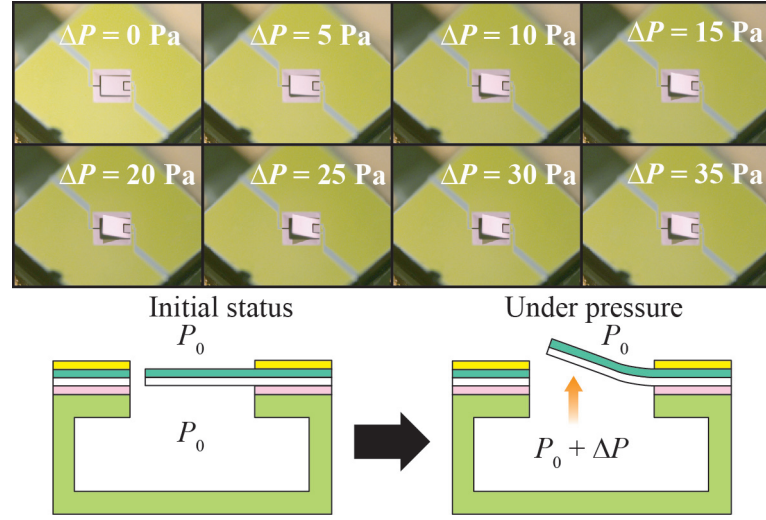


Fig. 1. 3 Behavior of the sensor during barometric pressure measurement

which is based on a piezo-resistive cantilever. In the proposed sensor, an ultra-thin (300-nm-thick) piezo-resistive cantilever was placed on the opening of a cavity, which was used as the reference pressure (**Fig. 1. 2**). Here, the piezo-resistive cantilever was used to measure the time-variant differential pressure between the barometric pressure and the cavity's pressure. The behavior of the cantilever due to applied pressure is shown in **Fig. 1. 3**. The cantilever has an ultra-small spring constant because the spring constant is proportional to the thickness cubed. Therefore, the cantilever is sensitive and can measure a pressure of less than 0.1 Pa<sup>[67][68][70]</sup>. With respect to diaphragm types, in our sensor, there is a gap (air-gap) between the cantilever and its surrounding walls such that air can leak through the gap. In this study, I have demonstrated that miniaturizing the air-gap enables the sensor to measure pressure changes at a very low frequency, which was 0.05 Hz with an air-gap size of 1  $\mu\text{m}$ .

Furthermore, the measurable rate of pressure change should improve with a smaller air-gap size. The basic difference between the proposed sensor and conventional sensors is that while conventional sensors can provide a static reading of absolute pressure, our cantilever-based pressure sensor measures the change in barometric pressure. The other difference is that the cavity below the cantilever is normally open and does not need to be vacuum sealed. Thus, this sensor can be easily fabricated at a low cost. The principle for measuring the change in barometric pressure will be briefly described in **Chapter 2**. The point here is the displacement of the cantilever due to a change in barometric pressure

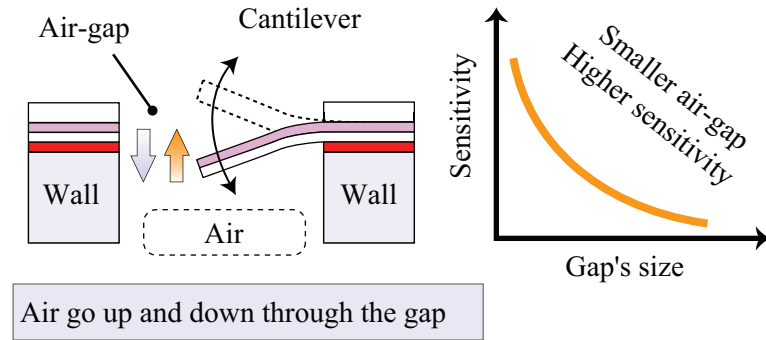


Fig. 1. 4 Concept of the scale effect of gap size in a piezo-resistive cantilever.

increases for a smaller air-gap. Hence, the sensor's sensitivity can be improved by using a miniaturized air-gap (Fig. 1. 4).

## 1.4 Objective and significance

(In this section, I have been allowed to reused some sentences and expressions from my previous paper, which is the reference <sup>[1]</sup> with the Copyright 2011 IEEE)

The main objective of this study is to provide a highly sensitive barometric pressure sensing based on the fluid structure interaction in cantilever-based structure. This research provides a theoretical calculations based on fluidic mechanics, materials mechanics and simulations of fluid structure interaction. This research also includes experimental evaluations of the proposed barometric pressure sensor. Using the theoretical calculations and the experiment results, this study discloses the scale effect of the gap size in a cantilever in barometric pressure sensing.

As presented in previous sections, conventional barometric pressure sensors are generally based on diaphragm structure, which is unable to measure small pressure of a few Pa. This research is the first study to provide barometric pressure measurement based on cantilever structure, which would lead to highly sensitive pressure sensing. The originality of this research is to disclose and take the advantage of the effect of gap size in a cantilever to improve the sensitivity. According to experiment, the proposed pressure sensor can measure barometric pressure change with high resolution of 0.01 Pa (10 mPa) order. Additionally, this research also provides a brief theoretical calculations of the measurement and that hints a way to have better sensing performance. Nevertheless, this research lead to many kinds

of applications in many fields such as automotive industry, mobile devices, medical devices, security market and so on.

## **1.5 Dissertation Structure**

---

### **Chapter 1: Introduction**

This chapter presents a background on barometric pressure measurement in general and conventional MEMS pressure sensors in specific. This chapter also provide a general concept of the sensing method of this study. The objective and significance of this study are also concerned in this chapter. At the end of this chapter, the structure of this thesis is shown.

### **Chapter 2: Sensing theory and experiment preparation**

In this chapter, a brief introduction about the measurement theory of the barometric pressure is provided. First, material mechanics of a cantilever is described. Next, theoretical calculation on the piezo-resistance of the cantilever is presented. The phenomenon of air leak through the cantilever gap is provided next. It followed by the measuring method of the barometric pressure sensor. At the end of this section, the preparation for experiments, which includes measurement electrical circuit and concept of experimental set-up, are presented.

### **Chapter 3: Fluid structure interaction simulation**

This chapter shows a fluid structure interaction simulation based on Finite Element Method to investigate the behavior of the cantilever in the process of pressure balance between cavity's pressure and external pressure. The simulations also investigated the influence of gap size, cavity volume, external pressure change on the cantilever's deflection.

### **Chapter 4: Evaluation experiments**

In this chapter, evaluation experiments on the characteristics of the sensor is described. The characteristics, including static and dynamic one, of the cantilever and of the proposed sensor were investigated. The dependence of sensor response on the change in external pressure, on cantilever's gap size and on cavity volume were clearly carried out. Noise measurement is also presented in this chapter in order to evaluate the measurement resolution of the sensor.



## **Conclusion**

Simulation results and experiment results are summarized. And conclusion of this research and its future works are presented in this chapter.

## **Reference**

This section shows the list of reference papers, from which my study cited and provided statements on literature researches.

## **Appendix**

This section provides informations related to this study. Appendix A presents a cantilever-based pressure sensor but in different approach. The gap of a cantilever is filled with liquid in order to prevent the air leakage. Appendix B demonstrate a simple theoretical calculations the relationship between the change external pressure and the resistance change of the piezo-resistor fabricated on a cantilever. Appendix C shows the list of important experiment equipment used in this study. Appendix D describes the fabrication process of a piezo-resistive cantilever. In appendix E, devices and chemicals used in MEMS fabrication processes are provided. And appendix F shows the mask design of a piezo-resistive cantilever.

## **Publication**

A list of related papers of the author is provided in this section.

## **Acknowledgement**

I would like to thank people who have been supported me to accomplish my Ph.D. thesis.

---

## Chapter 2 Sensing Theory and Experiment Preparation

In this chapter, theoretical calculation of mechanical properties of a micro cantilever is presented first. In the next section, theory of a piezo-resistive cantilever is provided, in which the relationship between cantilever displacement and resistance change of piezo-resistor and applied differential pressure is shown. This study also theoretically discuss about the influence of acceleration on the sensor response, and the Reynolds number considering the gap size as the characteristic length. It follows by the principle for measuring barometric pressure. Fabrication process of the sensor and preparation for experiments, including experimental setup and measurement electrical circuits, are described at the end of this chapter.

### 2.1 Physical properties of a cantilever

---

#### 2.1.1 Parameter definition

The parameters used in equations and graphs of this section are listed as follows. The unit for each parameter is also described.

**Terms associated with piezo-resistive cantilever. (see Fig. 2. 1)**

$L_1$	Total length of the cantilever [m]
$L_2$	Length of the body part of the cantilever [m]
$h$	Cantilever's thickness [m]
$b$	Cantilever's width [m]
$w$	Width of the cantilever's leg [m]

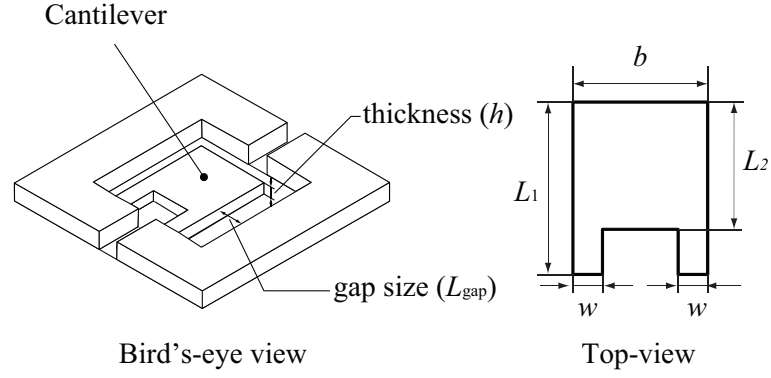


Fig. 2. 1 Dimensions of a cantilever beam.

$L_{\text{gap}}$	Cantilever's gap size [m]
$R$	Cantilever's resistance [ $\Omega$ ]
$\Delta R$	Cantilever's resistance change [ $\Omega$ ]
$\varepsilon$	Silicon's strain gauge[-]
$\rho$	Silicon's specific resistance [ $\Omega \cdot \text{m}$ ]
$\Delta \rho$	Specific resistance change [ $\Omega \cdot \text{m}$ ]
$\pi$	Piezo-resistive coefficient
$E$	Young's modulus [Pa]
$\nu$	Poisson ratio [-]
$I$	Geometrical moment of inertia [ $\text{m}^4$ ]
$f$	Frequency [Hz]
$m$	Mass [kg]
$\rho_{\text{Si}}$	Mass density of Silicon (Si)

**Terms associated with fluid dynamics.**

$\mu$	Viscosity [Pa.s]
$\nu$	Kinematic viscosity [ $\text{m}^2/\text{s}$ ]
Re	Reynolds numbers [-]
$P$	Pressure [Pa]
$\rho_{\text{air}}$	Mass density of the air [ $\text{kg}/\text{m}^3$ ]

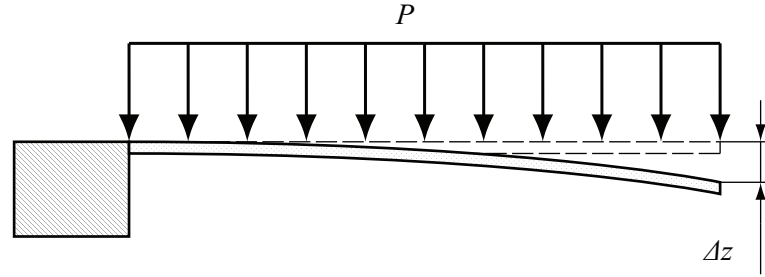


Fig. 2. 2 Cantilever deformed while being applied by an uniform mechanical load.

### 2.1.2 Material mechanics of a simple cantilever beam

A simple model of cantilever affected by a pressure is described in **Fig. 2. 2**. Consider that a pressure  $P$  is applied on the entire surface of the cantilever. According to the theory of material mechanics, the displacement at the free end of the cantilever  $\Delta z$  is expressed by <sup>[73]</sup>

$$\Delta z = \frac{PL_1^3}{8EI} \quad (2.1)$$

The geometrical moment of inertia  $I$  is expressed by

$$I = bh^3/12 \quad (2.2)$$

From the above equation, we can see the linear relationship between applied pressure and the deflection of a cantilever.

### 2.1.3 Piezo-resistive effect

The core of this research is the piezo-resistive cantilever. Indeed there are many methods to convert the bending of a cantilever to an electrical signal such as piezo-electric type, capacitive type or optical type. however, to fabricate an ultra thin cantilever, piezo-resistive type has advantage of simple fabrication at a low cost. **Fig. 2. 3** shows the general concept of a piezo-resistive cantilever, which is fabricated on a SOI wafer. A piezo-resistive layer is created on the surface of the cantilever by a process of thermal expansion, which will be described in detail in the chapter of fabrication and

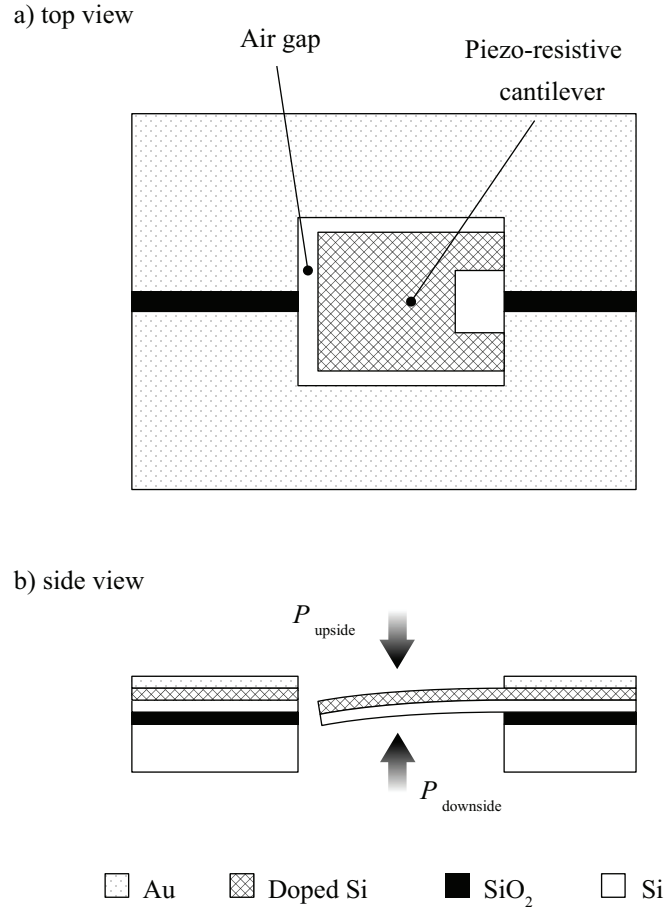


Fig. 2. 3 (a) Top view (b) Side view of a piezo-resistive cantilever.

experiment preparation. Due to this piezo-resistive layer, the resistance of the cantilever changes with the deformation of the cantilever. In other words, the resistance change occurs when the cantilever is acted by an external pressure. In the following sub-section, the relationship between the resistance change of the piezo-resistive cantilever and the applied pressure. Consider the case when a piezo-resistive element is applied a stress. The fractional resistance change of that piezo-resistive element ( $\Delta R/R$ ) can be expressed as follows.

$$\frac{\Delta R}{R} = (1 + 2\nu) \cdot \varepsilon + \frac{\Delta \rho}{\rho} \quad (2.3)$$

where  $\nu$  is the Poisson ratio,  $\varepsilon$  is the strain gauge,  $\rho$  is the specific resistance and  $\Delta\rho$  is the change of the specific resistance due to the applied pressure on the piezo-resistive element. In semiconductor crystal structure (e.g. Si), a slight deformation in the structure would cause the large change in the carrier concentration and lead to a huge change in the specific resistance. Thus, the fractional change of specific resistance  $\frac{\Delta\rho}{\rho}$  is much larger than  $(1 + 2\nu)\varepsilon$ . Therefore, for piezo-resistive cantilever,

$$\frac{\Delta R}{R} \approx \frac{\Delta\rho}{\rho} = \pi \cdot \sigma \quad (2.4)$$

Here  $\pi$  is the piezo-resistive coefficient of Si in the direction corresponding with x-axis in **Fig. 2. 4**.

#### 2.1.4 Fractional resistance change of a piezo-resistive cantilever

The definition of parameters in cantilever structure is provided in the top of this chapter. In 2012, we have demonstrated a brief calculation for the fractional resistance change of a piezo-resistive cantilever<sup>[68]</sup>. According to the material mechanics for general cantilever beam, the geometrical moment of inertia  $I$  is expressed by

$$\begin{aligned} I &= \frac{wh^3}{6} \quad (\text{for } 0 \leq x \leq L_1 - L_2) \\ I &= \frac{bh^3}{12} \quad (\text{for } L_1 - L_2 \leq x \leq L_1) \end{aligned} \quad (2.5)$$

The small displacement of the cantilever  $y(x)$  can be expressed using moment  $M$ , Young modulus  $E$  and the moment of inertia of area. We have,

$$\frac{d^2 y(x)}{dx^2} = \frac{-M}{EI} \quad (2.6)$$

The moment  $M$  can be obtained as the following.

$$\begin{aligned} M &= \frac{b\Delta P}{2} [2L_2(L_1 - x) - L_2^2] + w\Delta P [(L_1 - L_2) - x]^2 \quad (0 \leq x \leq L_1 - L_2) \\ M &= \frac{b\Delta P}{2} (L_1 - x)^2 \quad (L_1 - L_2 \leq x \leq L_1) \end{aligned} \quad (2.7)$$

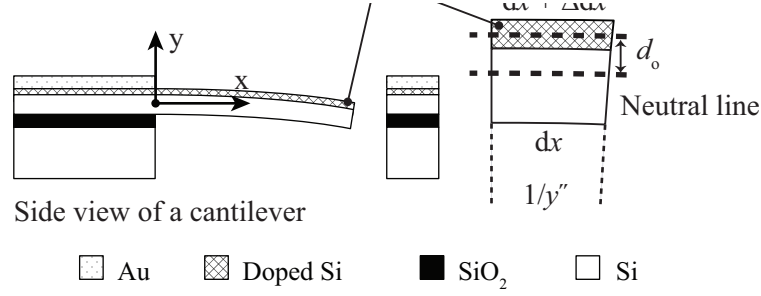


Fig. 2. 4 Cantilever deformation.

where  $\Delta P$  is the differential pressure applied on the cantilever. The boundary conditions here are

$$\frac{dy(0)}{dx} = 0, y(0)=0 \quad (2.8)$$

As shown in **Fig. 2. 4**, the relationship between the displacement of a cantilever  $y(x)$  and the corresponding strain  $\varepsilon(x)$  is expressed by

$$\varepsilon(x) = \frac{\Delta dx}{dx} = d_0 \cdot \frac{d^2 y(x)}{dx^2} \quad (2.9)$$

where  $d_0$  is the distance from the neutral plane of the cantilever to central plane of the piezo-resistive layer, considering that the impurity concentration within the piezo-resistive layer is uniform. The fractional resistance change of the piezo-resistive cantilever can be calculated as follows.

$$\frac{\Delta R}{R} = \int_0^{L_1-L_2} \pi \cdot \sigma \cdot dx / (L_1 - L_2) \quad (2.10)$$

Here  $\sigma$  is the stress in the direction of  $x$ -axis (**Fig. 2. 4**) of the cantilever and  $\pi$  is the piezo-resistive coefficient in that direction. Since  $\sigma = E \cdot \varepsilon$ , from **Eq. 2.9** and **Eq. 2.10** we have the theoretical calculation for the fractional resistance change of the piezo-resistor on the cantilever as follows.

$$\frac{\Delta R}{R} = \frac{\pi d_0 E}{L_1 - L_2} \int_0^{L_1-L_2} \frac{d^2 y(x)}{dx^2} \cdot dx \quad (2.11)$$

Indeed, as shown in our previous research<sup>[68]</sup>, **Eq. 2.11** is to calculate the fractional resistance change of the two hinges of the cantilever.  $\Delta R$  and  $R$  respectively represents the resistance change and the resistance of the hinges. However, from the view point of material mechanics, when a cantilever is deflected, the stress concentrated mostly at the hinges. Therefore, the resistance change of the hinges is dominant in compared with other parts of the cantilever. Therefore, **Eq. 2.11** can be used for representing the fractional resistance change of a piezo-resistive cantilever. We can replace the hinge's resistance ( $R$ ) by the cantilever's resistance, without losing the proportional relationship between both sides of the equation.

### 2.1.5 Reynolds number in gap area

(In this section, I have been allowed to reused some sentences and expressions from my previous paper, which is the reference<sup>[1]</sup> with the Copyright 2011 IEEE)

When the cantilever is in an airstream, the air gap cause air leak. The air gap is the gap between the cantilever and its surrounding walls. Consider the case in which the air flow leak through the gap is an ideal gas. According to Bernoulli equation for ideal gas, the characteristic velocity of air flow, which leaks through the air gap due to the differential pressure  $\Delta P$ , can be obtained by the following equation.

$$U = \sqrt{\frac{2K\Delta P}{\rho_{\text{air}}}} \quad (2.12)$$

The coefficient  $K$  in **Eq. 2.12** is used to represents the percentage of the potential energy (of the differential pressure) converted to kinetic energy.  $K$  is always smaller than 1. If  $K$  is equal to 0, it means that there is no air that leaks through the gap. Consider the gap size as the characteristic length, Reynolds number of the flow leak through the air gap can be calculated as follows.

$$\text{Re} = \frac{UL}{\nu} = \frac{L_{\text{gap}} \cdot \sqrt{\frac{2K\Delta P}{\rho_{\text{air}}}}}{\nu} \quad (2.13)$$

## 2.2 Design of a piezo-resistive cantilever

---

### 2.2.1 Cantilever deformation and the fractional resistance change



In this study, the dimensions of the piezo-resistive cantilever was determined with the value shown in the following **Table 2. 1**.

**Table 2. 1 Dimensions of a piezo-resistive cantilever**

$L_1$	125 [ $\mu\text{m}$ ]
$L_2$	100 [ $\mu\text{m}$ ]
$h$	0.3 [ $\mu\text{m}$ ]
$b$	100 [ $\mu\text{m}$ ]
$w$	25 [ $\mu\text{m}$ ]

The dimensions of the cantilever chip, which was fabricated from an n-type SOI wafer, was 1.5 mm×1.5 mm×0.3 mm. The dimension of the piezo-resistive cantilever was 125  $\mu\text{m}$ ×100  $\mu\text{m}$ ×0.3  $\mu\text{m}$ . The dimension of the hinges (legs) was 25  $\mu\text{m}$ ×25  $\mu\text{m}$ ×0.3  $\mu\text{m}$ . The piezo-resistive layer was formed by the thermal expansion process, which will be described in detail in the section of fabrication. The  $x$ -axis of the cantilever was designed to have the orientation corresponding with the (1,0,0) crystal orientation of the SOI wafer. In this case, the Young modulus is 130 GPa. Considered the thickness of the piezo-resistive layer is 100 nm ( $h_p$ ) and the impurity concentration is  $1\sim 2\times 10^{19} \text{ cm}^{-3}$ , we can calculate the piezo-resistive coefficient  $\pi = -9.2\times 10^{-10} \text{ Pa}^{-1}$  [69].

In the corresponding cantilever model, due to stress concentration, the resistance change at the hinges cantilever is dominant in compared with that change at other parts of the cantilever. Here, let us simplify the calculation by providing the resistance change of the hinges only. By combining **Eq. 2.5**, **Eq. 2.6**, **Eq. 2.7** and **Eq. 2.11**, we obtain the following relationship between the resistance change  $\Delta R$  and applied pressure  $\Delta P$ .

$$\frac{\Delta R}{R} = -\frac{6\Delta P\pi h_p}{wh^3(L_1-L_2)} \int_0^{L_1-L_2} \left( \frac{b}{2} [2L_2(L_1-x) - L_2^2] + w[(L_1-L_2)-x]^2 \right) \cdot dx \quad (2.14)$$

thus,

$$\frac{\Delta R}{R} \propto \Delta P \quad (2.15)$$

**Eq. 2.15** means the fractional resistance change of a piezo-resistive cantilever is proportional to the differential pressure applied on the cantilever. For specific value of the parameters that were mentioned above, the proportional coefficient is calculated to be in the range of  $10^{-4}[\text{Pa}^{-1}]$  order. Since the value of fractional resistance change can be measured with resolution of sub  $10^{-5}$  [70], we can understand that the resolution of pressure measurement by this piezo-resistive cantilever is expected to be sub 0.1 Pa.

### 2.2.2 Calculation the amount of air leak and Reynolds number

Consider the gap size is  $1\text{ }\mu\text{m}$  and the differential pressure applied on the cantilever is 10 Pa. Kinematic viscosity and density of air are taken as  $15.5 \times 10^{-6}\text{ }^\circ\text{C m}^2/\text{s}$  and  $1.25\text{ kg/m}^3$  at 1 atm and 20. According to **Eq. 2.13**, Reynolds number in this case is calculated as the following.

$$\text{Re} = \frac{UL}{\nu} = \frac{L_{gap} \cdot \sqrt{\frac{2K\Delta P}{\rho_{\text{air}}}}}{\nu} \leq 0.26 \quad (2.16)$$

Indeed, at this range of Reynolds number, the air can not be considered as inviscid gas. The effect of viscous gas should be considered in all calculation. However, in theoretical calculation and simulations of this study, the physic model was simplified by considering only the case of inviscid gas.

## 2.3 Theory on cantilever-based barometric pressure measurement

---

(In this section, I have been allowed to reused some sentences and expressions from my previous paper, which is the reference <sup>[1]</sup> with the Copyright 2011 IEEE)

In the proposed sensor, an ultra-thin (300-nm-thick) piezo-resistive cantilever was placed on the opening of a cavity, which was used as the reference pressure. Here, the piezo-resistive cantilever was used to measure the time-variant differential pressure between the barometric pressure and the cavity's pressure. Because one end of the cantilever is free, the cantilever-based pressure sensors should be more sensitive than diaphragm-based sensors. Additionally, the cantilever has an ultra-small spring constant because the spring constant is proportional to the thickness cubed. With respect to diaphragm types, in our sensor, there is a gap (air-gap) between the cantilever and its surrounding walls such that air can leak through the gap. The basic difference between the proposed sensor and conventional

sensors is that while conventional sensors can provide a static reading of absolute pressure, our cantilever-based pressure sensor measures the change in barometric pressure. The other difference is that the cavity below the cantilever is normally open and does not need to be vacuum sealed.

The principle for measuring the change in barometric pressure is simple. we define the initial state as the state in which the pressure inside the cavity and the ambient pressure are equal. The cantilever does not deform, and there is no air leakage through the air-gap at the initial state. Now, consider the case in which the barometric pressure increases (e.g., due to an altitude change). As a result, the cantilever bends and the air-gap gradually becomes larger to allow air to leak through the gap. Due to the air leakage, the pressure inside the cavity increases to match the barometric pressure. When the pressure inside the cavity equals the barometric pressure, the cantilever returns to its initial state. The key factor here is the size of the air-gap.

Indeed, the behavior of air-leakage through the gap, which is merely a few micrometers wide, is different from the behavior that would be observed in macroscopic space. Here, the shear force (i.e., the viscosity) of the air within the air-gap is dominant and prevents air from leaking through the air-gap. Therefore, the pressure loss due to air leakage becomes small, and the differential pressure experienced by the cantilever increases as the air-gap decreases. In other words, the displacement of the cantilever due to a change in barometric pressure increases for a smaller air-gap. Hence, the sensor's sensitivity can be improved by using a miniaturized air-gap.

A simple calculation model is presented in **Appendix B**, in which we assume that the air leaks through the cantilever's gap obeys the Bernoulli equation for ideal gas. We also assume that the change in gap size during the cantilever's bending is small such that it can be ignored.

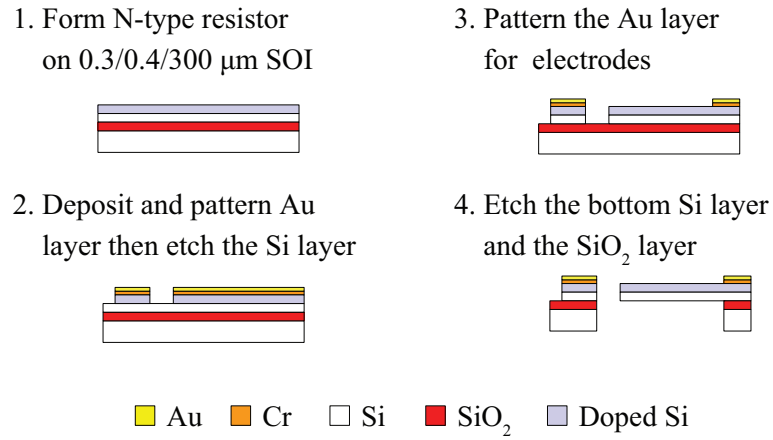


Fig. 2. 5 Fabrication process of a piezo-resistive cantilever (Copyright 2011 IEEE<sup>[1]</sup> )

## 2.4 Fabrication of a piezo-resistive cantilever and the sensor device

(In this section, I have been allowed to reused some sentences and expressions from my previous paper, which related to the reference <sup>[1][3]</sup> with the Copyright 2011 IEEE and the Copyright 2013 AIP Applied Physics Letters)

In this section, fabrication process flow of a piezo-resistive cantilever is provided in detail. The design and dimensions of the cantilever was presented in **Section 2.2** .

The cantilever was fabricated using a P-type 0.3- $\mu\text{m}$  / 0.4- $\mu\text{m}$  / 300- $\mu\text{m}$ -thick SOI (silicon-on-insulator, G6P-020-01, Soitec Asia) wafer. That means the thickness of the device silicon, the buried oxide layer and the handle silicon were 0.3- $\mu\text{m}$  , 0.4- $\mu\text{m}$  and 300- $\mu\text{m}$  , respectively. The dimensions of a SOI wafer used in the process were 1 square inches.

First, an one-square inches SOI wafer was created from a large 6 inch SOI by using dicing saw machine (A-WD-10A, Tokyo Seimitsu, Japan). An SOI wafer was then put in HF solution to remove the silicon oxide layer on the wafer surface. After that the wafer was spin-coated with n-type dopant (OCD (P-59230), Tokyo Ohka Kogyo Co., Ltd., Japan). Then 100-nm-thick of a piezo-resistive layer was formed on the surface of the SOI wafer by rapid thermal diffusion using diffusion furnace (SSA-

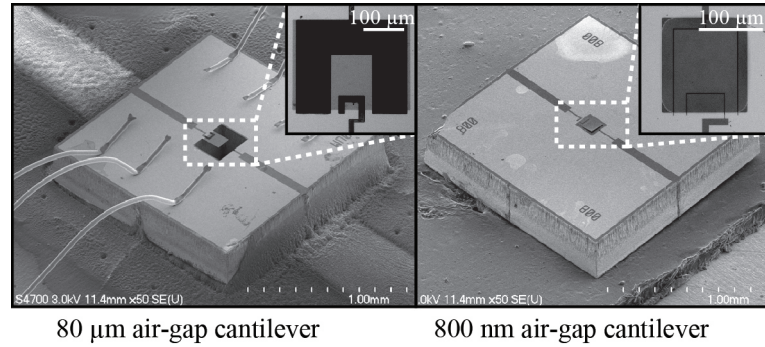


Fig. 2. 6 SEM images of the fabricated piezo-resistive cantilever chip (Copyright 2013 AIP Applied Physics Letters<sup>[3]</sup>)

P610CP, ULVAC-ROKO, JAPAN). Considering the carrier density the piezo-resistive layer, the value at the depth of 50 nm and 100 nm are about  $10^{19} \text{ cm}^{-3}$  and  $10^{15} \text{ cm}^{-3}$ , respectively. Additionally, the electrical resistivity at the depth of 50 nm is about  $10^{-3} \sim 10^{-2} \Omega \text{ cm}$ .

Next, chromium (Cr) and gold (Au) layers were deposited with thicknesses of 3 nm and 30 nm, respectively. In the next step, the Cr/Au layers were patterned (Mask Aligner, Type PEM-800, Union Kouki, Japan) to form the shape of the cantilever. The upper-side Si layer was then dry-etched by ICP-RIE (inductively coupled plasma - reactive ion etching, (MUC-21 HR, Sumitomo Precision Products)). Then, the Au and Cr layers were etched again to remove the metal layers from the surface of the piezo-resister. The lower-side Si layer was etched using ICP-RIE from the backside. Then, the cantilever was released by etching the box layer ( $\text{SiO}_2$ ) using vaporized HF gas.

The dimensions of the cantilever itself were fixed, as shown in **Section 2.2**. However, to investigate the effect of the gap size, various sizes of air-gap was designed. **Fig. 2. 6** shows two examples of the fabricated piezo-resistive cantilever. The SEM (scanning electron microscope) images show the cantilever with gap size of  $0.8 \mu\text{m}$  and  $80 \mu\text{m}$ . The dimensions of the chip was  $1.5 \text{ mm} \times 1.5 \text{ mm} \times 0.3 \text{ mm}$ . The cantilever was in right the center of the chip.

From an 1 square inches wafer, ideally 81 cantilever chip can be fabricated. However, due to the conditions of clean room process, the yield was about 80%, which means about 60 cantilever chips can be

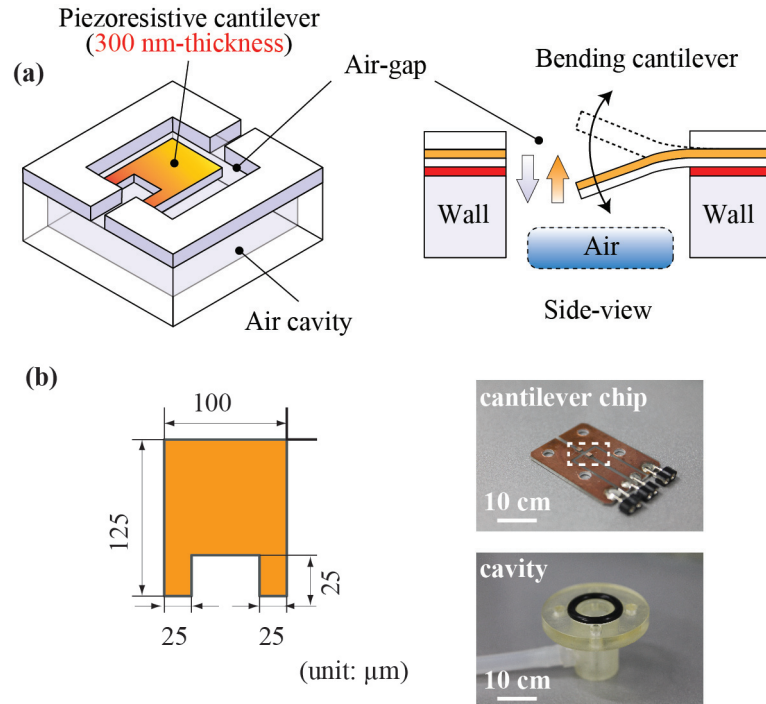


Fig. 2. 7 (a) Schematic diagram of the sensor device (b) Dimensions of the cantilever and image of the sensor device (Copyright 2013 AIP Applied Physics Letters<sup>[3]</sup>)

successfully fabricated at once.

The fabricated cantilever was then attached to a circuit board by using an instant adhesive (Aron Alpha, Toagosei Company, Ltd.) and UV curable resin. The cavity was fabricated using a modeling machine, which enabled the cavity volumes to be precisely controlled. Then the circuit board was attached to the opening of the cavity with screws. A plastic O-ring was sandwiched between the circuit board and the cavity to prevent air leak. In all of the test samples, the dimensions of the piezo-resistive cantilever were fixed. The image of the fabricated sensor device is shown in **Fig. 2. 7**.

## 2.5 Preparation for evaluation experiments

In this section, two methods for measuring the fractional change of piezo-resistive cantilevers are given. The first one uses voltage divider circuit and the second one uses Wheatstone bridge circuit. In

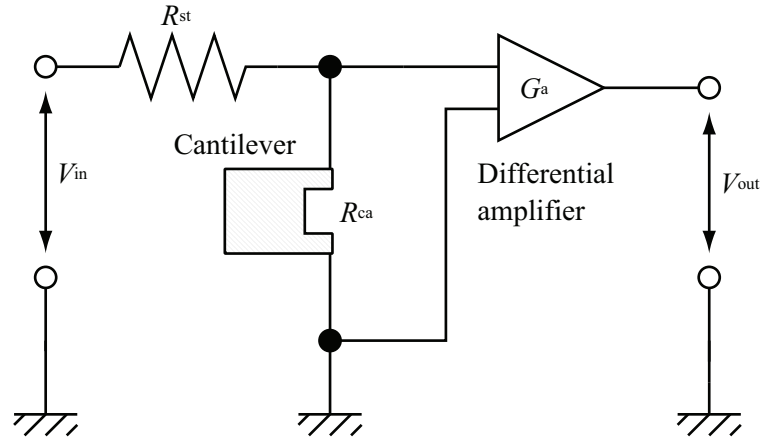


Fig. 2. 8 Combination of voltage divider and differential amplifier

both methods, the small change in cantilever's resistance is converted into the change into voltage. However, due to the specification of experimental machines, the first method was for investigating the frequency response of the cantilever and the second method was for measuring the differential pressure.

### 2.5.1 Voltage divider circuit

Related parameters are defined as follows.

$V_{in}$	Input voltage [V]
$V_{out}$	Output voltage [V]
$G_a$	Amplifier's gain [-]
$R_{st}$	Reference resistance [ $\Omega$ ]
$R_{ca}$	Cantilever's resistance [ $\Omega$ ]

Since the fractional resistance change of the piezo-resistive cantilever is small, in an order of 0.01%, a reference resistor and differential amplifier are used (**Fig. 2. 8**). The output voltage  $V_{out}$  is expressed by

$$V_{out} = G_a \frac{R_{ca}}{(R_{st} + R_{ca})} V_{in} \quad (2.17)$$

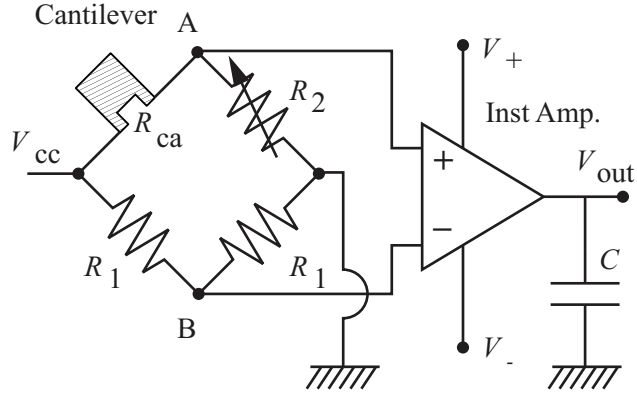


Fig. 2. 9 Combination of H-bridge and amplifier circuit

Concerning the output voltage when the cantilever's resistance  $R_{ca}$  changes,  $V_{out}$  is suggested by

$$V_{out} + \Delta V = G_a \frac{R_{ca} + \Delta R}{(R_{st} + R_{ca} + \Delta R)} V_{in} \quad (2.18)$$

Because  $\Delta R$  is small enough to be neglected, from **Eq. 2.17** and we have

$$\Delta V = G_a \frac{R_{st}}{(R_{st} + R_{ca})^2} V_{in} \Delta R \quad (2.19)$$

By measuring this voltage change, we can obtain the resistance change of the cantilever.

### 2.5.2 Wheatstone bridge circuit

Here the Wheatstone bridge circuit is combined with an Inst amplifier (**Fig. 2. 9**). Related parameters are defined as follows.

$V_{cc}$	Bias voltage [V]
$R_2$	Variable resistance [ $\Omega$ ]
$R_0$	Initial resistance of cantilever (without bending)
C	Noise-cut condenser



Here, the value of  $R_2$  is equal to that of  $R_0$ . Consider the variable resistance of cantilever  $R = R_0 + \Delta R$ , the voltage difference between point A and point B is determined by

$$\Delta V = V_A - V_B \quad (2.20)$$

$$\Delta V = \frac{V_{cc}}{2} - \frac{V_{cc}}{1 + R/R_0} \quad (2.21)$$

$$\Delta V = \frac{\Delta R/R_0}{2(2 + \Delta R/R_0)} V_{cc} \quad (2.22)$$

Because  $\Delta R/R_0 \ll 2$ , we obtain

$$\Delta V \cong \frac{V_{cc}}{4} \cdot \frac{\Delta R}{R_0} \quad (2.23)$$

In experiment, the resistance  $R_1$  of Wheatstone bridge circuit was determined to be 1.0 [k $\Omega$ ]. The variable resistance  $R_2$  has the value from 0.2 [k $\Omega$ ] to 5.2 [k $\Omega$ ]. In fact, a combination of two variable resistance were used to represent  $R_2$ . The first one, which has value from 0 [k $\Omega$ ] to 5 [k $\Omega$ ], was for large adjustment. The second one, which has value from 0 [k $\Omega$ ] to 0.2 [k $\Omega$ ], was for small adjustment. Amplifier AD623 with gain of 1000 was used to enhance the output voltage. A shunt regulator AD510 was used to provide a stable voltage of 2.5 [V]. The output voltage was then converted by an A/D converter. Finally, the signal was read by USB Data Logger Program to visualize the change in the resistance of the cantilever.

### 2.5.3 Setup for measuring cantilever's frequency characteristic

A speaker was used as a sound source and its sound frequency can be varied by using a network analyzer (see **Appendix E**). The sound emitted by the speaker produces pressure on the cantilever and causes it to bend. It results in the change in the resistance of the cantilever. The sound pressure is calibrated by a commercial microphone (B&K microphone, see **Appendix E**).

The change in the resistance of the cantilever is then measured by a voltage divider circuit (**Fig. 2.**

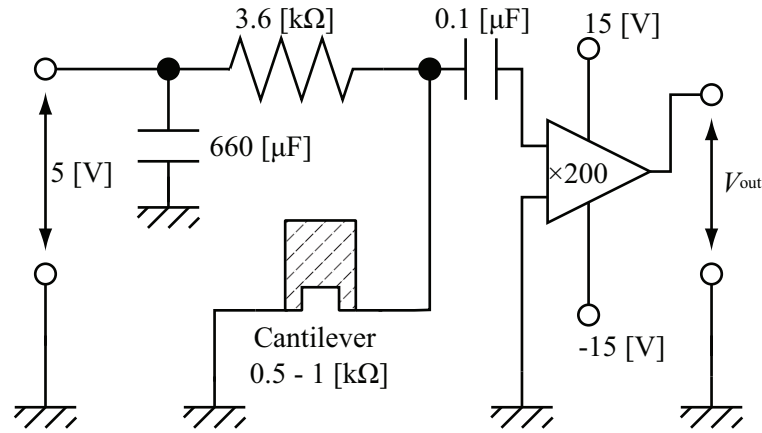


Fig. 2. 10 Voltage divider circuit

10). The concept and calculation for this circuit was described in **Subsection 2.5.1**. Here, a bypass capacitor ( $660\text{ }\mu\text{F}$ ) and a bypass filter capacitor ( $0.1\text{ }\mu\text{F}$ ) were used to stabilize the input and output voltage. By observing the fractional resistance change of cantilever at a certain range of sound frequency, we can determine the frequency characteristic of the cantilever. From this characteristic, we can observe the natural frequency of the cantilever as well as the its high-sensitive range.

#### 2.5.4 Setup for evaluating the sensor characteristic at low frequency

(In this section, I have been allowed to reused some sentences and expressions from my previous paper, which is related to the reference<sup>[3]</sup> with the Copyright 2013 AIP Applied Physics Letters)

We investigated the characteristics of the proposed barometric pressure sensor over a range from 0.05 Hz to 1 Hz. In many applications, the response in this range is of particular interest. For example, in indoor navigation applications, subjects move (e.g., climb stairs) with a relatively low speed and the rate of change of the barometric pressure is often approximately 1 Hz.

The experiments were performed in a closed room with no wind and no air flow. The environmental conditions were identical for each of the experiments. The room temperature was maintained at  $25\text{ }^{\circ}\text{C}$ , and the humidity was 70%. The sensor was fixed on a rotating wheel with a radius of 150 cm. The absolute altitude of the sensor and thus the absolute pressure experienced by the sensor changed with

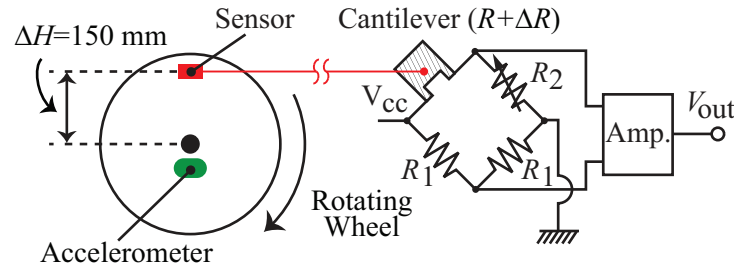


Fig. 2. 11 Concept of the rotating experiment to evaluate the sensor characteristic at low frequency (Copyright 2013 AIP Applied Physics Letters<sup>[3]</sup>)

the rotation rate of the wheel. The rotating velocity of the wheel was controllable.

In the rotating experiment (**Fig. 2. 11**), the maximum altitude change of the sensor was 30 cm (0.3 m), which was the diameter of the rotating orbit of the sensor. An accelerometer (HAAM-302B, Hokuriku Electric Industry Co., Ltd, Japan) was used to calculate the position of the sensor, which was obtained by measuring the gravitational acceleration. From the positional relation of the accelerometer and the proposed sensor, which was known, the position of the sensor was calculated. We also used the accelerometer to determine the phase lag of the barometric sensor's response.

The circuit used to measure the sensor's response is also shown in **Fig. 2. 11**. The fractional resistance change ( $\Delta R/R$ ) of the sensor was measured. As mentioned above, a piezo-resistor layer was formed on the cantilever's surface. Under the deformation of the cantilever, the resistance of the piezo-resistor layer changes. In the measurement circuit, the piezo-resistor was used as one of the four resistors in a Wheatstone-bridge circuit. The output was amplified with an amplifier (AD623, Analog Devices) with the gain of 1000.

### 2.5.5 Relationship between barometric pressure and absolute altitude

(In this section, I have been allowed to reused some sentences and expressions from my previous paper, which is related to the reference<sup>[3]</sup> with the Copyright 2013 AIP Applied Physics Letters)

The relationship between the change in barometric pressure and the change in absolute altitude is obtained as follows. According to *U.S. Standard Atmosphere*<sup>[62]</sup>,

$$\frac{p}{p_0} = e^{-\frac{g_0(h-h_0)}{RT}} \quad (2.24)$$

where  $h_0$  and  $p_0$  are the absolute altitude and absolute pressure at the base, respectively;  $g_0$  is the gravitational acceleration; and  $T$  is the ambient temperature, which is considered to be constant.

In our experiment, the change in altitude was less than 30 cm, which was the diameter of the orbit that the proposed sensor was rotating. Therefore, we have,

$$\frac{g(h-h_0)}{RT} \ll 1 \quad (2.25)$$

Thus,

$$e^{-\frac{g_0(h-h_0)}{RT}} \cong 1 - \frac{g_0(h-h_0)}{RT} \quad (2.26)$$

Hence,

$$\frac{p_0 - p}{p_0} = \frac{g_0(h-h_0)}{RT} \quad (2.27)$$

Therefore, we have the relationship between the change in barometric pressure and the change in absolute altitude as follows:

$$\Delta p = \left( \frac{p_0 g_0}{RT} \right) \cdot \Delta h = \rho g_0 \Delta h \quad (2.28)$$

where  $\rho$  is the air density. Here, we take  $g_s = 9.80665 \text{ (m/s}^2\text{)}$  and  $\rho = 1.192 \text{ (kg/m}^3\text{)}$ . Consider the temperature is maintained at  $25^\circ \text{ C}$ , we have

$$\Delta p = 11.69 \Delta h \quad (2.29)$$

In the rotating experiment, the maximum change in the altitude of the sensor was 30 cm (0.3 m). Therefore, the maximum change in barometric pressure was 3.5 Pa. The variance in air density due to absolute pressure and temperature was small enough to be neglected.

---

## Chapter 3 Fluid structure interaction simulation

In this study, an FEM (Finite Element Method) based simulation software was used in order to clarify the effect of fluid structure interaction (FSI) in the proposed cantilever-based barometric pressure sensor. This chapter provides a brief description on FSI of the cantilever-based pressure sensing model. The main purpose of this chapter is to evaluate the effect of the gap size of a cantilever on the sensor response. Additionally, the influence of cavity volume, applied pressure, cantilever's thickness, absolute pressure on the sensing are also carried out by simulations.

### 3.1 Cantilever deformation

---

In this section, simulation on the static deformation of a cantilever is presented. As shown in **Fig. 3.1**, the dimensions of the cantilever is  $100\text{ }\mu\text{m} \times 125\text{ }\mu\text{m}$  with the thickness of  $0.3\text{ }\mu\text{m}$ . The hinge dimension is  $25\text{ }\mu\text{m} \times 25\text{ }\mu\text{m}$ . In this simulation, let us assume that the cantilever is loaded with a pressure of 10 Pa. Consider that the cantilever is made of poly-crystal silicon with the following properties.

Young's modulus  $E = 160 \times 10^9\text{ Pa}$

Silicon density  $\rho = 2320\text{ kg/m}^3$

Thermal conductivity  $K = 34\text{ W/(m} \cdot \text{K)}$

Poisson's ratio  $\nu = 0.22$

Relative permittivity  $\epsilon = 4.5$

The static deformation of the cantilever is shown in **Fig. 3.2**. According to this result, the maximum deformation, which occurs at the free end of the cantilever, is approximately  $3.2\text{ }\mu\text{m}$ . Consider the rela-

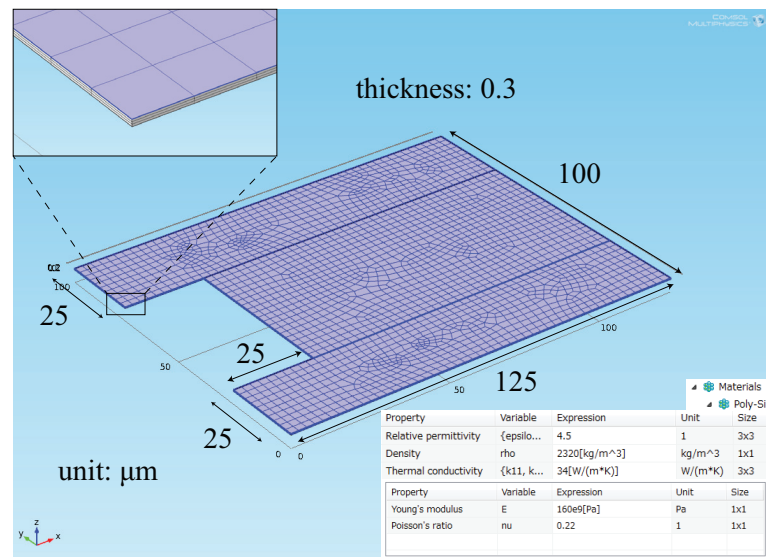


Fig. 3. 1 Cantilever model in FEM simulation

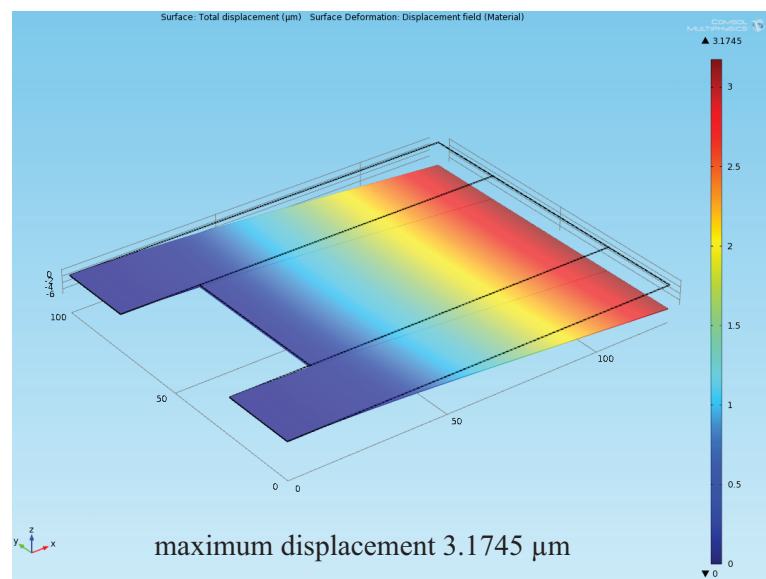


Fig. 3. 2 Cantilever's static deformation under a pressure of 10 Pa.

tionship between cantilever's deformation and applied pressure is a linear one, the deformation at the free end is approximately 300 nm for 1 Pa.

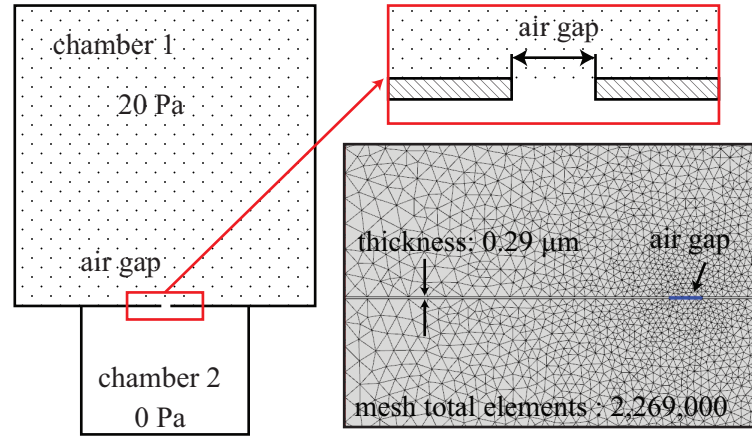


Fig. 3. 3 Simulation model for evaluating pressure decay between two chambers.

### 3.2 Pressure decay and dependence on gap size

In the proposed pressure sensor, the changing of external pressure lead to the bending of the cantilever and also the increasing or decreasing of the cavity pressure. Before doing simulation on the properties of the barometric pressure sensor, it is necessary to investigate the pressure decay of a chamber with an opening of a few micrometers. I suppose that the decay process is dependent on the dimensions of the opening.

Here, let us build a model with two chambers connected with an opening **Fig. 3. 3**. In this model, the volume of chamber 1 is much larger than that of chamber 2. In detail, chamber 1 is a circular cylinder with dimensions of  $\Phi 100 \text{ mm} \times H 100 \text{ mm}$ , and chamber 2 is a circular cylinder with dimensions of  $\Phi 10 \text{ mm} \times H 50 \text{ mm}$ . The volume ratio between chamber 1 and chamber 2 is 200 times. Hence we can consider chamber 1 is atmosphere and chamber 2 is the sensor cavity. As shown in **Fig. 3. 3**, the total elements of mesh in this simulation is 2269000 elements.

In the area between the two chambers, there is a plate with thickness of  $0.3 \text{ } \mu\text{m}$ , with a slit or gap at microscale. We can image that this plate is a cantilever but it is not deformed in this simulation. The gap size here is designed to have value of  $5 \text{ } \mu\text{m}$ ,  $10 \text{ } \mu\text{m}$ ,  $20 \text{ } \mu\text{m}$  and  $50 \text{ } \mu\text{m}$ . In this physics model, at initial status the pressure in chamber 2 is 0 Pa. The pressure of chamber 1 is kept constantly at 20 Pa and we will see the change in the pressure of chamber 2.



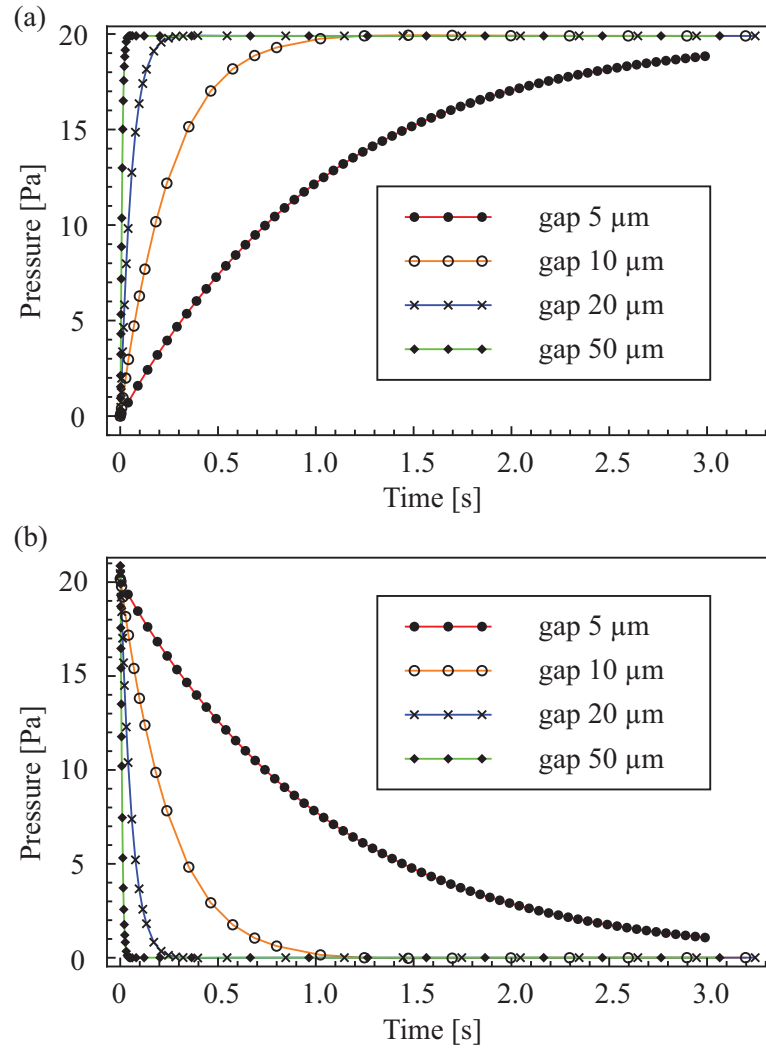


Fig. 3. 4 (a) Pressure inside chamber 1. (b) Differential pressure of the two chambers.

**Fig. 3. 4 (a)** shows the changing process of the cavity pressure with those gap sizes. **Fig. 3. 4 (b)** shows the change of the differential pressure, which is the difference of pressure in chamber 1 and chamber 2. The horizontal axis represents the duration of the changing process and the vertical axis represents the pressure.

From this results, we can observe that the pressure in chamber 2 increases to balance with the pressure in chamber 1. This process occurs due to the gap between the two chamber. However, the difference in the changing process with different gap size is obvious. The relaxation time, which is the

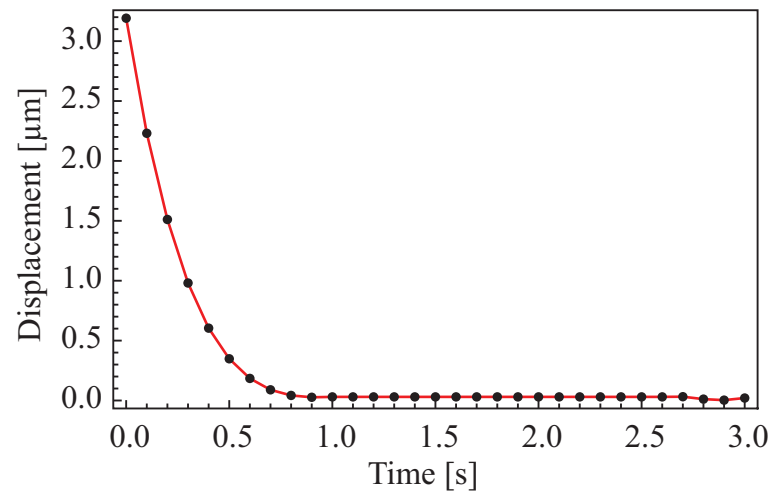


Fig. 3. 5 Calculated cantilever displacement based on the differential pressure in case of 10  $\mu\text{m}$  gap size.

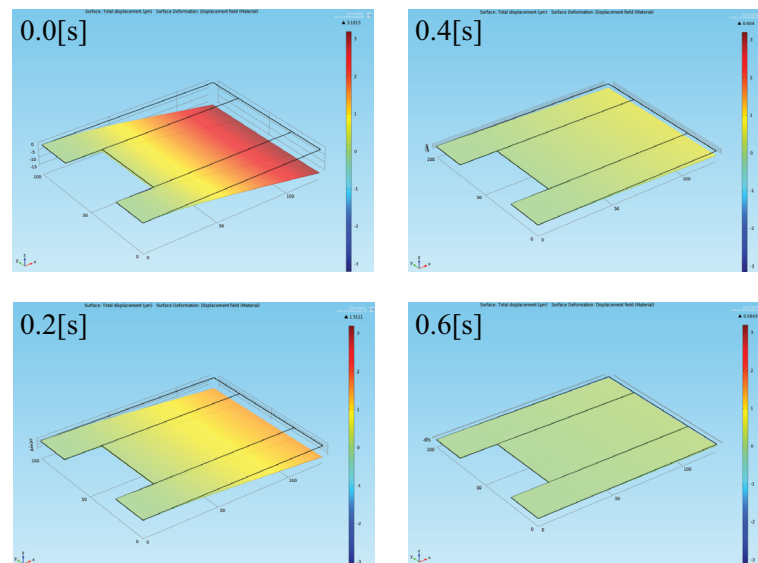


Fig. 3. 6 Images of the cantilever during the pressure change process at certain time (0 s, 0.2 s, 0.4 s and 0.6 s).

time needed for the chamber 2 to balance in pressure with chamber 1, is longer with smaller gap size. In detail, to reach pressure of 20 Pa, the models with gap size of 10  $\mu\text{m}$ , 20  $\mu\text{m}$  and 40  $\mu\text{m}$  need a

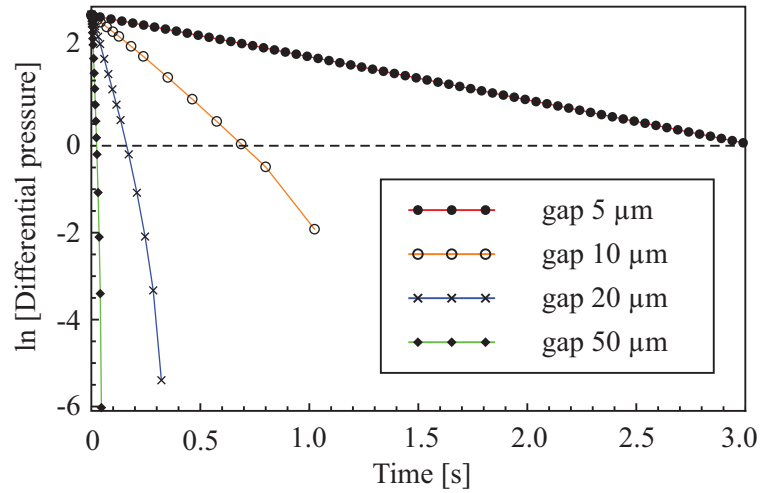


Fig. 3. 7 Relationship between cantilever displacement and time during pressure balance process. The result indicates that the cantilever displacement decreases in an exponential curve.

relaxation time of 1.3 s, 0.4 s and 0.09 s, respectively. However, the model with gap size of 5  $\mu\text{m}$  needs more than 3 s to reach 20 Pa. At the moment of 3 s from the initial status, the model of 5  $\mu\text{m}$  gap only reaches approximately 19 Pa.

Next, the change of differential pressure in the model of 10  $\mu\text{m}$  gap size (**Fig. 3. 4 (b)**) is used and converted to the cantilever displacement. The cantilever is designed with the same dimensions that was described in **Section 3.1**. The result is shown in **Fig. 3. 5**. The horizontal axis represents time and vertical axis represents the displacement of the cantilever. Note that in **Chapter 2**, the displacement of the cantilever is supposed to be proportional with the applied differential pressure. Therefore, the relationship between displacement and variant time can be considered as the decay process of the differential pressure. **Fig. 3. 6** shows the images of the cantilever during the deforming process. The cantilever displacement reaches its maximum at 0 s and then gradually returns to the its stable position with no deformation (see the images at 0.2 s, 0.4 s and 0.6 s).

To investigate the relationship of the decreasing cantilever's displacement with variant time during the pressure change process, the displacement is expressed in term of natural logarithm. **Fig. 3. 7** shows

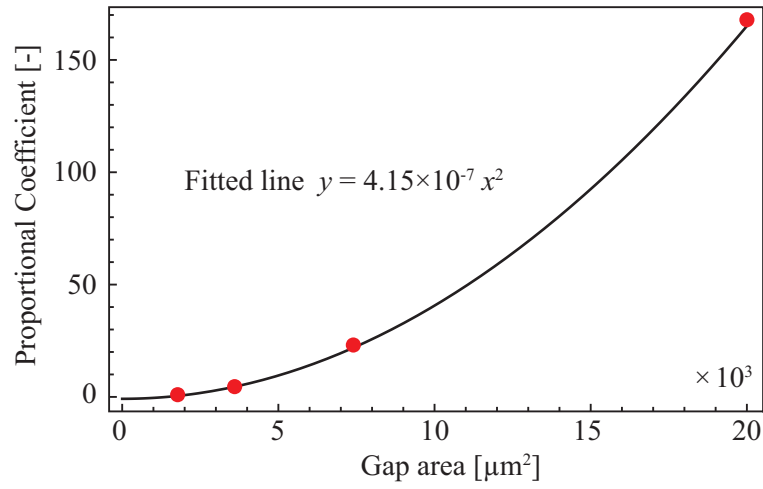


Fig. 3. 8 Relationship between decrement factor of cantilever displacement and cantilever's gap area.

that the cantilever displacement decreases in an exponential curve. Furthermore, by calculating the decrement factor of exponential curves corresponding with each gap size (**Fig. 3. 8**), it is obvious that the decrement factor is proportional to square of gap area.

**Section 3.1** has shown simulation on the structure deformation of the cantilever based on material mechanics. **Section 3.2** has shown fluidic simulation with a variation of gap size. However, the issue here is all of the above simulations are taken without considering the fluid structure interaction between the flexible cantilever and air flow. Indeed, the gap size of the cantilever is changing when the cantilever is being deformed. And the change in gap size would have influence on the behavior of air flow leaking through the gap. The change in behavior of the air flow then has influence on the cantilever deformation. Therefore, it is necessary to do a simulation such the interaction between fluids and structure are both considered at the same time. This will be provided in the next section.

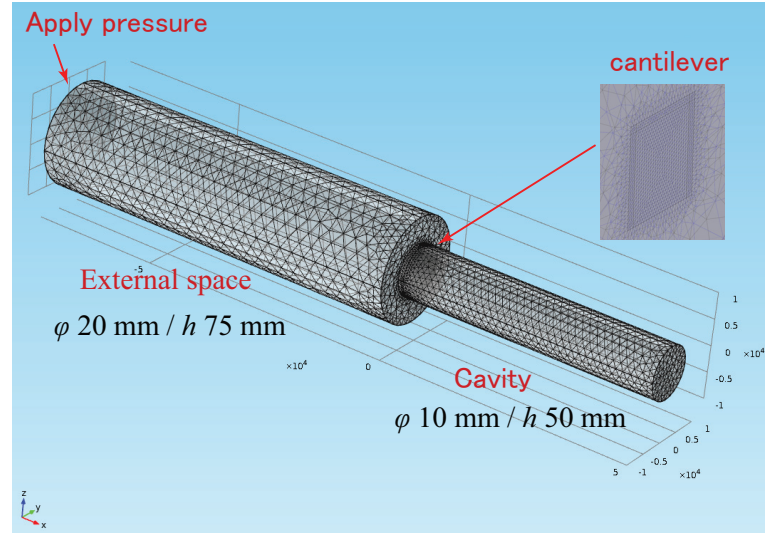


Fig. 3. 9 Fluid structure interaction model.

### 3.3 Simulations of fluid structure interaction

The simulation model is shown in **Fig. 3. 9**. Two circular cylinders are considered as the atmosphere and the sensor's cavity. The volume of atmosphere chamber is 6 times larger than that of the cavity chamber. In detail, the dimensions of the atmosphere chamber are  $\Phi 20 \text{ mm} \times H 75 \text{ mm}$  and the dimensions of cavity chamber are  $\Phi 10 \text{ mm} \times H 50 \text{ mm}$ . As shown in **Fig. 3. 9**, a cantilever beam with an air gap is placed between the two chambers. The dimensions of the cantilever are  $100 \mu\text{m} \times 125 \mu\text{m}$  with thickness of  $1 \mu\text{m}$ . In the next sub sections, the gap size, applied pressure and atmosphere pressure are the varied parameters to investigate the properties of the proposed sensor. In the following simulations, the air is considered as continuous, incompressible and inviscid gas with no slip at wall.

#### 3.3.1 Gap size variation

Here simulation with gap size of  $5 \mu\text{m}$ ,  $10 \mu\text{m}$ ,  $20 \mu\text{m}$  and  $40 \mu\text{m}$  (**Fig. 3. 10**) is carried out. I investigated the cantilever displacement with these gap size in two case. In the first case, which is shown in **Fig. 3. 11**, we assume that the differential pressure between the two chambers is kept at  $10 \text{ Pa}$  by a pressure supplying source. Then at moment of  $0 \text{ s}$ , the pressure supplier is switched off. Obvi-

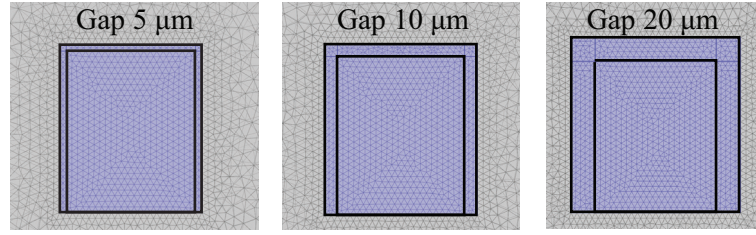


Fig. 3. 10 Variation of gap size.

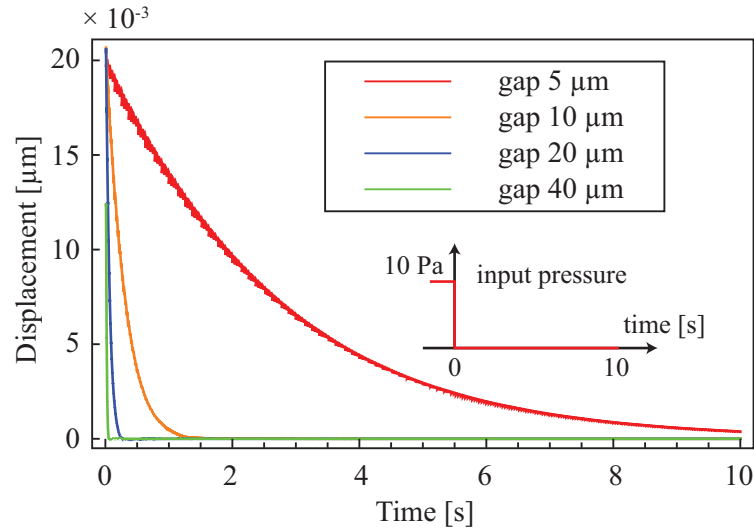


Fig. 3. 11 Cantilever displacement with various air-gap sizes. At initial status the differential pressure is kept at 10 Pa and then the input pressure is turned off.

ously, when the differential pressure is kept constant at 10 Pa, cantilevers with different gap size would bend with the same displacement, which is  $0.02 \mu\text{m}$  in this case. When the pressure supplier is switched off, the differential pressure gradually decrease to 0 Pa due to the air leak through the gap. According to the result in **Fig. 3. 11**, the process of pressure decay is different with different gap size. In detail, with gap size of  $40 \mu\text{m}$ , the differential pressure of 10 Pa needs 0.1 s to decrease to 0 Pa. That time with gap size of  $20 \mu\text{m}$ ,  $10 \mu\text{m}$  and  $5 \mu\text{m}$  are 0.4 s, 1.5 s and approximately 10 s. **Fig. 3. 12** presents the displacement change in terms of natural logarithm and its dependency on time. Obviously, the result shows that when the pressures on both sides of a cantilever balance, the cantilever displace-

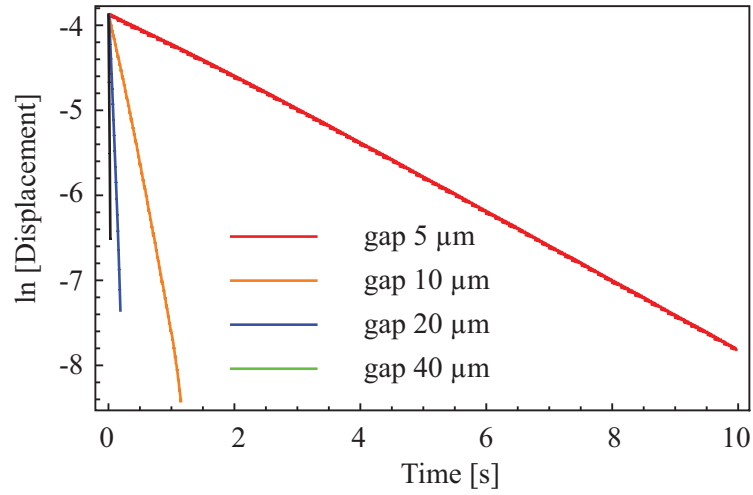


Fig. 3. 12 Relationship between cantilever displacement and time during pressure balance process. The cantilever displacement decreases in an exponential curve.

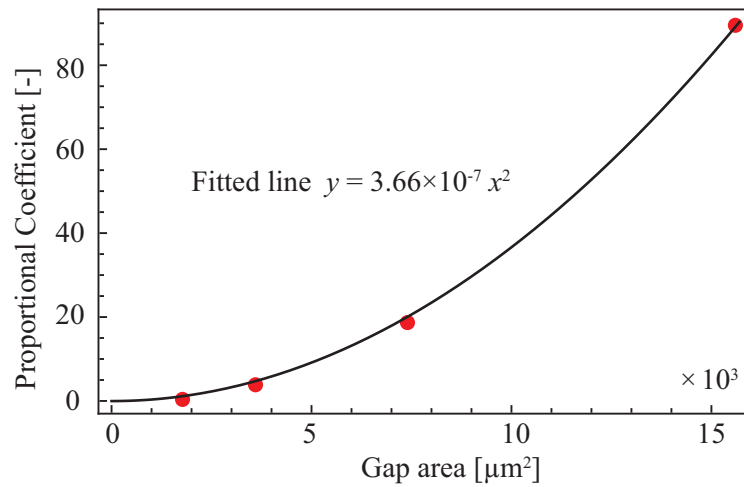


Fig. 3. 13 Relationship between decrement factor of cantilever displacement and cantilever's gap area.

ment decreases in an exponential curve. However, the way decrement factor is different for each gap size. The tendency here is that the decrement gets bigger with larger gap size. **Fig. 3. 13** shows the relationship between the decrement factor in **Fig. 3. 12** and the cantilever's gap area. We can observe that

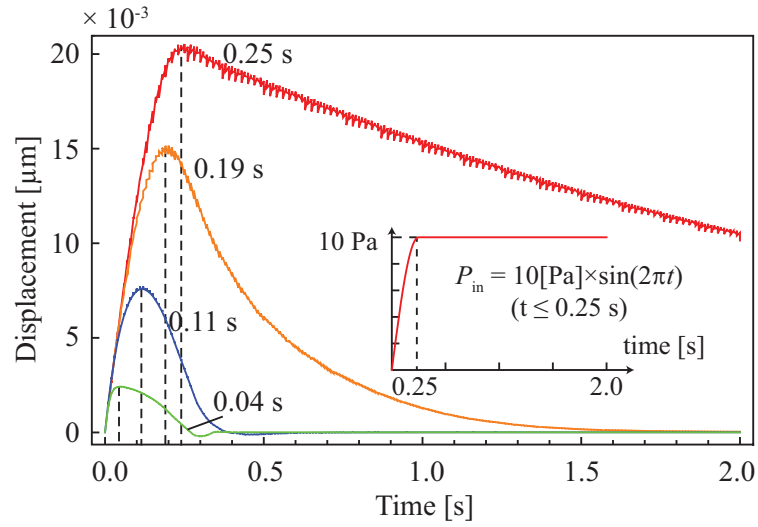


Fig. 3. 14 Cantilever displacement with various air-gap sizes. At initial status input pressure is 0 Pa and then gradually charged up to 10 Pa.

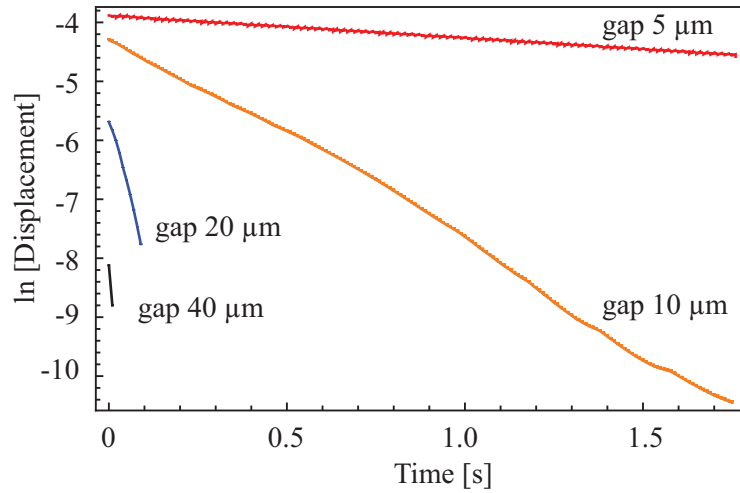


Fig. 3. 15 Relationship between cantilever displacement and time during pressure balance process. The cantilever displacement decreases in an exponential curve.

the decrement factor is proportional to square of gap area. Consider that the applied pressure ( $P_{in}$ ) is a function of time as follows.



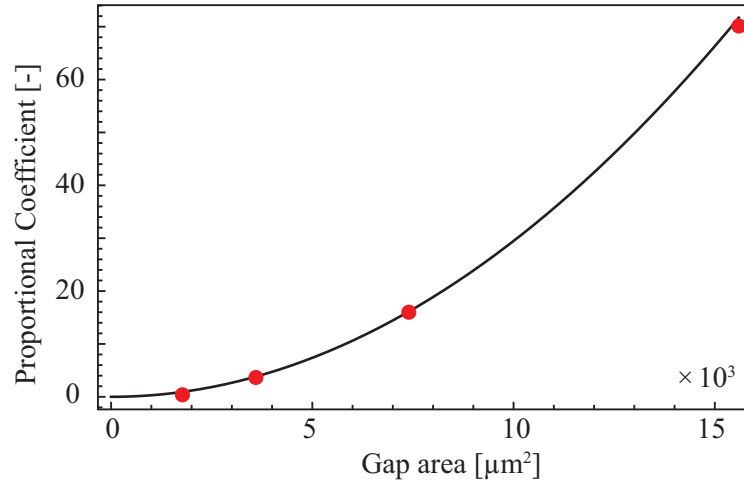


Fig. 3. 16 Relationship between decrement factor of cantilever displacement and cantilever's gap area.

$$P_{in} = 10 \text{ [Pa]} \times \sin(2\pi t) \{ (t \leq 0.25 \text{ s}) \}$$

$$P_{in} = 10 \text{ [Pa]} \{ (t \geq 0.25 \text{ s}) \}$$

The graph of applied pressure ( $P_{in}$ ) is shown in **Fig. 3. 14**. The displacement of cantilever with different gap sizes is also shown in **Fig. 3. 14**. Normally the cantilever displacement is proportional to the differential pressure applied on it. Hence, from this graph we can observe the behavior of the cavity chamber. When the atmosphere pressure is increasing to 10 Pa, the cavity pressure also increase to balance with the atmosphere pressure. As shown in **Fig. 3. 4**, with a gap size of larger than 10  $\mu\text{m}$ , the cavity needs less than 1 s to balance a pressure of 10 Pa. Since the atmosphere pressure only reaches the maximum pressure (10 Pa) at 0.25 s, the differential pressure between the two chambers should reaches its peak before 0.25 s, as shown in **Fig. 3. 14**.

In detail, with gap sizes of 10  $\mu\text{m}$ , 20  $\mu\text{m}$ , 40  $\mu\text{m}$ , the cantilever displacement is maximum at 0.19 s, 0.11 s and 0.04 s, respectively. For the case of 5  $\mu\text{m}$  gap size, the cantilever displacement peaks at 0.25 s. The reason is that the relaxation time with gap size of 5  $\mu\text{m}$  is longer than 0.25 s, which suits with the result in **Fig. 3. 4**. Another observation is that the maximum displacement is larger with smaller gap size. This result is meaningful because we can conclude that with for pressure change of

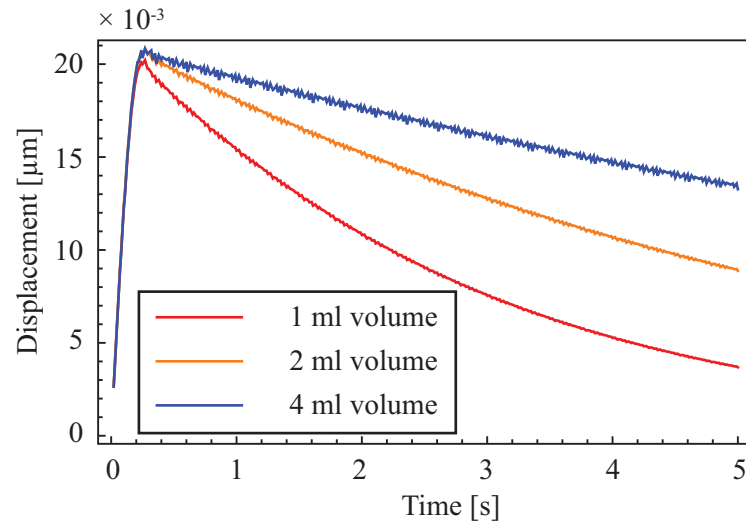


Fig. 3. 17 Cantilever displacement with various cavity volume.

less than 0.25 s, the cantilever gap should be designed with gap size smaller than  $5 \mu\text{m}$  in order to have larger displacement, which means higher sensitivity for the pressure sensing. **Fig. 3. 15** presents the displacement change in terms of natural logarithm and its dependency on time. The result shows that the cantilever displacement decreases in an exponential curve. The tendency here is that the decrement gets bigger with larger gap size. **Fig. 3. 16** shows the relationship between the decrement factor in **Fig. 3. 15** and the cantilever's gap area. We can observe that the decrement factor is proportional to square of gap area. It is the same result with previous simulations.

### 3.3.2 Cavity volume variation

The cavity volume is also a factor that has influence on the response of the sensor. From the general principle for gases, the time needed for an air cavity's pressure changes to balance with external pressure is obviously dependent on that cavity's volume. Normally, larger cavity should need more time for that process and vice versa. In this sub-section, a model with various cavity is presented. The cantilever's gap size and the applied pressure are kept to be constant. In detail, the gap size was  $5 \mu\text{m}$  and the applied pressure was 10 Pa. The input function of applied pressure is the same with the model in **Section 3.3.1**.

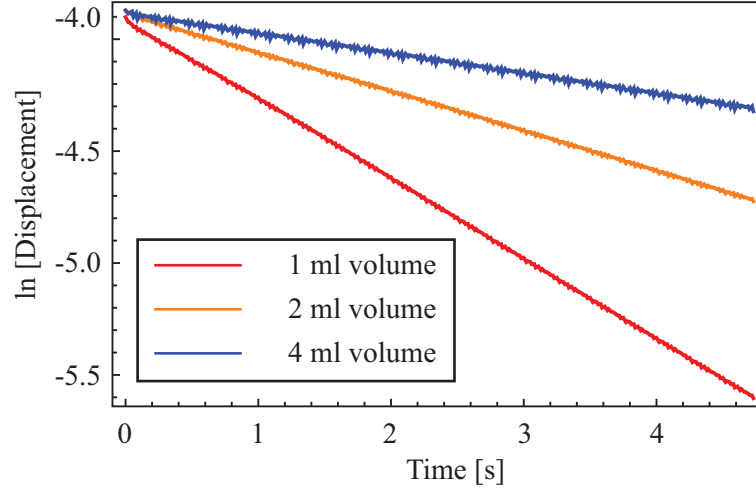


Fig. 3. 18 Relationship between cantilever displacement and time with various cavity volume (1 ml, 2 ml and 4 ml).

The simulation result of **Fig. 3. 17** shows that the value at the peak corresponding with each cavity's volume is almost the same for all cases. However, the process of pressure relaxation is different, in which larger cavity requires longer time for pressure balancing. Consider the process the cantilever's displacement decreasing from the peak, the change of displacement is expressed in terms of natural logarithm in **Fig. 3. 18**. This result indicates that the cantilever's displacement decreases in an exponential curve. Moreover, the decrement factor is inversely proportional to the cavity's volume.

### 3.3.3 Applied pressure variation

The applied pressure is varied in this simulation. Similar with the above section, the input pressure is expressed as follows.

$$P_{in} = P_0 \sin(2\pi t) \{ (t \leq 0.25 \text{ s}) \}$$

$$P_{in} = P_0 \{ (t \geq 0.25 \text{ s}) \}$$

Where  $P_0$  is varied with values of 5 Pa, 10 Pa, 20 Pa and 40 Pa. The result is shown in **Fig. 3. 19**. The gap size is set to be 5  $\mu\text{m}$  in this case. We can observe that in all the cases, the cantilever displacement

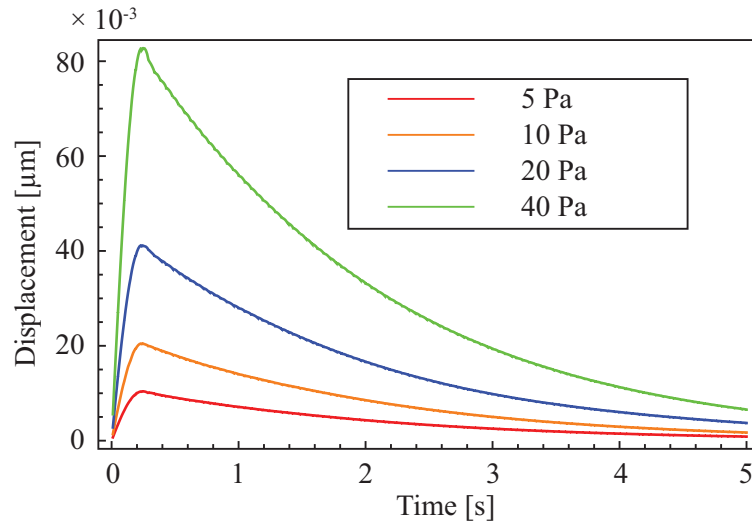


Fig. 3. 19 Cantilever displacement with various input pressure ( $P_0$  is varied with value of 5 Pa, 10 Pa, 20 Pa, 40 Pa)

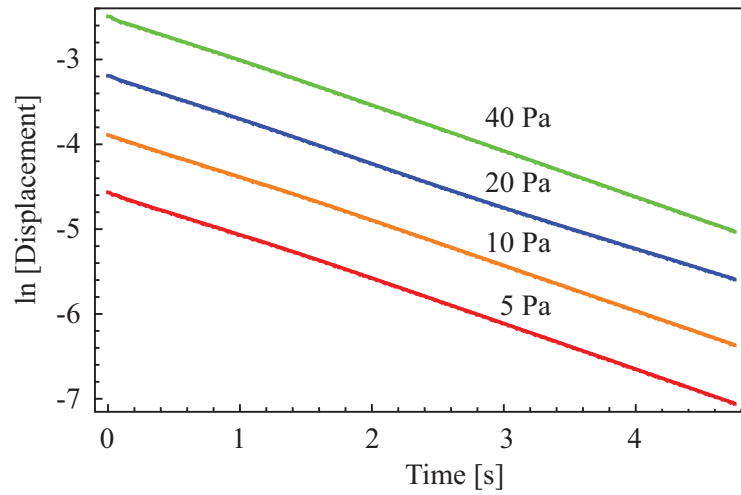


Fig. 3. 20 Relationship between cantilever displacement and time with various applied pressures.

reaches its peak at the same time of 0.25 s due to the same gap size, which is explained in **Section 3.3.1**. The maximum value is also proportional with the applied pressure  $P_0$ . For example, we can see that the

peak of 40 Pa is two times bigger than that of 20 Pa. Consider the process the cantilever's displacement decreasing from the peak of each graph, the change of displacement is expressed in terms of natural logarithm in **Fig. 3. 20**. This result indicates that the cantilever's displacement decreases in an exponential curve in which the decrement factor is not dependent on the applied pressure.

### 3.4 Summary of simulation results

---

In this chapter, an FEM based simulation software was used in order to clarify the effect of fluid structure interaction in a microcantilever with small gap size. The physic model includes a cantilever placed at the opening of a small air cavity and a chamber that are large enough to be considered as the ambient atmosphere. The simulations investigated the behavior of the cantilever when the ambient pressure changes, and its dependency on the gap size, the cavity's volume and the applied pressure. In this chapter, simulations were for calculating the cantilever's displacement due to the change in external pressure. In **Chapter 2**, the displacement of a cantilever is calculated to be proportional with the applied differential pressure. It also has linear relationship with the resistance change of the piezo-resistive layer fabricated on the cantilever. Therefore, the relationship between displacement and variant time can be considered as the decay process of the differential pressure, or as the change in piezo-resistance. The simulation results indicate that after being bent, the cantilever turns back to its initial balanced position in which the displacement decreases in an exponential function of time. Moreover, the decrement factor is calculated to be proportional to square of gap area and inversely proportional to the cavity's volume. In addition, the decrement factor does not change for various applied pressure. Note that in all the simulations, the gas was considered as continuous, incompressible and inviscid gas, and the boundary condition was no slip at wall.

---

## Chapter 4 Evaluation experiments

This chapter will provide an evaluation on the sensing performance of the proposed sensor. First, experiment for evaluating the static characteristics of a piezo-resistive cantilever, which included cantilever's deformation under an applied pressure and cantilever's static sensitivity, were done. Then the frequency characteristic of the cantilever was investigated in acoustic experiments. The phenomenon of air leak and pressure decay is shown next. The dependence of the decrement factor of pressure decay on the gap size of the cantilever, on the cavity volume, and on the change in external pressure were investigated. A full evaluation of the proposed barometric pressure sensor is presented in the next section. The evaluation includes static characteristics and dynamic characteristics at high frequency range and low frequency range. At the end of this chapter, a evaluation on the ability of a piezo-resistive cantilever in measuring differential pressure was shown. The result demonstrates that the cantilever was able to measure pressure at 10 mPa order.

### 4.1 Static characteristics of a piezo-resistive cantilever

---

#### 4.1.1 Cantilever deformation

The theoretical calculation on material mechanics of a cantilever beam was described in Section 2.1.2. In this section, the deformation of the fabricated piezo-resistive cantilever was measured. As presented in **Chapter 2**, the dimensions of the cantilever was designed as  $100\ \mu\text{m} \times 125\ \mu\text{m} \times 0.3\ \mu\text{m}$  with hinges of  $25\ \mu\text{m} \times 25\ \mu\text{m}$  (**Fig. 4. 1(a)**). The gap size of the cantilever in this experiment was  $5\ \mu\text{m}$ .

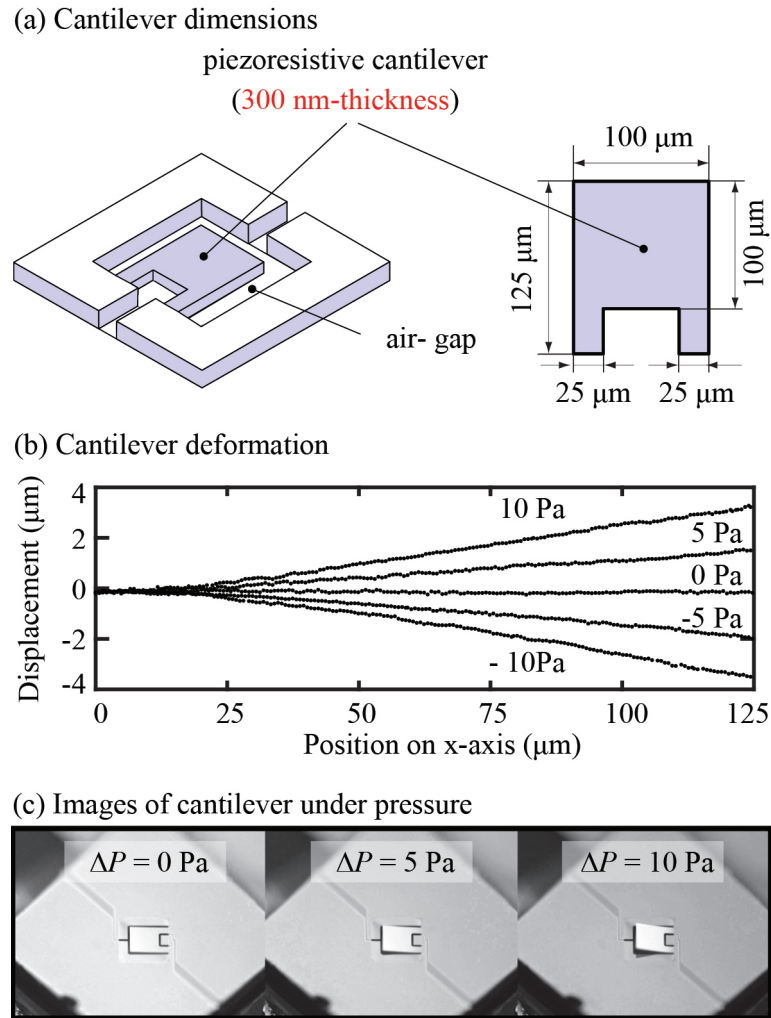


Fig. 4. 1 (a) Dimensions of the fabricated piezo-resistive cantilever. The gap size in this experiment was 5  $\mu\text{m}$  (b) Cantilever displacement under various differential pressure. (c) Images of the piezo-resistive cantilever during the pressurization process.

Pressure was created by a pressure generator with controlled pressure (KAL100, Halstrup-Walcher GmbH). The applied differential pressure were -10 Pa, -5 Pa, 0 Pa, 5 Pa and 10 Pa. The displacement of the cantilever was measured with a displacement detector (VK-8700, Keyence). **Fig. 4. 1(b)** shows the result of this experiment. The horizontal axis represents the position of an element on the cantilever in longitudinal direction (see **Fig. 2. 4**). The vertical axis represents the displacement when the cantilever was applied a pressure. The result indicates that the maximum displacement, which was at the free end

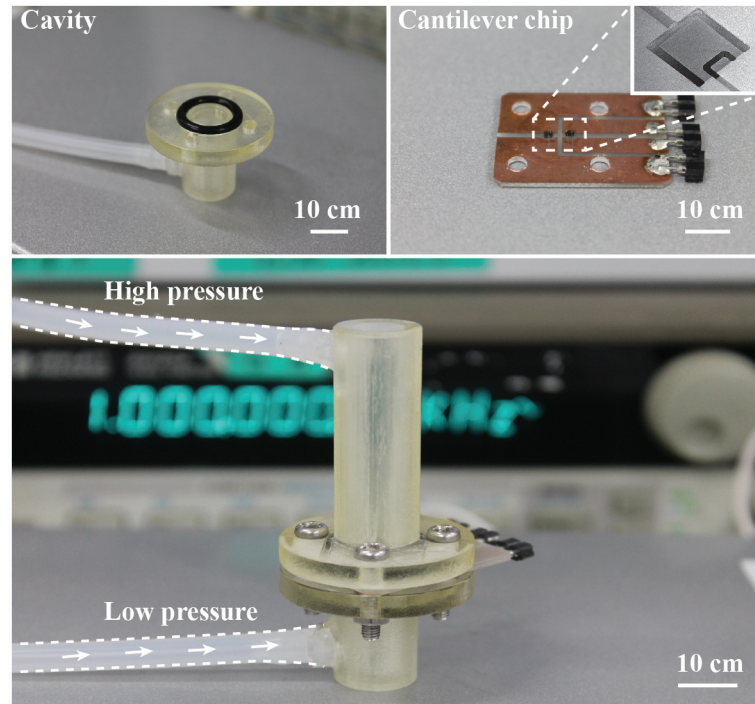


Fig. 4. 2 Image of the sensor and experimental setup.

of the cantilever, was approximately 300 nm for 1 Pa, which is suitable with simulation result in **Fig. 4. 1(c)** shows the images of the cantilever under pressurizing. The images show the behavior of the cantilever with pressures of 0 Pa, 5 Pa and 10 Pa. Obviously, the gap between the cantilever and its surrounding walls enlarges and allows the air to leak.

#### 4.1.2 Cantilever's sensitivity toward applied pressure

(In this section, I have been allowed to reused some sentences and expressions from my previous paper, which is related to the reference <sup>[1]</sup> with the Copyright 2011 IEEE)

Cantilever's sensitivity, which is expressed by the fractional resistance change under applied differential pressure of 1 [Pa], is determined in this section. The experimental set-up is shown in **Fig. 4. 2**, two air chambers were placed at upside and downside of the piezo-resistive cantilever. There was an air hole between the two chambers and the cantilever was put on that hole. A pressure generator was used



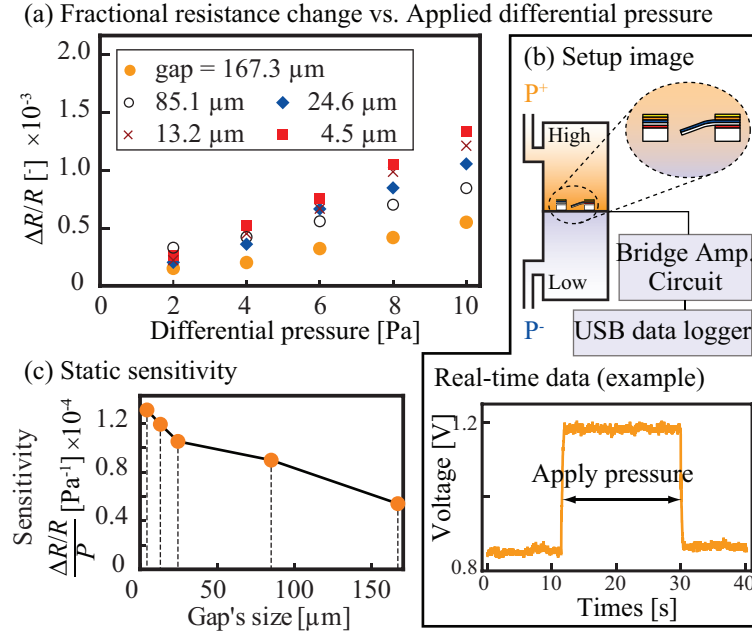


Fig. 4. 3 (a) Response of the piezo-resistive cantilever with various gap sizes to applied pressure. (b) Concept of the experimental set-up. (c) Static sensitivity of fabricated cantilevers.

to create pressure difference between the chambers. That differential pressure is exactly the pressure applied on the piezo-resistive cantilever. The pressurizing process consists of three steps. First, the cantilever was kept in initial status in which no pressure was applied. This status was 10 seconds. In the next 20 seconds, the pressure generator was switched ON and a certain differential pressure was created from the generator. Then the generator was switched OFF (**Fig. 4. 3**).

The resistance change of the cantilever was converted into the voltage change and then amplified and read with an oscilloscope. Indeed, the electrical circuit for measuring the resistance change of piezo-resistive cantilever was described in detail in **Chapter 2**, Section 2.5.2 and in our previous research<sup>[68]</sup>. The relationship between fractional resistance change and the change in output voltage is as follows.

$$\frac{\Delta R}{R} = \frac{1}{1000} \cdot \frac{\Delta V}{V} \quad (4.1)$$

The change in voltage, which was recorded by an oscilloscope, was used to calculate the fractional resistance change of the piezo-resistive cantilever. The result was shown in **Fig. 4.3 (a)**. In this experiment, cantilever with various gap sizes were evaluated and compared. The gap sizes were designed to be 5  $\mu\text{m}$ , 10  $\mu\text{m}$ , 20  $\mu\text{m}$ , 80  $\mu\text{m}$  and 160  $\mu\text{m}$ . However, due to the conditions of dry etching process, the fabricated gap sizes became 4.5  $\mu\text{m}$ , 13.2  $\mu\text{m}$ , 24.6  $\mu\text{m}$ , 81.5  $\mu\text{m}$  and 167.3  $\mu\text{m}$ . The value of applied pressure were controlled to be 0 Pa, 2 Pa, 4 Pa, 6 Pa, 8 Pa and 10 Pa.

We can observe a good linear relationship between fractional resistance change and applied pressure here. The proportional coefficient corresponding to each gap size was calculated (**Fig. 4.3 (c)**). Indeed, the proportional coefficient is the sensitivity of the cantilever to 1 Pa. The unit for sensitivity is hence  $[\text{Pa}^{-1}]$ . This result demonstrates that with the same pressure difference created by the pressure generator, the pressure loss due to the air gap could be higher with wider air gap size. For example, consider the sensitivity of the cantilever with gap size of 4.5  $\mu\text{m}$ , we have

$$\frac{\Delta R}{R} = 1.3 \times 10^{-4} \times \Delta P$$

which means the sensitivity in this case is  $1.3 \times 10^{-4} [\text{Pa}^{-1}]$ . The sensitivity of cantilever with gap sizes of 13.2  $\mu\text{m}$ , 24.6  $\mu\text{m}$ , 85.1  $\mu\text{m}$  and 167.3  $\mu\text{m}$  were  $1.1 \times 10^{-4} [\text{Pa}^{-1}]$ ,  $1.0 \times 10^{-4} [\text{Pa}^{-1}]$ ,  $0.9 \times 10^{-4} [\text{Pa}^{-1}]$ ,  $0.5 \times 10^{-4} [\text{Pa}^{-1}]$ , respectively.

---

## 4.2 Frequency characteristics of a piezo-resistive cantilever

---

(In this section, I have been allowed to reused some sentences and expressions from my previous paper, which is related to the reference <sup>[1]</sup> with the Copyright 2011 IEEE)

The measurement of frequency characteristics of a piezo-resistive cantilever is provided in this section. The preparation for measuring the frequency characteristic of the fabricated piezo-resistive cantilevers was given in **Subsection 2.5.3**. The image of this experiment is also in **Fig. 4.4**. Here the response of the cantilever to the sound pressure is investigated. The sound pressure is produced by a speaker (**Appendix C**) and is calibrated by a commercial microphone (B&K Co.) Network Analyzer (NA, see **Appendix C**) was used to record the cantilever's response. The frequency range was from 1

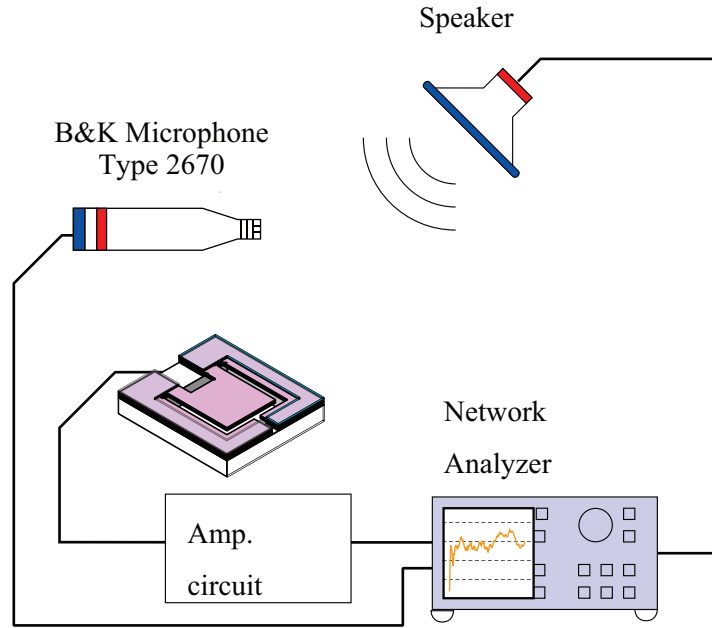


Fig. 4. 4 Setup for measuring the frequency characteristics of piezo-resistive cantilever.

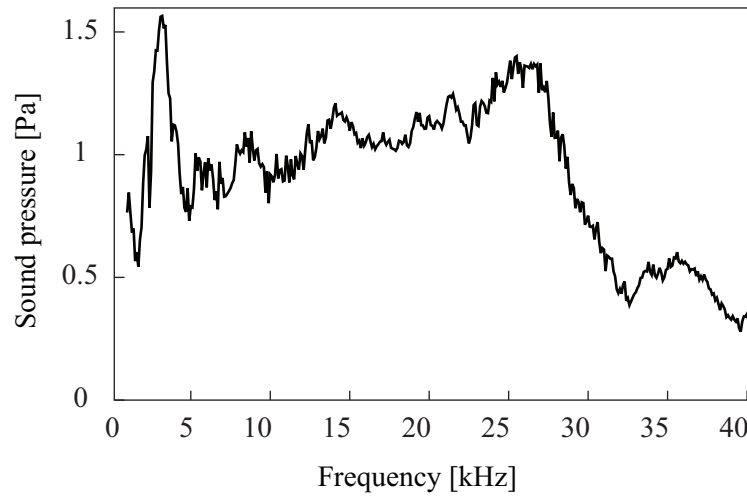


Fig. 4. 5 Sound pressure measured by the B&K microphone.

[kHz] to 40 [kHz], which is the stable range of the speaker. The output voltage of NA was 70.7 [mV] and the reference impedance was 50 [ $\Omega$ ]. The sensitivity of the B&K microphone was 100 [mV/A].

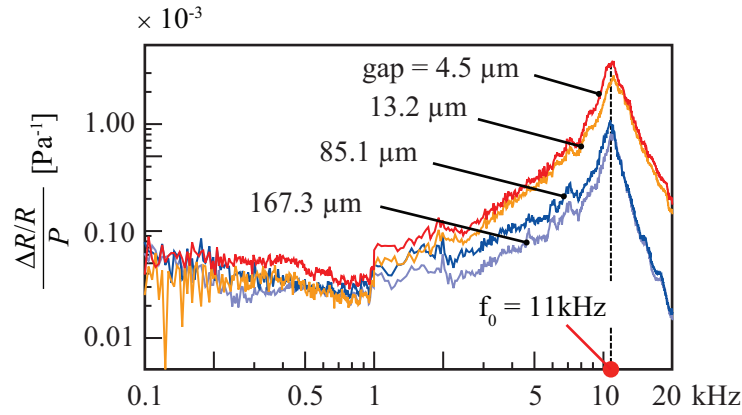


Fig. 4. 6 Frequency characteristics of piezo-resistive cantilever.

The sound pressure calibrated by B&K microphone is shown in **Fig. 4. 5**. As mentioned in **Chapter 2**, the responses of the cantilevers to the sound pressure were measured by the voltage divider and the amplifier circuit. For cantilevers of which its longitudinal directions were (1,0,0) and (1,1,0) of silicon crystal direction, the natural frequency were 14 kHz and 11 kHz. In the following experiments, all of the cantilevers were fabricated such that its longitude direction is on (1,1,0) direction. The frequency characteristics of cantilevers with various gap sizes (4.5  $\mu\text{m}$ , 13.2  $\mu\text{m}$ , 81.5  $\mu\text{m}$  and 167.3  $\mu\text{m}$ ) are shown in **Fig. 4. 6**. The horizontal axis represents the frequency of the sound wave emitted from the speaker. The frequency range here is from 100 Hz to 20 kHz. The vertical axis represents the fractional resistance change of the piezo-resistive cantilever to sound pressure of 1 Pa. Consider the fractional resistance change at the resonant frequency, we can observe that although the resonant frequencies were identical, the smaller gap size resulted in larger displacement. Indeed, the displacement of the cantilever with gap size of 4.5  $\mu\text{m}$  was three times bigger than with gap size of 167.3  $\mu\text{m}$ .

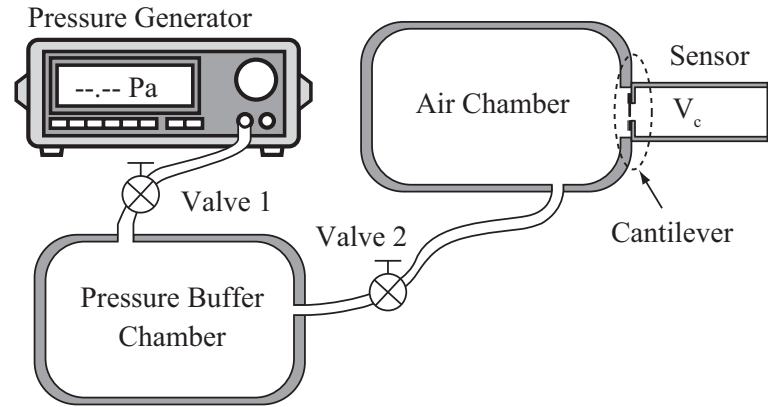


Fig. 4. 7 Experiment for evaluating the static characteristics of the proposed barometric pressure sensor.

### 4.3 Barometric pressure measurement

#### 4.3.1 Characteristics toward static applied pressure

(In this section, I have been allowed to reused some sentences and expressions from my previous paper, which is the reference <sup>[1]</sup> with the Copyright 2011 IEEE)

The experimental setup for evaluating the pressure sensor is shown in **Fig. 4. 7**. The sensor was connected to an air chamber (chamber 1), of which the volume was large enough ( $3.5 \times 10^6 \text{mm}^3$ ) in comparison with the cavity's volume. Thus we can consider the sensor is placed in the atmosphere. Chamber 1 was linked with a same volume chamber 2 by using silicone tube. A pressure generator was used to change the pressure inside the chamber 2. At initial state, the pressure in chamber 1 and in sensor's cavity was set to be the same with barometric pressure ( $P_0$ ). Valve 2 was closed. Valve 1 was opened to increase the pressure in chamber 2 up to  $P_0 + 2\Delta P$ . Next, valve 1 was closed and valve 2 was opened to investigate the response of the sensor. Consider that the pressure in chamber 1 was supposed to increase to  $P_0 + \Delta P$  immediately after opening valve 2. The principle for measuring the change in barometric pressure is simple (**Fig. 4. 8**). Let us define the initial state as the state in which the pressure inside the cavity and the ambient pressure are equal. The cantilever does not deform at the initial state. Now, consider the case in which the barometric pressure increases (e.g., due to an altitude change). As

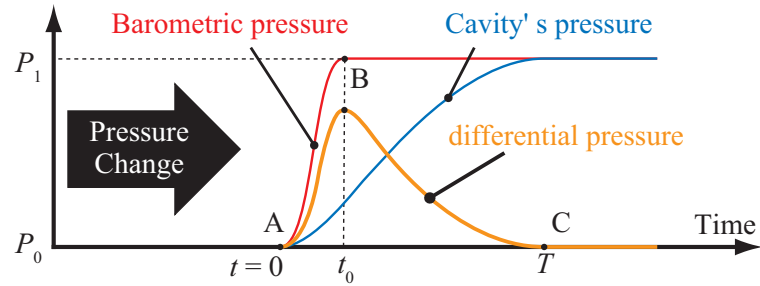
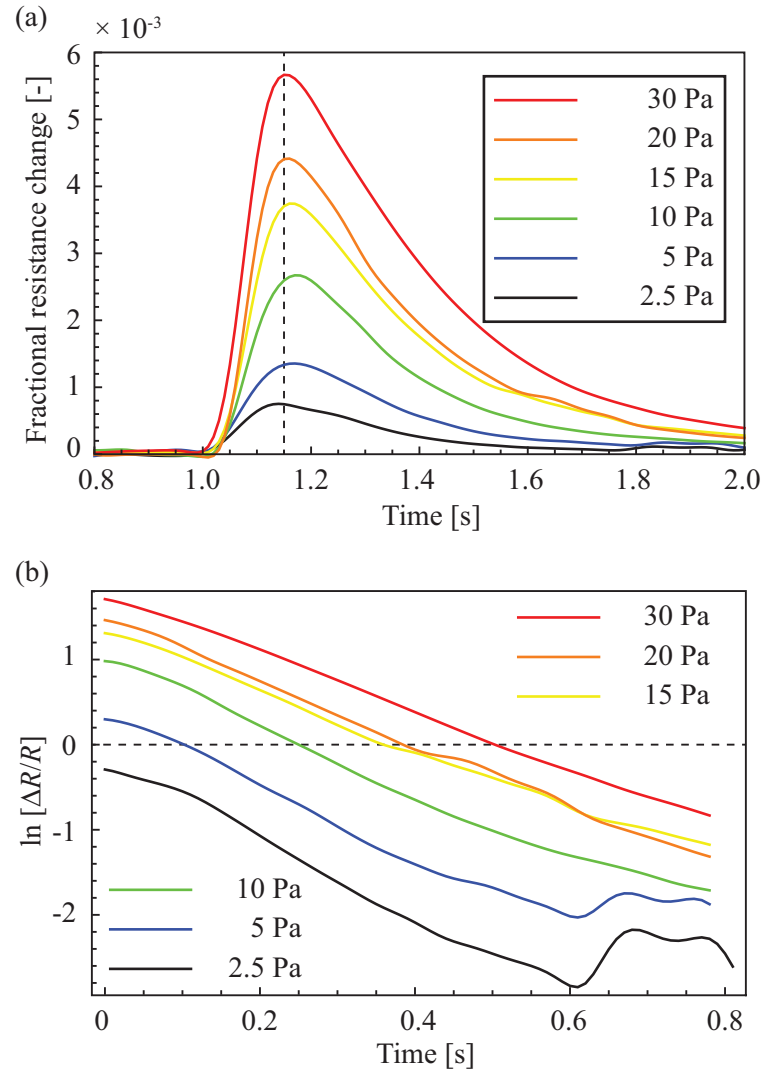


Fig. 4. 8 Concept of the pressure change process.

a result, the cantilever bends and the air-gap gradually becomes larger to allow air to leak through the gap. Due to the air leakage, the pressure inside the cavity increases to match the barometric pressure. When the pressure inside the cavity equals the barometric pressure, the cantilever returns to its initial state.

The key factor here is the size of the air-gap. As mentioned in previous sections, when the gap size is down-scaled, the pressure loss due to air leakage becomes smaller, and the differential pressure experienced by the cantilever is bigger. Hence, the sensors sensitivity toward pressure can be improved by miniaturizing the gap. The results of evaluation experiments are shown in **Fig. 4. 9**. First, the cavity's volume was fixed at  $10^3 \text{ mm}^3$  and the applied  $\Delta P$  was varied at 2.5 Pa, 5 Pa, 10 Pa, 15 Pa, 20 Pa, and 30 Pa (**Fig. 4. 9 (a)**). The horizontal axis shows the time of pressure balance process. The vertical axis represents the fractional resistance change of the piezo-resistive cantilever. As shown in previous sections, the fractional resistance change is proportional to the differential pressure experienced by the cantilever. Therefore, conclusions for the relationship between fractional resistance change with time can be applied for differential pressure.

In this experiment, the gap size was  $13.2 \text{ }\mu\text{m}$ . With the same experimental setup, we can observe that the bigger applied  $\Delta P$  produced higher peak. Now let consider the process from the moment the cantilever reached its maximum deflection to the moment it returned to the initial position. In **Fig. 4. 9 (b)**, the fractional resistance change is expressed in terms of natural logarithm. The result demonstrates that the fractional resistance change (i.e. differential pressure experienced by the cantilever) decays in an



**Fig. 4.9** a) Calibration data while varying the ambient pressure change. The gap size was  $13.2 \mu\text{m}$ , the cavity volume was 1 ml. b) Behavior of resistance change during pressure relaxation process is expressed in terms of natural logarithm. The start point is the moment the sensor response reached its peak.

exponential function of time. Moreover, although the change in external pressure (2.5 Pa, 5 Pa, 10 Pa, 15 Pa, 20 Pa, 30 Pa) was different for each graph, the slope was almost the same. It means that logarithmic decrement does not depend on the change in external pressure.

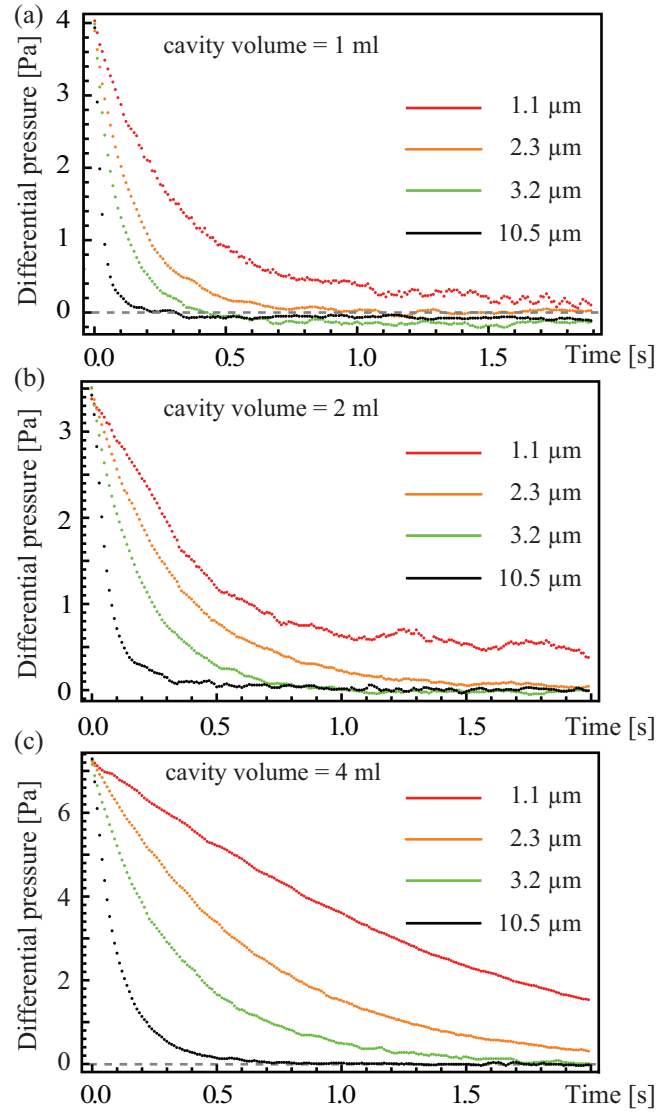


Fig. 4. 10 Differential pressure decay for various gap sizes when cavity volume was fixed at (a) 1 ml (b) 2 ml (c) 4 ml

#### 4.3.2 Effect of gap size on differential pressure decay

The phenomenon of differential pressure decay due to the air leak through the gap is the most significant physics of this study. Therefore, it is necessary to investigate the effect of gap size during the pres-



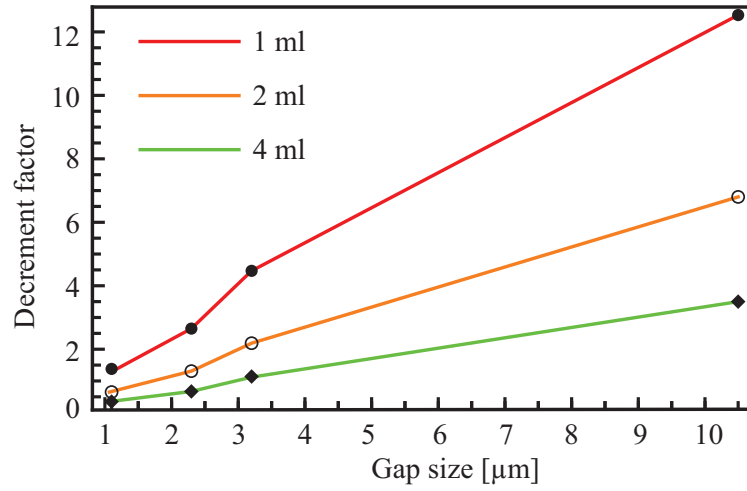


Fig. 4. 11 Relationship between decrement factor and gap size.

sure relaxation process. It is easy to imagine that in case of diaphragm, there is no air leak such that the time for pressure relaxation is infinite. In case with the existence of air gap, the relaxation time is obviously finite. As shown in **Chapter 3**, the fluid structure interaction (FSI) simulation demonstrates that the differential pressure decreases in an exponential function with the decrement proportional to square of gap area. However, the boundary condition of FSI simulation is no wall slip and for inviscid and incompressible gas, while the conditions in the device may be different. Therefore, in this sub section, the effect of gap size was investigated.

Four samples of the cantilever with different gap sizes ( $1\ \mu\text{m}$ ,  $2\ \mu\text{m}$ ,  $3\ \mu\text{m}$  and  $10\ \mu\text{m}$ ) were used in experiments. Due to the variance of equipment' conditions in fabrication process, the actual sizes were  $1.1\ \mu\text{m}$ ,  $2.3\ \mu\text{m}$ ,  $3.2\ \mu\text{m}$  and  $10.5\ \mu\text{m}$ , respectively. The experimental setup was the same with that in **Subsection 4.3.1**. The differential pressure decay with these gap sizes is shown in **Fig. 4. 11**. For a certain cavity volume, the differential pressure decreases differently with different gap size. The obvious tendency here is that the relaxation time for smaller gap size is longer. In addition, the differential pressure in this process is a exponential function of time. This results suit with theoretical calculation. However, the relationship between decrement factor and gap size in this experiment is a proportional one. This result is different with simulation result, in which decrement factor of differential pressure decay is

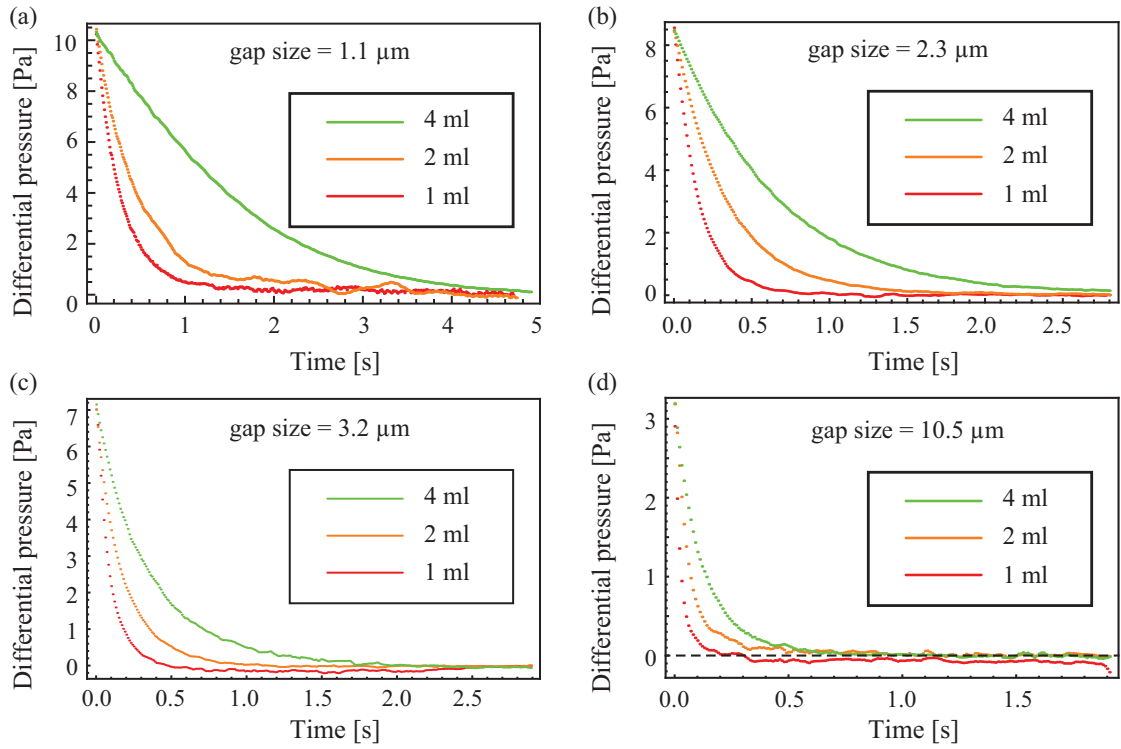


Fig. 4. 12 Differential pressure decay for various cavity volume when the gap size was fixed at (a) 1.1  $\mu\text{m}$  (b) 2.3  $\mu\text{m}$  (c) 3.2  $\mu\text{m}$  (d) 10.5  $\mu\text{m}$

proportional to square of gap size. Indeed, due to the ability of simulation processing computer, the gap size in simulation was larger than 5  $\mu\text{m}$  and the cantilever thickness was 1  $\mu\text{m}$ . For a few micron gap size, the Reynolds number is supposed to be around 1. Therefore, the different in gap size could bring into a significant difference in air viscosity. This could be the reason for the difference of experiment result and simulation result.

Nevertheless, in both of experiment and simulation, the differential pressure decay is confirmed to be an exponential function of time. In addition, the decrement factor is larger for bigger gap size. From experiments we can conclude that the decrement factor is proportional to gap size.

#### 4.3.3 Effect of cavity volume on differential pressure decay

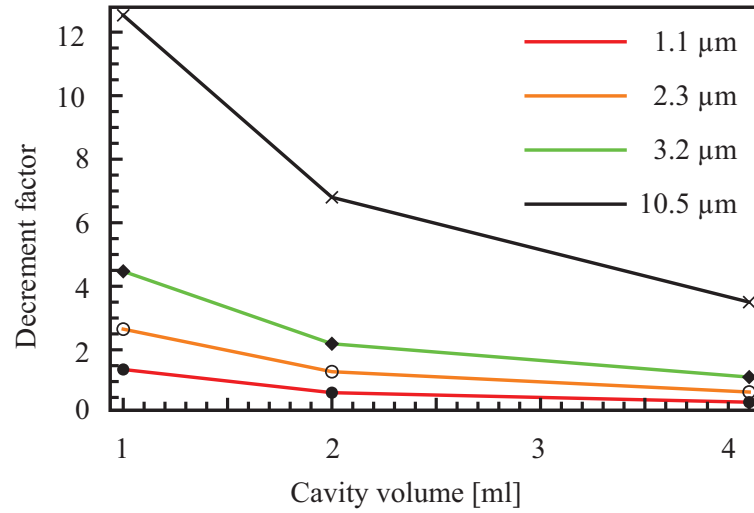


Fig. 4. 13 Relationship between decrement factor and cavity volume.

In the previous sub-section, the effect of gap size on differential pressure decay was presented. Cavity volume is also an important parameter in the sensing model. Simulation results have indicated that larger cavity require longer pressure relaxation process, which means that the decrement factor of differential pressure is bigger. Here, the effect of cavity will be described. There cavities with different volume (1 ml, 2 ml and 4 ml) were used in experiments. The gap size was kept constant to compare the difference between those cavities. The result is shown in **Fig. 4. 12**. This result agrees with simulation results, in which the differential pressure decreases in an exponential function of time.

The dependence of decrement factor and cavity volume is presented in **Fig. 4. 13**. Simulation results have shown that the decrement factor is inversely proportional to cavity volume. From the above experiment result, we can not completely conclude that relationship. However, the tendency in which larger cavity makes longer pressure relaxation process was confirmed. According to this fact, the sensor should be designed with small gap size and large cavity in order to improve the sensing performance. In applications, the idea of making larger cavity is not favorable. Hence, the key for this device is to narrowing the gap size as much as possible.

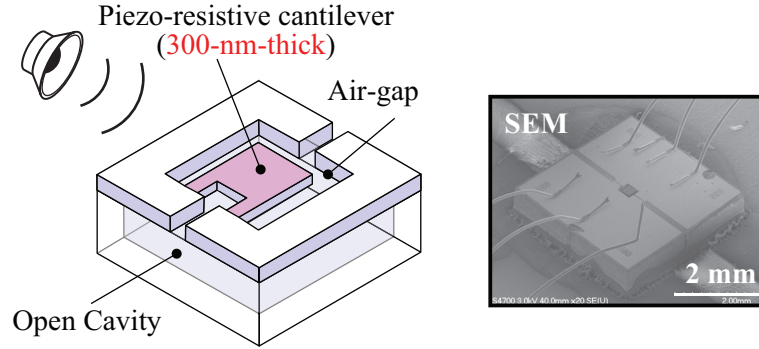


Fig. 4. 14 Schematic diagram of the sensor and SEM image of the cantilever.

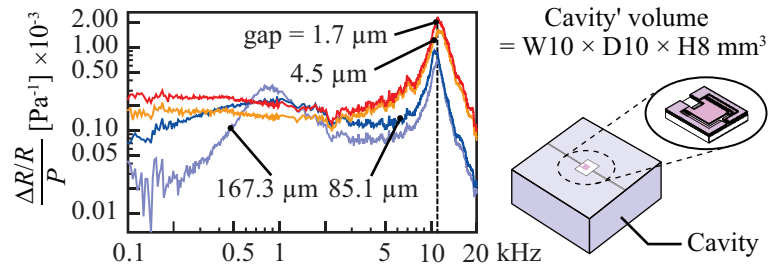


Fig. 4. 15 Frequency characteristic of the proposed sensor with various gap sizes.

#### 4.3.4 Measurement at high frequency range

In this section, dynamic characteristics of the proposed barometric pressure sensor in frequency range from 100 Hz to 20 kHz is described (**Fig. 4. 14**). As a pressure sensor, cantilever type is much more sensitive than diaphragm type. Nevertheless, cantilever-based microphones have been supposed to be insufficient because it is gradient type, thus their frequency response is commonly non-flat. In this research, we suppose that if the air-gap is small enough, cantilever-based microphones can obtain flat frequency response on broad band as well. **Fig. 4. 15** shows the scale effects of air-gap in the proposed sensor. Three values of cavity's volume  $\{V_0, 2V_0, 4V_0\}$ , in which the dimensions for cavity volume  $V_0$  was  $10 \text{ mm} \times 10 \text{ mm} \times 5 \text{ mm}$ , was varied for each size of air-gap. Compare with the result shown in **Fig. 4. 6**, we found that cantilever with cavity has higher sensitivity than cantilever its self. We also found that in the case of smaller cavity, the frequency response becomes gradually non-flat (**Fig. 4. 16**

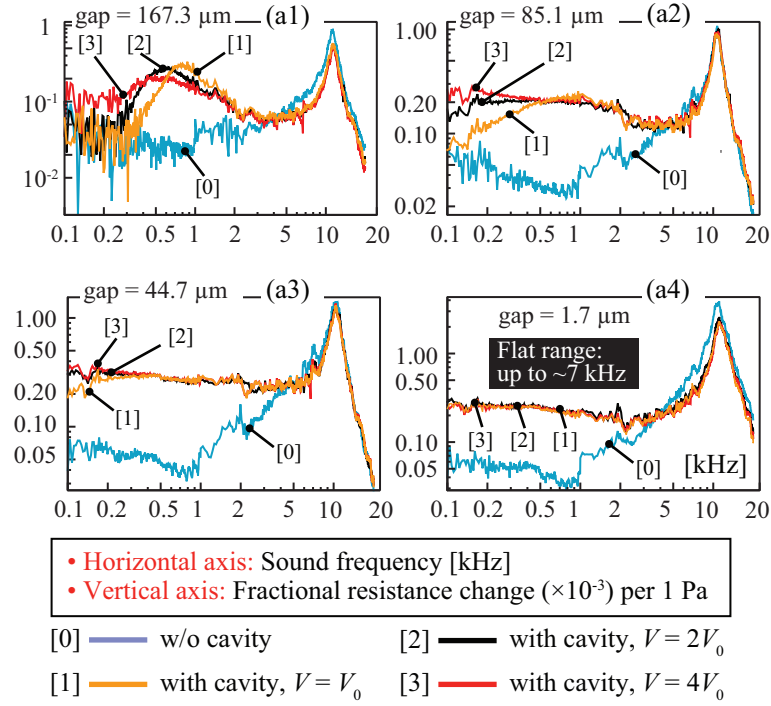


Fig. 4. 16 Frequency characteristics of the proposed sensor with various gap sizes and various cavity volume.  $V_0$  was 4 ml.

(a1)(a2)(a3)(a4)). It means that in order to miniaturize the microphone while keeping the flat frequency response unchanged, the air-gap should be miniaturized. The result showed in **Fig. 4. 16 (a4)**, with air-gap of  $1.7 \mu\text{m}$ , presents an agreement with this speculation. The frequency response of  $1.7 \mu\text{m}$  air-gap was flat up to 7 kHz, with sensitivity of approximately  $2.8 \times 10^{-4} \text{ Pa}^{-1}$ . We suggest that if the resonant frequency is designed to be higher, the flat range can be obtained broader. And the sensitivity of the sensor, as a microphone, can be also improved due to the design of the cantilever.

#### 4.3.5 Measurement at low frequency range

(In this section, I have been allowed to reused some sentences and expressions from my previous paper, which is the reference<sup>[3]</sup> with the Copyright 2013 AIP Applied Physics Letters)

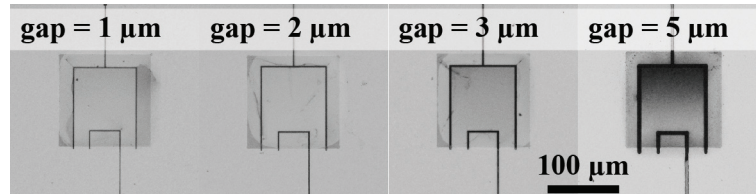


Fig. 4. 17 Images of cantilever with different gap sizes. (Copyright 2013 AIP Applied Physics Letters<sup>[3]</sup>)

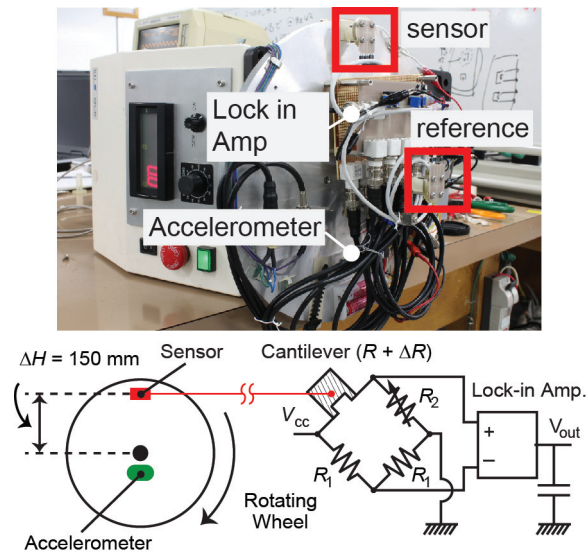


Fig. 4. 18 Image of the rotating experiment. (Copyright 2013 AIP Applied Physics Letters<sup>[3]</sup>)

In our experiments, we evaluated the response of the sensor to variations in the frequency, the air-gap size and the cavity volume. In all of the test samples, the dimensions of the piezo-resistive cantilever were fixed. The dimensions of the piezo-resistive cantilever are shown in **Fig. 4. 1**. With this design, the mass of the piezo-resistive cantilever was small enough that the influence of inertial forces on the sensors response could be neglected. In other words, the proposed sensor is not affected by acceleration. In detail, with the above dimensions, the mass of the cantilever was  $7.8 \times 10^{-9}$  g. For example, let us consider a case in which the cantilever experiences an acceleration of 1 G. The pressure that is applied to

the cantilever surface is calculated to be 6.7 mPa, which is negligible.

The fabricated cantilever was then attached to a circuit board by using an instant adhesive (Aron Alpha, Toagosei Company, Ltd.) and UV curable resin. The cavity was fabricated from ABS (acrylonitrile butadiene styrene) using a modeling machine, which enabled the cavity volumes to be precisely controlled. Then the circuit board was attached to the opening of the cavity with screws. A plastic O-ring was sandwiched between the circuit board and the cavity to prevent air leak.

We investigated the characteristics of the proposed barometric pressure sensor over a range from 0.05 Hz to 1 Hz. In many applications, the response in this range is of particular interest. For example, in indoor navigation applications, subjects move (e.g., climb stairs) with a relatively low speed and the rate of change of the barometric pressure is often approximately 1 Hz. As mentioned above, miniaturizing the air-gap should result in high measurement stability and sensitivity. In this experiment, I fabricated cantilevers with air-gap sizes of 1  $\mu\text{m}$ , 2  $\mu\text{m}$ , 3  $\mu\text{m}$  and 5  $\mu\text{m}$ . In fact, because the conditions of fabrication process were not always maintained to be the same, the actual sizes were 1.1  $\mu\text{m}$ , 2.3  $\mu\text{m}$ , 3.2  $\mu\text{m}$  and 5.9  $\mu\text{m}$ . The images of fabricated cantilevers are shown in **Fig. 4. 17**. The cavity volume was precisely controlled at 1 ml, 2 ml and 4 ml.

The experimental setup is shown in **Fig. 4. 18**. The experiments were performed in a closed room with no wind and no air flow. The environmental conditions were identical for each of the experiments. The room temperature was maintained at 25 C, and the humidity was 70%. The sensor was fixed on a rotating wheel with a radius of 150 cm. The absolute altitude of the sensor and thus the absolute pressure experienced by the sensor changed with the rotation rate of the wheel, and this rate was controllable. As shown in Section 2.5.4, the relationship between the change in barometric pressure and the change in absolute altitude is as follows:

$$\Delta p = 11.69 \Delta h$$

In the rotating experiment, the maximum altitude change of the sensor was 30 cm (0.3 m), which was the diameter of the rotating orbit of the sensor. Therefore, the maximum change in barometric pressure was 3.5 Pa. An accelerometer (HAAM-302B, Hokuriku Electric Industry Co., Ltd, Japan) was used to calculate the position of the sensor, which was obtained by measuring the gravitational acceleration.

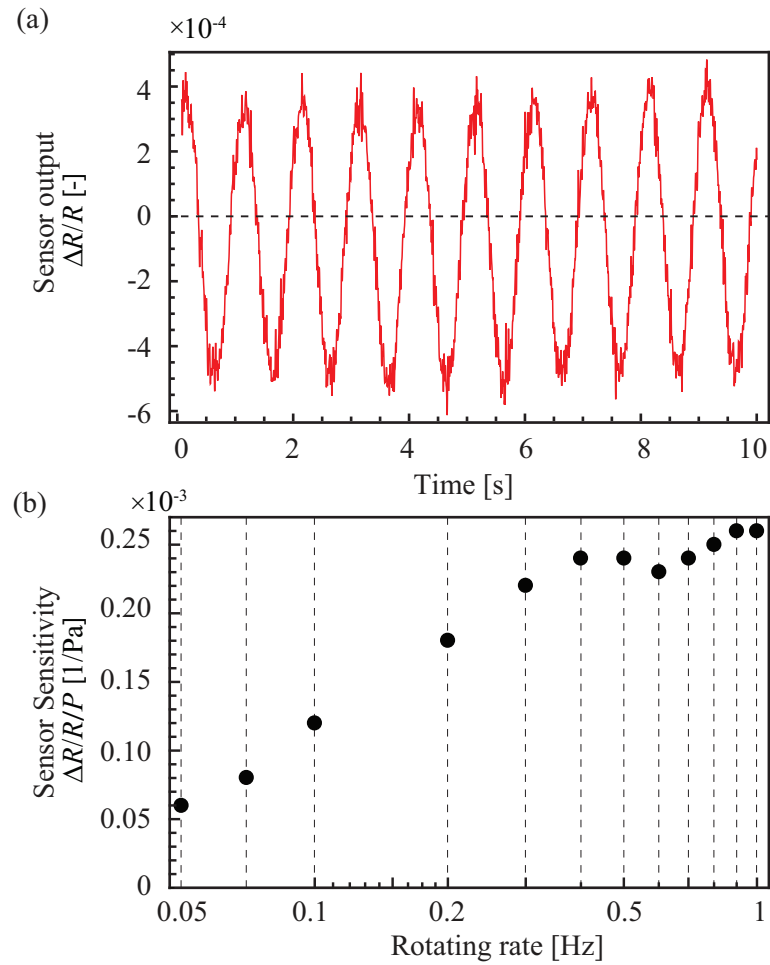


Fig. 4. 19 (a) Response of the sensor with gap size of  $1.1 \mu\text{m}$  and cavity volume of 2 ml  
 (b) Sensor sensitivity (fractional resistance change per 1 Pa) as a function of the rotating frequency.

From the positional relation of the accelerometer and the proposed sensor, which was known, the position of the sensor was calculated. We also used the accelerometer to determine the phase lag of the barometric sensors response. The circuit used to measure the sensors response was described in Section 2.5.2 . The sensor response was compensated by using a reference sensor placed in the center of the rotating wheel. The reference sensor consisted of a piezo-resistive cantilever and a cavity that had the same dimensions with the main sensor. During the rotation, the reference sensor was not influ-



enced by the change in barometric pressure. Additionally, by subtracting the reference sensor's response from the main sensor, influence of noises such as thermal noise, light, mechanical vibration of the rotating wheel and ambient air flow, should be reduced. The compensated response of the sensor for

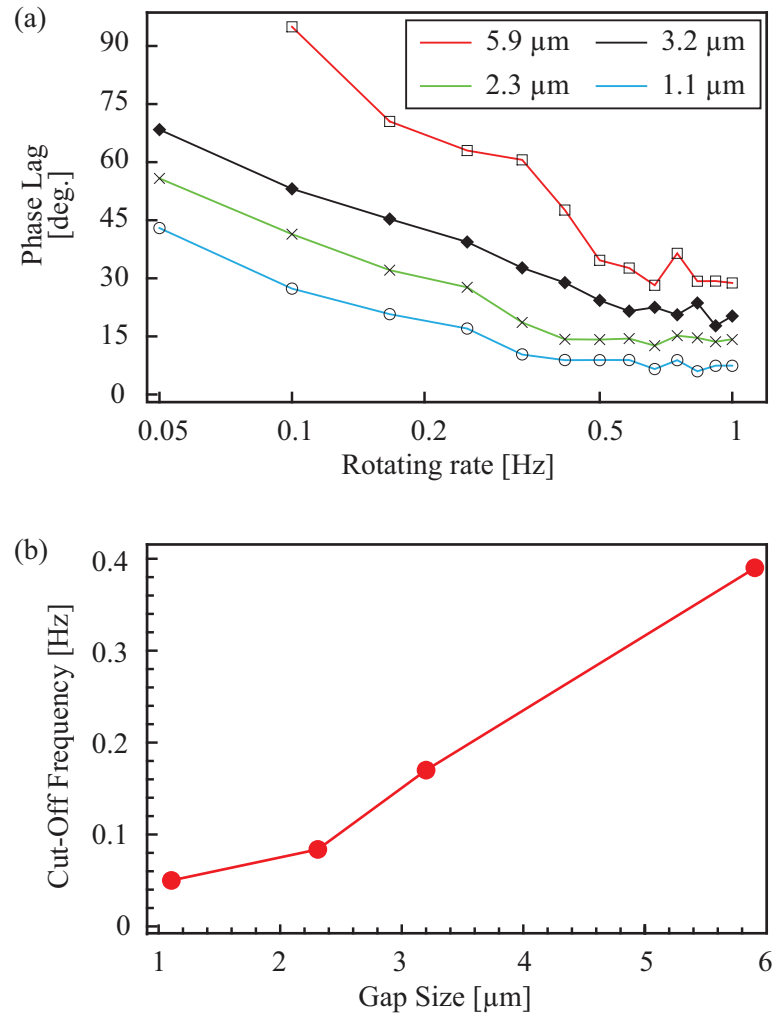


Fig. 4. 20 (a) Phase lags for various air-gap sizes with a cavity volume of 4 ml. (b) Cut-off frequencies for different gap sizes with a cavity volume of 4 ml.(Copyright 2013 AIP Applied Physics Letters<sup>[3]</sup>)

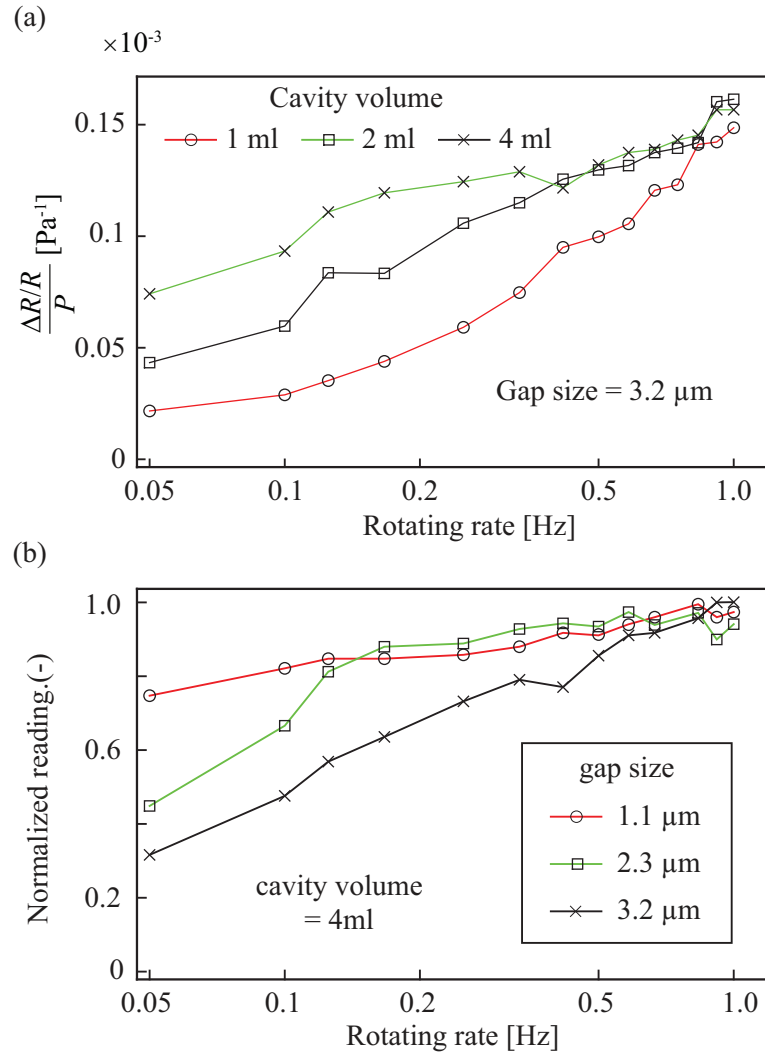
a rotation rate of 1 Hz is shown in **Fig. 4. 19 (a)**. The air-gap size was 1.1  $\mu\text{m}$  and the cavity volume

was 2 ml. Based on the data shown in **Fig. 4. 19 (a)**, we calculated the sensor sensitivity, which is presented as the fractional resistance change of the cantilever versus 1 Pa of change in barometric pressure. For example, the sensitivity of the sensor at rate change of 1 Hz and 0.05 Hz was  $0.26 \times 10^{-3} \text{ Pa}^{-1}$ . According to the result, which is shown in **Fig. 4. 19 (b)**, the sensitivity dropped when the rotation rate decreased. This result is reasonable because in the case of the lower rotation rate, air leakage occurred when the barometric pressure changed. Air leakage results in a smaller pressure difference between the upper and lower sides of the piezo-resistive cantilever.

Phase lag data for the different air-gap sizes are shown in **Fig. 4. 20 (a)**. Here, the phase lag was the phase lag of the sensor compared to that of the conventional accelerometer. The cavity volume was fixed at 4 ml. Note that the sensor response could not be measured when the gap size was  $5.9 \mu\text{m}$  for the rotation rate of 0.05 Hz. According to **Fig. 4. 20 (a)**, for a fixed rotation rate, a smaller air-gap size resulted in a smaller phase lag. Because the deformation of the cantilever due to pressure is a simple first-order lag system, we defined the cut-off frequency of the systems to be the frequency at which the phase lag is 45 degrees. The variation of the cut-off frequency for the various gap sizes is shown in **Fig. 4. 20 (b)**. This result indicates that by miniaturizing the gap size, we enabled the sensor to measure a smaller range of pressure change rates. Specifically, we could measure a pressure change of 0.05 Hz using an air-gap size of  $1.1 \mu\text{m}$ .

We investigated the frequency characteristics of the sensor for different cavity volumes with a fixed air-gap size of  $3.2 \mu\text{m}$ . The results are shown in **Fig. 4. 21 (a)**. The vertical axis of the graph presents the fractional resistance change for a pressure change of 1 Pa. Here, we observed that a larger cavity enabled the sensor to have a greater response. Because the air leaks through the air-gap and the cavity pressure changes to balance the change in the barometric pressure, a smaller cavity volume enables the sensor to take less time to reach equilibrium. Therefore, the maximum pressure difference between the cavity pressure and the barometric pressure is smaller for a smaller cavity volume. As a result, the maximum displacement of the piezo-resistive cantilever becomes smaller. This phenomenon explains the results shown in **Fig. 4. 21 (a)**.

We also investigated the frequency characteristics of the sensor for various air-gap sizes when the cavity volume was fixed at 4 ml (**Fig. 4. 21 (b)**). Although the cantilevers dimensions were intended to



**Fig. 4. 21** Frequency characteristics of the sensor for various cavity volumes and air-gap sizes. a) The air-gap size was  $3.2 \mu\text{m}$ , and the cavity volume was controlled to be 1 ml, 2 ml and 4 ml. b) Cavity volume was 4 ml and the air-gap sizes were  $1.1 \mu\text{m}$ ,  $2.3 \mu\text{m}$  and  $3.2 \mu\text{m}$ , respectively. (Copyright 2013 AIP Applied Physics Letters<sup>[3]</sup>)

remain constant, the fabrication process had an influence on the sensitivity of the piezo-resistive cantilever. Therefore, in this experiment, we normalized the sensor response in a manner such that the response at a certain frequency was divided by the response at 1 Hz. The key result in this case is the slope of the graph for the various air-gap sizes. The results show that the sensor response for a smaller

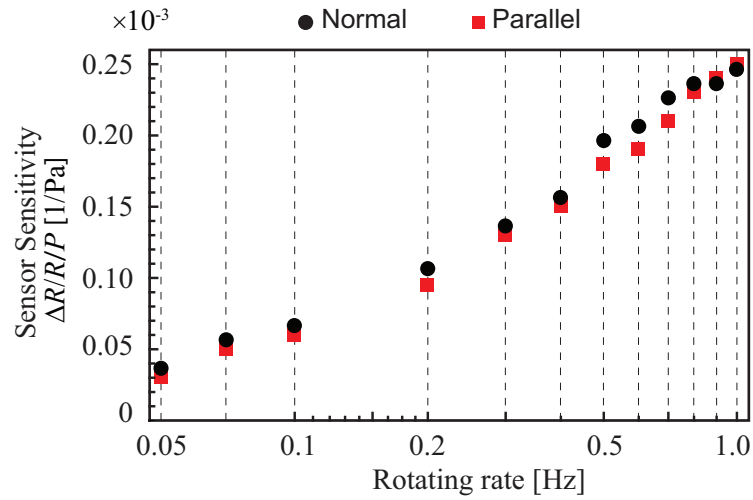


Fig. 4. 22 Response of the sensor in different orientation. Normal orientation indicates that the cantilever was placed normal to the flow direction. Parallel orientation indicates that the cantilever was parallel to the surface of the rotating wheel.

gap was flatter. In other words, a small gap size was able to maintain high sensitivity even in a low frequency range, which allows us to conclude that by fabricating a small air-gap size and a large cavity volume, we can achieve better sensitivity.

In the aforementioned experiments with the rotating wheel, we hypothesized that the sensor is influenced to some extent by the air drag when the cantilever is normal to the flow direction. The effect of orientation was investigated and the result is shown in **Fig. 4. 22**. The result demonstrates that there was almost no difference in sensor response when the sensor was placed in different direction. Indeed, in our previous work, we reported that when the direction of air flow is parallel to the cantilever surface, the influence of air drag is almost zero<sup>[68]</sup>. Therefore, we can neglect the influence of air drag in this experiment.

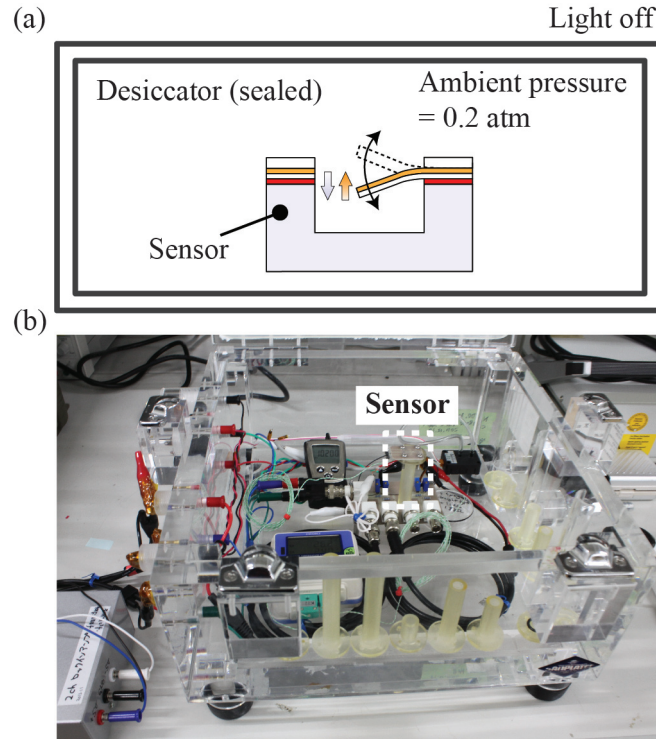


Fig. 4. 23 (a) Concept of the experimental set-up for measuring electrical noise of the sensor. (b) Image of the experimental setup.

#### 4.4 Noise evaluation

There are two inherent noise sources in the measurement using a piezo-resistive cantilever. They are named as Johnson noise and  $1/f$  noise. <sup>[63]</sup>

Johnson noise is caused by the thermal energy in the piezo-resistor. The voltage fluctuation due to a piezo-resistor is expressed by the following equation.

$$V_{\text{thermal}} = \sqrt{4k_B TR \Delta f} \quad (4.2)$$

where  $k_B$  is the Boltzmann constant,  $T$  is the absolute temperature,  $R$  is the resistance of the cantilever.  $\Delta f$  is the corresponding bandwidth. Particularly, the proposed barometric pressure sensor is expected to be used in a frequency range below 100 Hz. Hence, the bandwidth  $\Delta f$  is determined as 100 Hz.

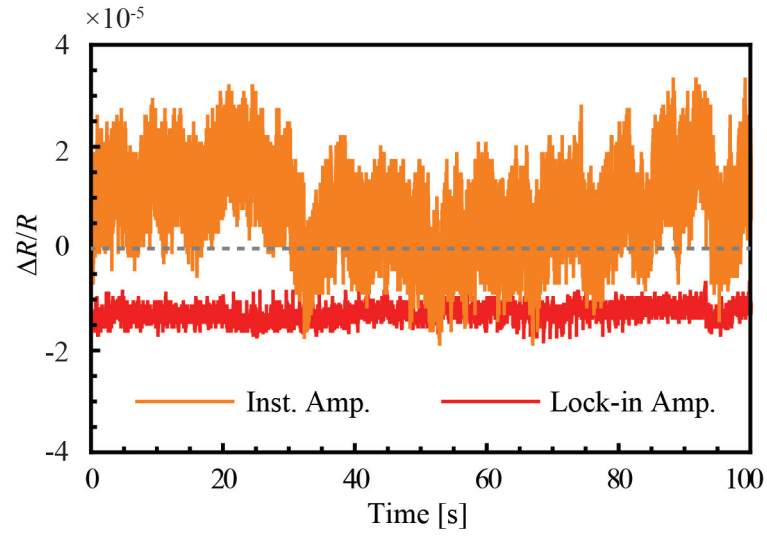


Fig. 4. 24 Sensor's noise level is expressed in fractional resistance change in two ways with instrumentation amplifier and lock-in amplifier.

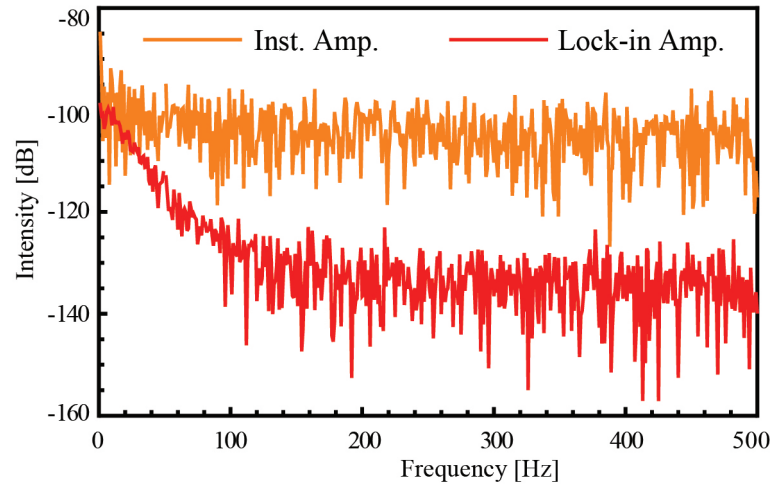


Fig. 4. 25 Fast fourier transform of the sensor output signal. The function of low pass filter of lock-in amplifier was clearly observed.

1/f noise is mainly caused by the conductance fluctuation at low frequencies. Generally, the voltage

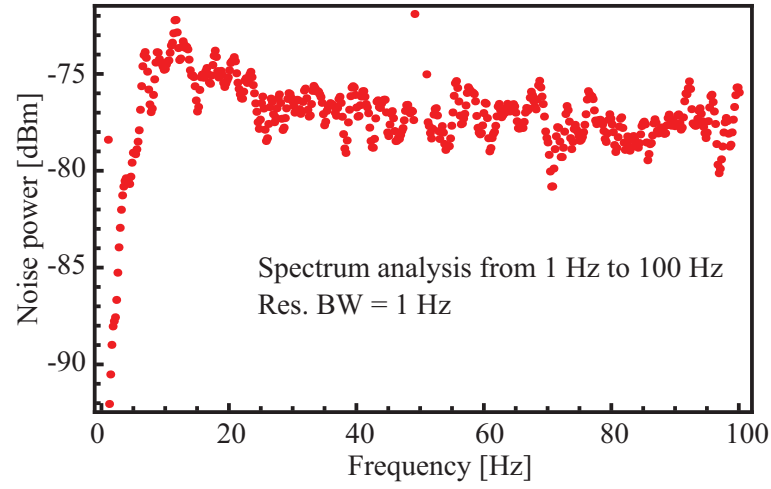


Fig. 4. 26 Measurement of noise spectrum using a network analyzer. The range was from 1 Hz to 100 Hz with the resolution band width of 1 Hz. Cantilever resistance was  $500 \Omega$ .

fluctuation across the piezo-resistor of a cantilever is given by:

$$V_{1/f} = \sqrt{\frac{\alpha V^2}{N} \ln \frac{F_{\max}}{F_{\min}}} \quad (4.3)$$

where  $\alpha$  is a dimensionless constant,  $V$  is the applied voltage difference between the two electrodes of a piezo-resistive cantilever,  $N$  is the total number of effective carriers,  $F_{\max}$  and  $F_{\min}$  are the upper and lower limits of the corresponding frequency band.

Indeed, in actual measurement, there are other minor noise sources such as light, mechanical vibration (e.g. in rotating experiment) and external air flow. In order to measure the true ability of the sensor in measuring pressure, an experimental set-up in low vacuum using a desiccator (**Fig. 4. 23**) was provided to eliminate the influence of those minor noise sources. In other words, the experimental set-up of **Fig. 4. 23** was for measuring the response of the proposed sensor under influence of only Johnson noise and  $1/f$  noise.

In detail, the sensor was placed inside a desiccator. The gap size was  $1 \mu\text{m}$  and the cavity volume was 1 ml. Air inside the desiccator was pumped down to 0.2 atm. Experiment was taken with light off. The sensor's output voltage was amplified by an amplifier. Indeed, in this experiment, two type of

amplifier was used. The first type is an instrumentation amplifier (AD623) with no filter. The second type is a lock-in amplifier with reference frequency of 1 kHz and with cut-off frequency of 13.6 Hz.

The electrical signal from the amplifier was processed in two ways. First, the electrical signal and the corresponding fast Fourier transform (FFT) was displayed and recorded with an oscilloscope. The noise level of the sensor expressed in the fractional resistance change ( $\Delta R/R$ ) is shown in **Fig. 4. 24**. Obviously, using a lock-in amplifier with low-pass filter produces smaller noise than using an instrumentation amplifier. The FFT analysis is shown in **Fig. 4. 25**. We can observe that in the lock-in amplifier, which had a cut-off frequency of 13.6 Hz, the signals at high frequency were eliminated. Especially, signals at frequency larger than 100 Hz were almost zero.

The root mean square (RMS) of the noise level with lock-in amplifier and instrumentation amplifier were  $2.7 \times 10^{-6}$  and  $14.9 \times 10^{-6}$ , respectively. The sensor's sensitivity was calibrated to be  $1.2 \times 10^{-4} \text{ Pa}^{-1}$  in similar method presented in **Subsection 4.1.2**. Hence, the resolution of pressure measurement can be calculated as 0.02 Pa for using lock-in amplifier, and 0.12 Pa for using instrumentation amplifier.

Noise spectrum analysis is another important method to evaluate exactly the noise level of a sensor in certain frequency range. The sensor in this study is expected to be used in applications such as car navigation, human activity log. The frequency range of these applications is normally smaller than 100 Hz. Therefore, in the next experiment, noise spectrum of the sensor was evaluated from 1 Hz to 100 Hz, with the highest resolution bandwidth of 1 Hz. Indeed, the lock-in amplifier was not used in this experiment because it cut all of frequency components larger than 13.6 Hz. The sensor's noise spectrum using instrumentation amplifier is shown in **Fig. 4. 26**. Based on this noise spectrum, the sensor's resolution in measuring pressure was calculated. The calculation is shown as follows.

Deviding the integral of the graph in **Fig. 4. 26** by the frequency span, which was 99 Hz, we have the representative value of the corresponding frequency span. The representative noise power ( $P_{\text{an}}$ ) was calculated to be 77.07 dBm. In this experiment, resolution bandwidth ( $RBW$ ) was 1 Hz. Hence, the noise density was derived by as follows.



$$P_{\text{and}} = P_{\text{an}} - 10\log(RBW) + 3 = -74.07 \text{ dBm/Hz} \quad (4.4)$$

Converting this value in unit of power (W), we have  $P_{\text{and}} = 39 \text{ pW/Hz}$ . Now consider the filtering bandwidth in the sensor's measurement to be 10 Hz. Note that this bandwidth should be designed in proper value for each application. For example, when we want to use this sensor in personal activity logging systems, 10 Hz may be enough. However, for faster movement such as vehicles, the bandwidth is supposed to be about 100 Hz. The noise power for a bandwidth (BW) of 10 Hz is calculated by the following.

$$P_{\text{sn}} = P_{\text{and}} \times BW = 0.39 \text{ nW} \quad (4.5)$$

The piezo-resistance of the cantilever was  $R_{\text{cantilever}} = 500 \text{ } \Omega$  and it was implemented in a Wheastone-bridge circuit. Therefore, we can consider the input impedance in this case was

$$R = R_{\text{cantilever}} / 2 = 250 \text{ } \Omega \quad (4.6)$$

Hence, the noise level expressed in unit of voltage is obtained as follows.

$$V_{\text{sn}} = \sqrt{R \times P_{\text{sn}}} = 0.99 \times 10^{-3} \text{ V} \quad (4.7)$$

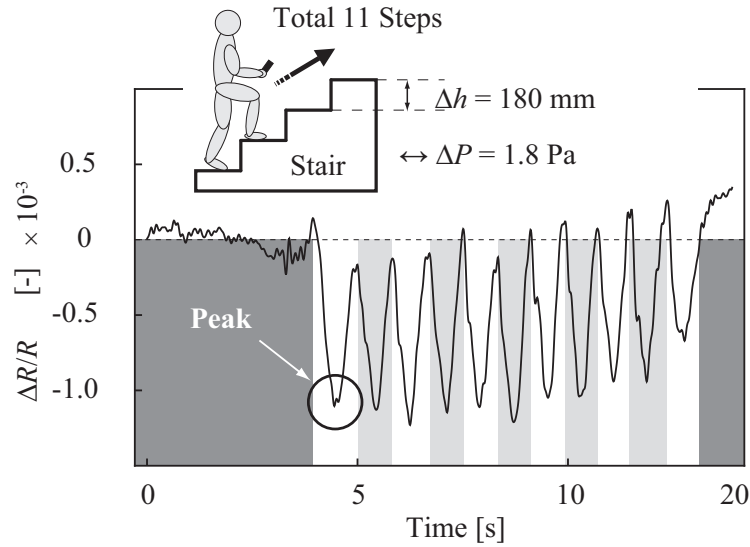
Since the gain of the amplifier circuit was 1000, the noise level of the sensor was  $0.99 \times 10^{-6} \text{ V}$ . Thus, the fractional resistance change of the cantilever is calculated as the following.

$$\frac{\Delta R}{R} = 4 \times V_{\text{sn}} = 1.25 \times 10^{-6} \quad (4.8)$$

Since the fractional resistance change of the sensor for a pressure of 1 Pa was  $1.2 \times 10^{-4} \text{ Pa}^{-1}$ , from **Eq. 4.8**, the resolution of pressure measurement can be obtained as 10 mPa. Note that this result is applied for the frequency range from 1 Hz to 100 Hz. The noise level at frequency smaller than 1 Hz was not evaluated due to the ability of the analyzing equipment. The resolution of pressure measurement for various value of bandwidth is shown in **Table 4. 1**.

**Table 4. 1 Sensor's resolution in pressure measurement for various bandwidth**

	$BW = 1 \text{ Hz}$	$BW = 10 \text{ Hz}$	$BW = 100 \text{ Hz}$
Resolution	3 mPa	10 mPa	33 mPa



**Fig. 4. 27** Demonstration: stair climbing with barometric pressure sensor. There were 11 steps in total. (Copyright 2011 IEEE<sup>[1]</sup>)

## 4.5 Demonstration

(In this section, I have been allowed to reuse some sentences and expressions from my previous paper, which is the reference<sup>[1]</sup> with the Copyright 2011 IEEE)

A demonstration of stair climbing is shown in **Fig. 4. 27**. The cavity's volume was  $8 \times 10^3 \text{ mm}^3$ . One step had the height of 180 mm, which was equivalent to 1.8 Pa of barometric pressure change. The result shows fully 11 local curves with 11 peaks, and thus it demonstrates that our sensor can measure the steps with relatively high sensitivity. As shown in previous section, the proposed sensor is supposed to be able to measure pressure at approximately 10 mPa order, which is superior to conventional barometric pressures. Therefore, the fluctuation existed in the graph (e.g. from 0 s to 4 s), can not be considered as noise. It might be the slight change in the ambient pressure, or the influence of an external air flow. We also performed a demonstration for the proposed barometric pressure sensor<sup>[67]</sup> (follow the link in the published paper to see the demonstration video on the internet). The sensor signal was processed and visualized in real-time on a computer screen. For the graph shown on the computer screen, the horizontal and vertical axes were the present time and the output voltage, respectively. The results indicate that when the sensor moved in the vertical direction by more than 20 cm, with a corresponding

absolute barometric pressure change of 2.3 Pa, the output voltage also changed. however, when the sensor moved in the horizontal direction, in which the absolute barometric pressure did not change, the output voltage did not change. It is clear that the sensor functions as a barometric pressure sensor, and the influence of inertial forces was not observed.

---

## Chapter 5 Conclusion

### 5.1 Conclusion

---

Conventional barometric pressure measuring methods have its limit in the sensitivity due to the structure based on diaphragm. In order to break through that limit, this study has proposed a method for measuring pressure with high sensitivity by taking advantage of the scale effect of the gap size in a micro cantilever. The proposed sensing device has a piezo-resistive cantilever placed on the opening of a cavity. The interaction between the external pressure and the cavity pressure causes the cantilever to bend. This study has found an phenomenon here is that the cantilever's displacement and the sensing sensitivity are determined by the size of the gap between the cantilever and the surrounding rigid walls. in this study, this scale effect of the gap size is investigated by theoretical calculations from the view of fluidic mechanics, material mechanics and fluid structure interaction simulation using Finite Element Method.

In the theoretical calculations based on fluidic mechanics and material mechanics, I have proposed an approximate calculation on the air leak through the gap and on the relationship between pressure change and the resistance fractional change of the cantilever. Additionally, the simulations have proved several significant phenomenons. The simulations proves that for a cantilever with gap size in micrometer order, simulations using fluidic mode or structure deformation mode separately are incorrect because the fluid structure interaction has an important role in microscale. Additionally, the simulations in fluid structure interaction mode have proved that the pressure relaxation time, which is the time needed for the sensor's cavity to change its internal pressure to a certain pressure, has great relationship with the gap size of the cantilever. Moreover, the maximum displacement of the cantilever,

which means the sensing sensitivity, is bigger with smaller gap size. From different point of view, the bigger displacement of the cantilever is indeed the result of smaller pressure loss due to smaller gap size. It is obvious that the pressure loss happens because of the air leak through the gap, which is clearly dependent on the gap size. The simulation results indicate that after being bent, the cantilever turns back to its initial balanced position in which the displacement decreases in an exponential function of time. Moreover, the decrement factor is calculated to be proportional to square of gap area and inversely proportional to the cavity's volume. In addition, the decrement factor does not change for various applied pressure.

However, in experiments the relationship between decrement factor and gap size in this experiment is a proportional one. This result is different with simulation result. Indeed, due to the ability of simulation processing computer, the gap size in simulation was larger than  $5\text{ }\mu\text{m}$  and the cantilever thickness was  $1\text{ }\mu\text{m}$ . For a few micron gap size, the Reynolds number is around 1, considering the differential pressure of a few Pa. Therefore, the different in gap size could bring into a significant difference in air viscosity. This could be the reason for the difference of experiment result and simulation result. Nevertheless, in both of experiment and simulation, the differential pressure decay is confirmed to be an exponential function of time. In addition, the decrement factor is larger for bigger gap size. In experiment, the tendency in which larger cavity makes longer pressure relaxation process was also confirmed. According to this fact, the sensor should be designed with small gap size and large cavity in order to improve the sensing performance. In applications, the idea of making larger cavity is not favorable. Hence, the key for this device is to narrowing the gap size as much as possible.

In experiment section, the natural properties of a piezo-resistive cantilever and the characteristics of the proposed barometric pressure sensor are shown. The dimensions of the cantilever was designed as  $100\text{ }\mu\text{m} \times 125\text{ }\mu\text{m} \times 0.3\text{ }\mu\text{m}$  with hinges of  $25\text{ }\mu\text{m} \times 25\text{ }\mu\text{m}$ . Experiment result shows that the sensitivity of the cantilever itself is approximately  $1.0 \times 10^{-4}\text{ Pa}^{-1}$ . The first resonant frequency of the cantilever was 11 kHz. In the experiments on dynamic characteristics of the cantilever and of the proposed sensor, the results demonstrate that the structure consists of a cantilever and a cavity should have sensitivity to pressure approximately 10 times higher than the cantilever its self, considering the cavity volume of a few ml. Moreover, the results also confirm that the proposed sensor can act as a microphone. Additionally, it is obviously from the results that smaller gap size and bigger cavity volume would provide flat-

ter frequency characteristic and higher sensitivity.

In the results of experiments on characteristics of the proposed sensing methods, this study investigated the characteristics of the proposed barometric pressure sensor over a range from 0.05 Hz to 1 Hz, with air-gap sizes of 1.1  $\mu\text{m}$ , 2.3  $\mu\text{m}$ , 3.2  $\mu\text{m}$  and 5.9  $\mu\text{m}$  and with cavity volume was precisely controlled at 1 ml, 2 ml and 4 ml. An inherent property of this sensor is that it has higher performance at higher rate change of pressure. However, the measurement resolution is bigger at lower rate change. The experiment results demonstrated that miniaturizing the air-gap of the cantilever enables the sensor to measure barometric pressure changes at a low pressure change rate, which was sub 0.05 Hz, for a gap size of 1.1  $\mu\text{m}$  and cavity volume of 1 ml. The sensitivity of a sensor with gap size of 1.1  $\mu\text{m}$  and volume cavity of 2 ml at the pressure change rate of 1 Hz was calculated to be  $0.26 \times 10^{-3} \text{ Pa}^{-1}$ . In fact, the sensitivity is proved to be decrease when the pressure change rate is slower. For example, when the rate is 0.05 Hz, the sensitivity is  $0.06 \times 10^{-3} \text{ Pa}^{-1}$ . The experiment results also indicate that the sensitivity here should be better with smaller gap size and bigger cavity volume.

The sensor's noise level was also evaluated. There are many noise sources. The two main sources are Johnson noise (or thermal noise) and 1/f noise. The other minor noises are caused by ambient light, mechanical vibration and external air flow. Experiment in low vacuum using a desiccator was provided to eliminate the influence of those minor noise sources. Calculating the root mean square of the recorded real-time noise, the sensor resolution in measuring pressure was 20 mPa using a lock-in amplifier, which had an cut-off frequency of 13.6 Hz. In the spectrum analysis of sensor noise, with a bandwidth of 10 Hz, amplifier gain of 1000, input resistance of 250  $\Omega$  and sensor's sensitivity of  $1.2 \times 10^{-4} \text{ Pa}^{-1}$ , the resolution of pressure measurement is calculated to be 10 mPa. Note that this spectrum analysis is applied for the frequency range from 1 Hz to 100 Hz.

The resolution is dependent on the determined bandwidth. It is obvious that a smaller bandwidth should provide a better resolution. Here, the sensor is supposed to be used in applications for a frequency range of sub 100 Hz. In that range, we conclude that the sensor's resolution in measuring pressure is approximately 10 mPa (0.01 Pa) order, providing the experiment conditions in low vacuum (0.2 atm). It means that the proposed sensor has a potential of measuring the change in absolute altitude with resolution of approximately 1 mm. This result demonstrates that the proposed sensor is superior in

comparison with conventional barometric pressure sensors. It can be expected to be used in various applications such as personal activity recording systems or three-dimensional car navigation, in which the altitude information is important.

## 5.2 Future works

---

As mentioned in previous section, because the sensitivity of sensors at low frequencies is an important factor for their implementation in certain applications, the air-gap should be made smaller, perhaps even on a nanometer scale. In our photolithography process, the resolution was a few micrometers. However, using techniques such as EB-lithography or FIB (focused ion beam) cutting, we expect that an air-gap on the order of tens of nanometers could be fabricated. Additionally, a thinner piezo-resistive cantilever results in greater sensitivity. In diaphragm-based structures, a thin diaphragm is fragile at high pressures. However, in our proposed structure, the cantilever is considered to be robust, even at high pressures, because the air is allowed to exit through the air-gap during the deformation of the cantilever. Indeed, the idea of using cantilever for measuring the change in barometric pressure with high sensitivity has given a hint for me to propose another approach for pressure measurement. That approach is shown in detail in **Appendix A**. In this approach, by using liquid to block the air leak through the gap, the sensor can measure the absolute pressure. Although the sensitivity is temporarily 0.9Pa, it can be improved by choosing appropriate liquid and gap size. Nevertheless, the proposed cantilever-based pressure sensor has the advantages of low-cost fabrication. This sensor is expected to be used in applications such as automotive navigation, personal mobile devices, acoustic systems in aqueous environment or even in medical industry.

## Reference

### Related Copyrights

---

In this paper, I have been allowed to requote some sentences and expression from my previous papers, which are as follows. The copyright is written at the end of each reference.

- [1] Nguyen Minh-Dung, Hidetoshi Takahashi, Kyoshi Matsumoto, Isao Shimoyama, "Barometric Pressure Change Measurement," *Proceedings of IEEE 16th International Conference on Solid-State Sensors, Actuators and Microsystems (Transducers 2011)*, Beijing, China, pp. 894-897, 2011. (**Copyright 2011 IEEE**)
- [2] Nguyen Minh-Dung, Hoang Phuong Phan, Kyoshi Matsumoto, Isao Shimoyama, "A Sensitive Liquid-Cantilever Diaphragm for Pressure Sensor," *Proceedings of IEEE 26th International Conference on Micro Electro Mechanical Systems (MEMS2013)*, Taiwan, pp. 617-620, 2013. (**Copyright 2013 IEEE**)
- [3] N. Minh-Dung, H. Takahashi, T. Uchiyama, K. Matsumoto, I. Shimoyama, "A barometric pressure sensor based on the air-gap scale effect in a cantilever," *Applied Physics Letters*, vol. 103, no. 14, article no. 143505, 2013. (**Copyright 2013 AIP Applied Physics Letters**)

### Barometric pressure measurement

---

- [4] A. McConnell, "Barometers," *Shire Library 2nd Revised Version*, 2008.
- [5] W. Tang, G. HoIll and Y-H. Tsai, "Barometric altimeter short-term accuracy analysis," *IEEE Aerospace and Electronic Systems Magazine*, vol. 20, no. 12, pp. 24-26, 2005.
- [6] E. Rodriguez and B. Polland, "Centimetric sea surface height accuracy using the Wide-Swath Ocean altimeter," *IEEE International Geoscience and Remote Sensing Symposium (IGARSS)*, vol. 5, pp. 3011-3013, 2003.
- [7] W.P. Eaton and J.H. Smith, "Micromachined pressure sensors: review and recent developments," *Smart Materials and Structures*, vol. 6, no. 5, pp. 530-41, 1997.
- [8] C.S. Smith, "Piezoresistance effect in germanium and silicon," *Physics Review*, vol. 94, pp. 42-49, 1954.
- [9] A. C. M. Gieles and G. H. J. Somers, "Miniature pressure transducers with a silicon diaphragm," *Philips Tech. Rev.*, vol. 33, pp. 14-20, 1973.
- [10] Samaun, K. D. Wise and J. B. Angell, "An IC piezoresistive pressure sensor for biomedical instrumentation," *IEEE Trans. Biomed. Eng.*, BME-20, pp. 101-109, 1973.
- [11] J. M. Borky, "Silicon diaphragm pressure sensors with integrated electronics," 1977.
- [12] K. D. Wise and S. K. Clark, "Diaphragm formation and pressure sensitivity in batch-fabricated silicon pressure sensors," *IEDM Dig. Tech. Papers*, pp. 96-99, 1978.
- [13] K. E. Petersen, "Silicon as a mechanical material," *Proc. IEEE*, vol. 70, pp. 420-457, 1982.



- [14] B. Puers, E. Peeters, A. Van Den Bossche, and W. Sansen, "A capacitive pressure sensor with low impedance output and active suppression of parasitic effects," *Sensors and Actuators*, vol. A21&A23, pp. 108 -114, 1990.
- [15] S. B. Crary, W. G. Baer, J. C. Coeles, and K. D. Wise, "Digital compensation of high-performance silicon pressure transducers," *Sensors and Actuators*, vol. A21&A23, pp. 70 -72, 1990.
- [16] J. B. Starr, "Squeeze film damping in solid state accelerometers," *Digest IEEE Solid State Sensor and Actuator Workshop*, pp. 44 -47, 1990.
- [17] M. Esashi, Y. Matsumoto, and S. Shoji, "Absolute pressure sensors by air-tight electrical feedthrough structure," *Sensors and Actuators*, vol. A21&A23, pp. 1048 -1052, 1990.
- [18] H. Henmi, S. Shoji, Y. Shoji, K. Yosimi, and M. Esashi, "Vacuum packaging for microsensors by glass and silicon anodic bonding," *Digest Transducers 93*, pp. 584 -587 1993.
- [19] Y. Zhang and K. D. Wise, "A high-accuracy multi-element silicon barometric pressure sensor," *Digest Int. Conf. on Solid-State Sensors and Actuators*, pp. 608 -611, 1995.
- [20] R. Ziermann, J. Berg, W. Reichart and E. Obermeier, "A high temperature pressure sensor with  $\beta$ -SiC piezoresistors on SOI substrates," *Int. Conf. on Solid State Sensors and Actuators (Transducers97)*, pp. 1411-1414, 1997.
- [21] A. V. Chavan, "An integrated high resolution capacitive barometric pressure sensing system", *The University of Michigan*, 1999.
- [22] B.P. Gogoi and C.H. Mastrano, "A low-cost batch sealed capacitive pressure sensor," *IEEE International Conference on Microelectromechanical Systems*, pp. 82-87, 1999.
- [23] A. V. Chavan and K. D. Wise, "A monolithic fully-integrated vacuum-sealed CMOS pressure sensor," *IEEE International Conference on Microelectromechanical Systems*, pp. 341 -346, 2000.
- [24] A.V. Chavan and K.D. Wise, "Batch-processed vacuum-sealed capacitive pressure sensors," *Journal of Microelectromechanical Systems*, vol.10, no.4, pp. 580-588, 2001.
- [25] A.V. Chavan and K.D. Wise, "A monolithic fully-integrated vacuum-sealed CMOS pressure sensor," *IEEE Transactions on Electron Devices*, vol.49, no.1, pp. 164-169, 2002.
- [26] S.P. Chang, J.B. Lee and M.G. Allen, "Robust capacitive pressure sensor array," *Sensor and Actuator A*, 101, pp. 231-238, 2002.
- [27] M. Fonseca, J. English, A.M Von and M. Allen, "Wireless micromachined ceramic pressure sensor for high-temperature applications," *J. Microelectromech. Syst.*, 11, pp. 337-43, 2002.
- [28] J. Bryzek, A. Flannery and D. Skurnik, "Integrating microelectromechanical systems with integrated circuits," *IEEE Instrumentation & Measurement Magazine*, vol. 7, iss. 2, pp. 51 - 59, 2004.
- [29] U. Schnakenberg, C. Kruger, J.-G. Pfeffer, W. Mokwa, G.v. Bogel, R. Gunther and T. Schmitz-Rode, "Intravascular pressure monitoring system," *Sens. Actuators A*, 110, pp. 61-67, 2004.
- [30] Aziz Ettouhami, Nouredine Zahid and Mourad Elbelkaacemi, "A novel Capacitive pressure sensor with high sensitivity and quasi-linear response," *Journal of C.R. Mecanique*, 332, pp. 141-146, 2004.
- [31] A.D. DeHenis and K.D. Wise, "A wireless microsystem for the remote sensing of pressure, temperature, and relative humidity," *Journal of Microelectromechanical Systems*, vol. 14, iss. 1, pp.12, 2005.

- [32] J.N.Palasagaram and R. Ramadoss, "MEMS capacitive pressure sensor array fabricated using printed circuit processing techniques," *31st Annual Conference of IEEE on Industrial Electronics Society (IECON)*, pp. 6-9, 2005.
- [33] M.X. Zhou, Q.A. Huang, M. Qin and Z. Li, "A novel capacitive pressure sensor based on sandwich structures," *Journal of Microelectromechanical Systems*, pp. 1272 - 1282, vol. 14, iss. 6, 2005.
- [34] M.X. Zhou, Q.A. Huang and M. Qin, "Modeling, design and fabrication of a triple-layered capacitive pressure sensor," *Sensors and Actuators A Physical*, vol. 117, iss. 1, pp. 71, 2005.
- [35] D. Dimitropoulos, C. Kachris, D. P. Karampatzakis and G. I. Stamoulis, "A new SOI monolithic capacitive sensor for absolute and differential pressure measurements," *Sensors and Actuators A Physical*, vol. 123-124, pp. 36, 2005.
- [36] C. B. Sippola and C. H. Ahn, "A ceramic capacitive pressure microsensor with screen-printed diaphragm," *4th IEEE Conf. on Sensors*, pp. 1271-4, 2005.
- [37] K. R. Lee, K. Kim, Y. K. Kim, H. D. Park, S. W. Choi, W. B. Choi and B. K. Ju, "Capacitive Absolute Pressure Sensor with Vacuum Cavity Formed by Bonding Silicon to SOI wafer for Upper Air Observations," *19th IEEE International Conference on Micro Electro Mechanical Systems (MEMS2006)*, pp. 618 - 621, 2006.
- [38] K.R. Lee, K. Kim, Y.K. Kim, H.D. Park, Y.K. Kim, S.W. Choi and W.B. Choi "Fabrication of capacitive absolute pressure sensor using Si-Au eutectic bonding in SOI wafer," *Journal of Physics Conference Series*, vol. 34, pp.393, 2006.
- [39] C. Pramanik, H. Saha and U. Gangopadhyay, "Design optimization of a high performance silicon MEMS piezoresistive pressure sensor for biomedical applications," *Journal of Micromechanics and Microengineering*, vol.16, issue 10, pp. 2060, 2006.
- [40] N. Liu, Q.A. Huang and M. Qin, "A novel monolithic CMOS capacitive pressure sensor," *8th International Conference on Solid-State and Integrated Circuit Technology (ICSICT '06)*, pp. 611 - 613, 2006.
- [41] K. Subramanian, J.B. Fortin and K. Kishore, "Scalable vertical diaphragm pressure sensors: device and process Design, Design for packaging," *IEEE Sensors Journal*, vol. 6, issue 3, pp. 618, 2006.
- [42] W. Soehren and W. Hawkinson, "Prototype personal navigation system," *Aerospace and Electronic Systems Magazine*, vol.23, no.4, pp. 10-18, 2008.
- [43] T. Pedersen, G. Fragiaco, O. Hansen and E.V. Thomsen, "Highly sensitive micromachined capacitive pressure sensor with reduced hysteresis and low parasitic capacitance," *Sensors and Actuators A Physical*, vol. 154, iss. 1, pp. 35, 2009.
- [44] M. Nie, Q-A. Huang, H-Y. Yu, M. Qin, I-H. Li, "A novel capacitive barometric pressure sensor based on the standard CMOS process," *10th IEEE International Conference on Solid-State and Integrated Circuit Technology (ICSICT)*, pp. 1480-1482, 2010.
- [45] E. G. Bakhoun and M. H. M. Cheng, "Capacitive Pressure Sensor With Very Large Dynamic Range", *IEEE Transactions on Components and Packaging Technologies*, pp. 79 - 83, vol. 33, iss. 1, 2010.
- [46] E. G. Bakhoun and M. H. M. Cheng, "Novel Capacitive Pressure Sensor", *Journal of Microelectromechanical Systems*, vol. 19, iss. 3, pp. 443, 2010.

- [47] C. B. Doody, C. Xiaoyang, C. A. Rich, D. F. Lemmerhirt and R.D. White, "Modeling and Characterization of CMOS-Fabricated Capacitive Micromachined Ultrasound Transducers," *Journal of MEMS*, vol.20, no.1, pp. 104-118, 2011.
- [48] E. G. Bakhoun and M. H. M. Cheng, "High-Sensitivity Inductive Pressure Sensor," *IEEE Transactions on Instrumentation and Measurement*, vol.60, no.8, pp. 2960-2966, 2011.
- [49] M. Nie, Q.A. Huang, H.Y. Yu, M. Qin and W.H. Li, "Complementary metal-oxide semiconductor compatible capacitive barometric pressure sensor," *Journal of Micro/Nanolithography MEMS and MOEMS*, vol. 10, iss. 1, pp.013018, 2011.
- [50] A. D. Sundararajan and S. M. R. Hasan, "A CMOS integrated MEMS capacitive pressure sensor design in a 3D SiGeMEMS process," *19th International Conference on Mechatronics and Machine Vision in Practice (M2VIP)*, pp. 150-155, 2012.
- [51] M. S. Tabarestani, B.A. Ganji and R. S. Nadooshan, "Design and simulation of new micro-electro-mechanical pressure sensor for measuring intraocular pressure," *16th IEEE Mediterranean Electrotechnical Conference (MELECON)*, pp. 208-211, 2012.
- [52] P. Gonzalez, M. Rakowski, D. S. Segundo, S. Severi, K. Meyer and A. Witvrouw, "CMOS-Integrated Poly-SiGe Piezoresistive Pressure Sensor," *IEEE Electron Device Letters*, vol.33, no.8, pp. 1204-1206, 2012.
- [53] P. Eswaran and S. Malarvizhi, "Simulation analysis of MEMS based Capacitive Differential Pressure sensor for aircraft application," *Journal on Advanced Material Research*, vol. 403-408, pp. 4152-4156, 2012.
- [54] P. Eswaran and S. Malarvizhi, "Sensitivity Analysis on MEMS Capacitive Differential Pressure Sensor with Bossed Diaphragm Membrane," *Proceeding of International Conference on Devices, Circuits and systems (ICDCS'12)*, pp. 703-704, 2012.
- [55] H.-C. Chang, S. Liao, H. Hsieh, S. Lin, C. Lai, R. Chen and W. Fang, "A novel inverse-magnetostrictive type pressure sensor with planar sensing inductor," *2013 IEEE 26th International Conference on Micro Electro Mechanical Systems (MEMS)*, pp. 685 - 688, 2013.
- [56] P. Eswaran and S. Malarvizhi, "Modeling of MEMS capacitive differential pressure sensor," *2013 International Conference on Circuits Polr and Computing Technologies (ICCPCT)*, pp. 699 - 702, 2013.
- [57] D. Wagner, J. Frankenberger and P. Deimel, "Optical pressure sensor using two Mach-Zehnder interferometers for the TE and TM polarizations," *J. Micromech. Microeng.*, vol. 4, pp. 35-39, 1994.
- [58] J. A. Dzuiban, A. Gorecka-Drzazga and U. Lipowics, "Silicon optical pressure sensor," *Sensors Actuators A*, vol. 32, pp. 628-631, 1992.
- [59] K. Hoppe, L. U. A. Anderson and S. Bouwstra, "Integrated Mach-Zehnder interferometer pressure transducer," *8th Int. Conf. on Solid-State Sensors and Actuators (Transducers95)*, pp. 590-595, 1995.
- [60] M. A. Chan, S. D. Collins and R. L. Smith, "A micromachined pressure sensor with fiber-optic interferometric readout," *Sensors Actuators A*, vol. 43, pp. 196-201, 1994.
- [61] H. Bartelt and H. Unzeitig, "Design and investigation of micromechanical bridge structures for an optical pressure sensor with temperature compensation," *Sensors Actuators A*, vol. 37-38, pp. 167-

170, 1993.

[62] US Standard atmosphere, *NASA-TM-X-74335*, 1976.

---

## Piezo-resistive cantilever

---

- [63] R. Dieme, et al., "Sources of excess noise in silicon piezoresistive microphones," *Journal of the Acoustical Society of America*, vol. 119, pp. 2710-2720, 2006.
- [64] J. C. Greenwood, "Silicon in Mechanical Sensors," *Journal of Physics E-Scientific Instruments*, vol. 21, pp. 1114-1128, 1988.
- [65] Y. Kanda, "A Graphical Representation of the Piezoresistance Coefficients in Silicon," *Ieee Transactions on Electron Devices*, vol. 29, pp. 64-70, 1982.
- [66] P. R. Scheeper, et al., "A review of silicon microphone," *Sensors and Actuators A*, vol.44, pp.1-11, 1994.
- [67] N. Minh-Dung, H. Takahashi, T. Uchiyama, K. Matsumoto, I. Shimoyama, "A barometric pressure sensor based on the air-gap scale effect in a cantilever," *Applied Physics Letters*, vol. 103, no. 14, article no. 143505, 2013.
- [68] H. Takahashi, N. Minh-Dung, K. Matsumoto, and I. Shimoyama, "Differential pressure sensor using a piezoresistive cantilever," *Journal of Micromechanics and Microengineering*, vol.22, no. 5, article no. 055015, 2012.
- [69] Y. Kanda, "A graphical representation of the piezoresistance coefficients in silicon," *IEEE Trans. Electron Devices*, vol.29, pp. 64-70, 1982.
- [70] G. Murat and I. Shimoyama, "Force sensing submicrometer thick cantilevers with ultra-thin piezoresistors by rapid thermal diffusion," *Journal of Micromechanics and Microengineering*, vol.14, pp. 423-428, 2004.

---

## Fluid Mechanics and Material Mechanics

---

- [71] Sighard, F. Hoerner, "Fluid Dynamic Drag: Practical Information on Aerodynamic Drag and Hydrodynamic Resistance," Hoerner Fluid Dynamics, 1965.
- [72] 東昭, "流体力学 (機械系基礎工学)," 朝倉書店, 1993.
- [73] 富田佳宏, 仲町英治, 中井善一, 上田整, "材料の力学," 朝倉書店, 2001.

---

## Appendix

### Appendix A : Application of the fluid structure interaction in cantilever structure

---

(In this section, I have been allowed to reused some sentences and expressions from my previous paper, which is the reference <sup>[2]</sup> with the Copyright 2013 IEEE)

Here I will describe a different approach to measure the absolute pressure by taking advantage of liquid's surface tension to fabricate a highly sensitive cantilever-based diaphragm, using liquid to bridge in the cantilever's gap. The concept of this research is shown in **Fig. A. 1**. An air cavity was designed under the liquid-cantilever diaphragm as a reference pressure. The point is that the gap's size was down-scaled to a few micrometers, so that liquids do not leak through the gap. The function of the liquid bridge here is to prevent the air leak through the cantilever's gap. As the result, when there is difference in pressure between the cavity and ambient environment, that pressure difference is applied to the liquid-cantilever diaphragm. Since both of cantilever and liquid are easy to be deformed, the proposed diaphragm is much sensitive than conventional rigid diaphragms. In addition, due to the low Reynolds number at the gap area, the viscous force is supposedly dominant in comparison with inertial force. Therefore, the motion of liquid within the gap space may have some effects on the deformation of the cantilever. However, since the total area of the gap was much smaller than the surface area of cantilever, the effects due to liquid motion can be ignored.

In experiments, I investigated the liquid leak with different gap sizes and different types of liquid. I also characterized the proposed sensor in response to pressure difference. The result demonstrates a tendency that using liquid with high viscosity would provide better linearity and stability, in

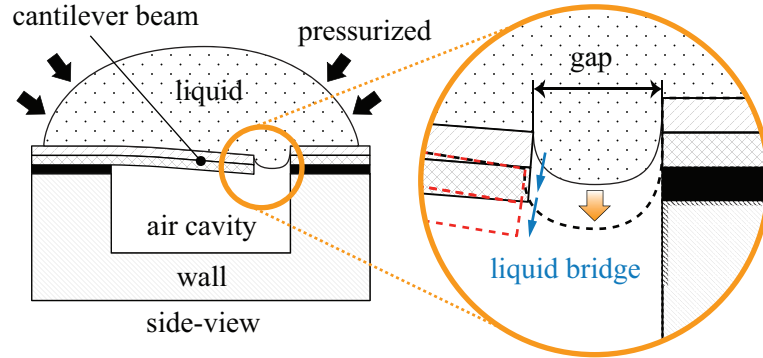


Fig. A. 1 Schematic design of the pressure sensor. Liquid was used to fill the gap between the cantilever and the surrounding walls.

comparison with the case of smaller viscosity. Furthermore, since surface tension and viscosity of liquid supposedly depends on the ambient temperature, the pressure response of the sensor with the variance of cavity's temperature was also evaluated. Experiment results indicate that the sensor's sensitivity can be improved by choosing proper liquid with proper design of piezo-resistive cantilever. In our prototype sensor, the piezo-resistive cantilever was ultrathin, with the thickness of 300 nm. Resolution of measurement was 0.9 Pa in case of using HIVAC-F5 silicon oil.

## A.1 DESIGN AND MEASUREMENT CONCEPT

The conceptual structure of our device is shown in **Fig. A. 1**. Different from diaphragm, a piezo-resistive cantilever has a gap through which air exchanges between the upper and the inner sides of the cantilever. An air cavity was placed under the diaphragm as a reference pressure source. The idea here is to use liquid to prevent air leak through the gap. Yet the original point of our proposed structure is that, the liquid is kept to hang within the gap and not to leak through the gap. By miniaturizing the cantilever's gap, I suppose that this structure is much more sensitive than conventional diaphragm, since the 300 nm thick cantilever is ultra-sensitive and easily deformed compared with rigid diaphragms.

Consider the surface tension of liquid within the gap, according to Young-Laplace equation, we have

$$P_1 - P_2 = \Delta P = 2\gamma H \quad (\text{A.1})$$

where  $\Delta P$  is the pressure difference between the pressure inside liquid ( $P_1$ ) and the pressure of the air cavity ( $P_2$ ),  $\gamma$  is the surface tension,  $H$  is the mean curvature of the liquid surface hanging within the gap. Since the maximum value of  $H$  is  $2/g$ , in which  $g$  is the gap's size, the threshold pressure for the proposed structure is expressed as the following

$$\Delta P_{max} = \frac{\gamma}{g} \quad (\text{A.2})$$

Threshold pressure here is defined as the maximum pressure difference across the liquid surface which allows the liquid not to leak through the gap. For a certain liquid at certain temperature, its surface tension is generally a constant. Therefore, according to equation **Equation (A.2)**, the threshold pressure of liquid leak is higher with smaller gap. In the other words, liquid is unlikely to leak if the gap is designed small enough.

Besides the liquid pressure and cavity's pressure, the ambient pressure must be concerned as well. Note that there are two air-liquid interfaces in our model. The first one is mentioned above, which is the interface within the gap, between liquid and air in the cavity. For convenience, I define this interface as the inner liquid surface. The second one is the surface between liquid and the ambient air outside ( $P_0$ ). I define the second interface as the external liquid surface. Surface tension at the external liquid surface can also be expressed by **Eq. (A.1)**. Without loss of generality, I assume the ambient pressure and the cavity's pressure is equal (i.e.  $P_0 = P_1$ ). Consider the ambient pressure changes in an amount of  $\Delta p$ , for example due to the change in absolute altitude. This pressure difference is the pressure applied on the liquid-cantilever diaphragm and causes the piezo-resistive cantilever to bend. This means that I can obtain  $\Delta p$  by measuring the displacement of the piezo-resistive cantilever. The displacement of the cantilever is indeed derived from its resistance change.

## A.2 FABRICATION PROCESS

The fabrication process steps of piezo-resistive cantilever and of the sensor device are described in this section. For fabricating cantilever with small gap (e.g. few mm size), photo-lithography is rather difficult. Thus, EB-lithography was used in our process. I used a 0.3 mm / 0.4 mm / 300 mm thick SOI wafer. In the first step, an N-type resistor layer was first formed on the surface of the SOI by the rapid thermal diffusion, and an EB-resist layer was spin-coated on the surface. Next, EB-lithography was

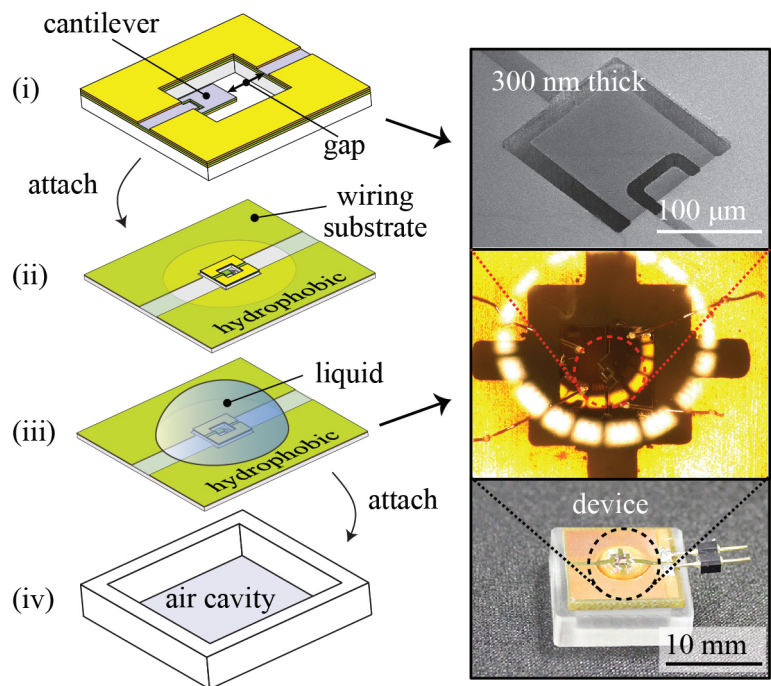


Fig. A. 2 Fabrication process flow of the device

gap size	HIVAC F-5*	HIVAC F-4*	water
1 $\mu\text{m}$	No leak	No leak	No leak
3 $\mu\text{m}$	No leak	No leak	No leak
5 $\mu\text{m}$	Leak	No leak	No leak
10 $\mu\text{m}$	Leak	Leak	No leak

\* HIVAC F-5, HIVAC F-4 were silicone fluidic oils (Shin-Etsu Chemical Co. Ltd, Japan).

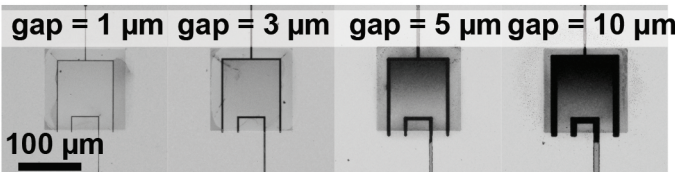


Fig. A. 3 Result of liquid leak test. HIVAC F-5 and HIVAC F-4 were silicone fluidic oils.

used to design the shape of the cantilever, with small gap. The smallest gap can be designed in our



method was 200 nm. After EB-lithography, I used electron beam physical vapor deposition to form a Cr/Au layer. The thickness of the Cr layer and Au layer were 3 nm and 30 nm, respectively. Then the Cr/Au layer deposited on EB-resist was lifted off by using piranha solution, which is a mixture of sulfuric acid ( $H_2SO_4$ ) and hydrogen peroxide ( $H_2O_2$ ). After that the device silicon layer was etched by using ICP-RIE (Inductive Coupled Plasma - Reactive Ion Etching). Then the Cr layer and Au layer were wet-etched to remove the metal layer on the surface of the piezo-resister. The bottom-side silicon layer (handle Si) was etched by ICP-RIE from the backside. And the piezo-resistive cantilever was released by etching the glass layer with hydrofluoric acid (HF) vapor.

The fabricated piezo-resistive cantilever chip was then attached to an electrode-patterned substrate. The substrate also had hydrophobic pattern (**Fig. A. 2**). Then liquid was put on the cantilever chip. The proposed sensor device was complete after attaching an air cavity under the substrate. The photographs of the fabricated piezo-resistive cantilever and sensor device are also shown in **Fig. A. 2**.

### A.3 EVALUATIONS

Experiment of liquid leak is described in this section. Since different liquid has different surface tension, it is necessary to design the gap size appropriate with the surface tension. I fabricated cantilevers with different gap, which were 1  $\mu m$ , 2  $\mu m$ , 3  $\mu m$ , 5  $\mu m$  and 10  $\mu m$ . The photographs are shown in **Fig. A. 3**. And I used 3 types of liquid, which were silicone oils (HIVAC F-5 and HIVAC F-4, Shin-Etsu Chemical Co. Ltd, Japan) and water. Among 3 types of liquid, HIVAC F-5 has lowest surface tension and water has highest one. The result of liquid leak test is shown in Table 1. The test was done in room temperature (25 °C). Water did not leak for all gap sizes, due to its high surface tension. Meanwhile, HIVAC F-4 showed leakage with gap size of 10  $\mu m$ . HIVAC F-5 leaked with gap size of 5  $\mu m$ . In fact, the surface tension of HIVAC F-4 and HIVAC F-5 are almost the same: 33.9 dyne/cm and 34.3 dyne/cm, respectively). But the viscosity of HIVAC F-5 (160 mm<sup>2</sup>/s) is much larger than that of HIVAC F-4 (37 mm<sup>2</sup>/s). Therefore, I suggest that not only surface tension but viscosity is also an important factor concerned with the liquid leak through the gap.

Pressure characteristic of the proposed pressure sensor was investigated. In this experiment, I evaluated the sensor by using the cantilever with gap size of 3  $\mu m$ , combined with different liquids. The experimental setup is shown in **Fig. A. 4**. A pressure generator was used to control the pressure differ-

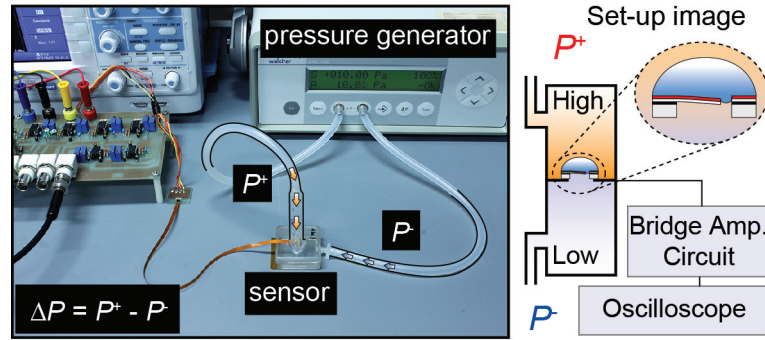


Fig. A. 4 Experimental setup. Pressure generator was used to control the pressure difference of upside and downside of the liquid-cantilever diaphragm.

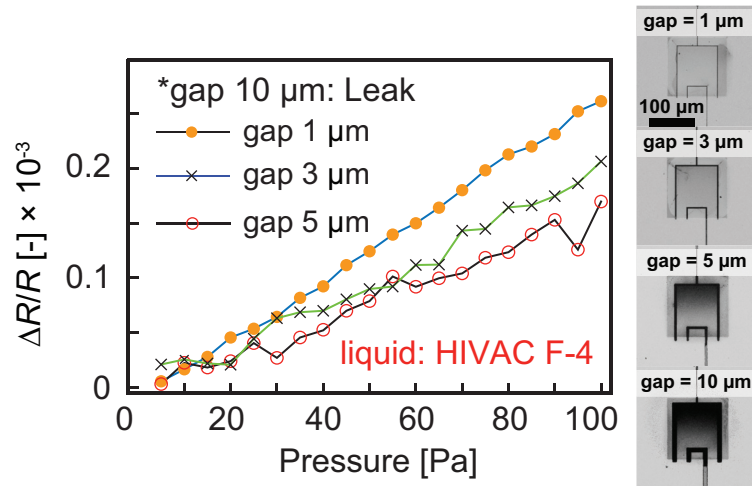


Fig. A. 5 Sensor response using three different types of liquid. HIVAC F-5 and HIVAC F-4 were silicon oils.

ence between the upside and the downside of the liquid-cantilever diaphragm. The pressure difference was varied from 0 Pa to 100 Pa. The resistance change of the piezo-resistive cantilever was measured by using Wheatstone bridge circuit.

The dependence of the sensor's response on liquid's viscosity is shown in **Fig. A. 5**. Among the 3 liquid samples, HIVAC F-5 had the highest sensitivity. The result indicates that the more viscous the liq-

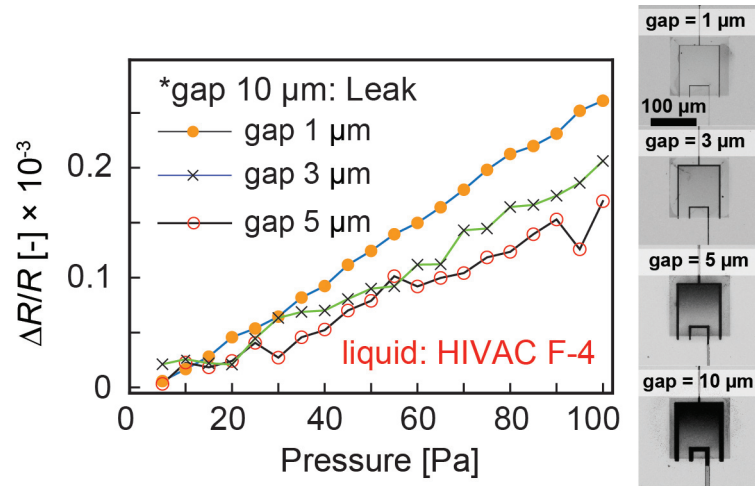


Fig. A. 6 Sensor response with various gap sizes.

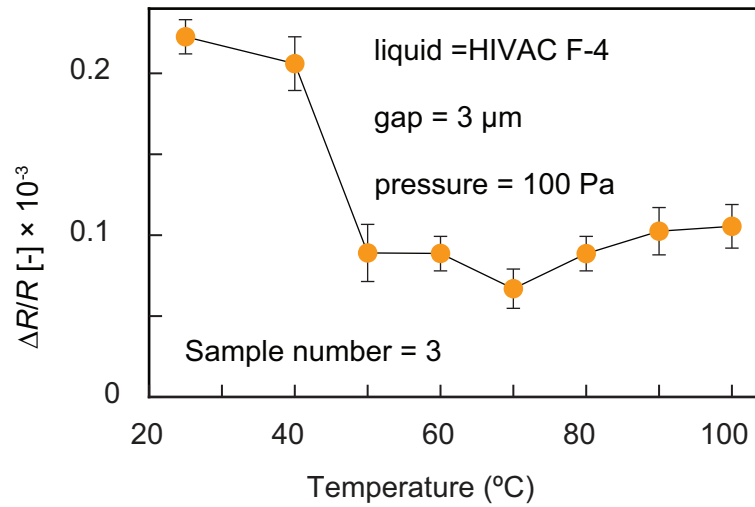


Fig. A. 7 Dependence on cavity's temperature.

uid was, the higher the sensitivity was.

The dependence on gap size is shown in **Fig. A. 6**, I suggest that the sensor's sensitivity got higher for smaller gap size. In addition, since the liquid's viscosity generally depends on ambient temperature, the dependence on air cavity's temperature was needed to be specified. According to the result in **Fig. A. 7**,

when the temperature was increased from 25 degrees to 50 degrees, the sensor's response dropped quickly. however, for temperature higher than 50 degrees, the response seemed to be converged. I suppose that in high temperature, liquid's viscosity decreases and that would lessen the dominance of viscous force.

In conclusion, I propose a highly sensitive diaphragm for pressure sensor, by using liquid to bridge the gap of a micro piezo-resistive cantilever. The liquid fills in but does not leak through the gap, as long as the gap is down-scaled to micro/nano size. I have characterized the pressure sensor, with different types of liquid, and different sizes of cantilever's gap as well. The experiment results demonstrated that, by miniaturizing the gap and choosing liquids with high dynamic viscosity, I can obtain measurement resolution of sub 1Pa. Silicone fluidic oil was used due to its physical stability and low evaporation rate. Although the sensitivity is 0.9 Pa, it can be improved by choosing appropriate liquid and gap size. Nevertheless, the proposed pressure sensor also has simple fabrication and low cost. The proposed sensor may lead to application in water, for example measuring the force applied on liquid surface.

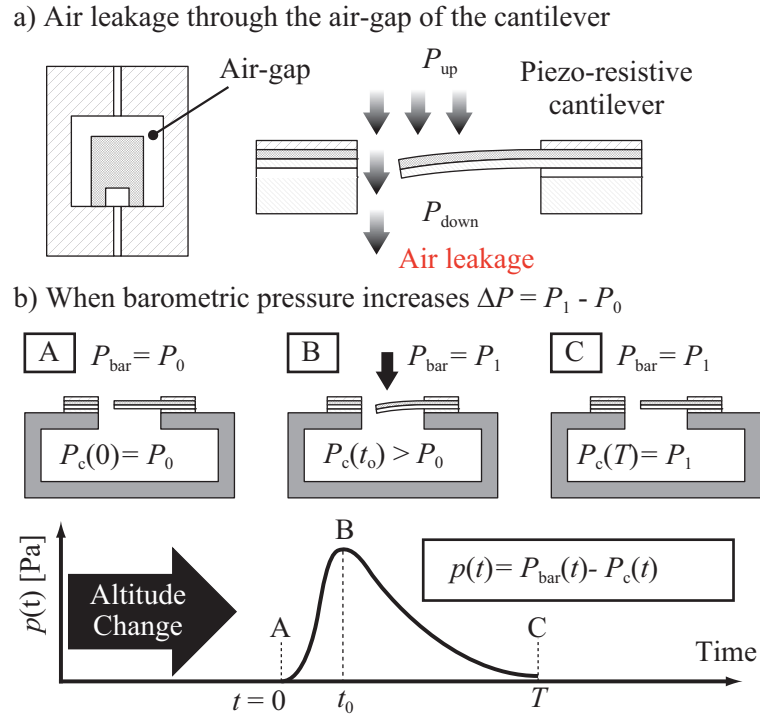


Fig. A. 8 Image of the proposed barometric pressure sensor

## Appendix B : Theoretical calculation for barometric pressure measurement

---

(In this section, I have been allowed to reused some sentences and expressions from my previous paper, which is the reference <sup>[1]</sup> with the Copyright 2011 IEEE)

Air leakage through the air-gap of the piezo-resistive cantilever is one important factor in the proposed sensing method. **Fig. A. 8** shows a model for investigating the behavior of the air leakage and the interaction between barometric pressure and the pressure inside the open cavity. As shown in **Fig. A. 8(a)**, the difference between the pressures at the upside and the downside of the cantilever causes the cantilever to bend down. At the same time, the air flows down through the air-gap. Thus, the pressure energy here is supposed to be converted into the kinetic energy of air particles flow through the air-gap, and the potential energy that stored in the cantilever's displacement. Note that the air stops leaking only if the pressure inside the cavity balances with barometric pressure.

In the following calculation, we assume that the air leaks through the cantilever's gap obeys the

Bernoulli equation for ideal gas. We also assume that the change in gap size during the cantilever's bending is small such that it can be ignored.

The model for estimating the time-variant interaction between barometric pressure and the cavity's pressure is shown in **Fig. A. 8(b)**. Assume that the barometric pressure,  $P_{bar}$ , increases from initial pressure  $P_0$  (status A) to  $P_1$  (status B). The air in the cavity leaks out and causes the cavity's pressure,  $P_c$ , to gradually increase and then it balances at  $P_1$  (status C). In this process, the differential pressure increases and peaks at status B and then decreases to 0 at status C. Consider the case of ideal gas, according to the general gas law, we have

$$\frac{dP_c}{dt} = \frac{dn}{dt} \frac{R_a T}{V} \quad (B.1)$$

where ( $P_c$ ,  $V$ ,  $T$ ) are pressure, volume and absolute temperature of the cavity, respectively.  $n$  is amount of substance and  $R_a$  is gas constant. To simplify the problem,  $V$  and  $T$  are assumed to be constant. Indeed, the air leakage is rather small in comparison with the entire volume  $V$ , the above assumption is acceptable. The change in amount of substance ( $dn/dt$ ) can be expressed as followed

$$\frac{dn}{dt} = n \cdot \frac{S \cdot u}{V} \quad (B.2)$$

here,  $S$  and  $u$  are the air-gap area and the average flow velocity through the air-gap. Combining Eq. (B.1) and Eq. (B.2), we obtain,

$$\frac{dP_c}{P_c} = \frac{S \cdot u}{V} dt \quad (B.3)$$

According to Bernoulli equation for ideal gas, the average flow velocity is given by

$$u = \sqrt{\frac{2(P_{bar} - P_c)}{\rho}} \quad (B.4)$$

in which  $\rho$  is air density. In the previous research of our group, the pressure difference of upside and

downside of a piezo-resistive cantilever, which is here, is proportional to the fractional resistance change of the cantilever.

$$P_{bar} - P_c = C \cdot \Delta R / R \quad (B.5)$$

where  $C$  is proportional coefficient. Therefore,

$$u = \sqrt{\frac{2C}{\rho} \cdot \frac{\Delta R}{R}} \quad (B.6)$$

Combining Eq. (B.3) and Eq. (B.6) , we have,

$$\frac{dP_c}{P_c} = \frac{S \cdot \sqrt{2C}}{V \sqrt{\rho}} \cdot \sqrt{\frac{\Delta R}{R}} \cdot dt \quad (B.7)$$

Taking the integral of both sides from  $t = 0$  (status A) to  $t = T$  (status C), the barometric pressure change is calculated as follows

$$\Delta P = P_1 - P_0 \cong K \int_0^T \sqrt{\frac{\Delta R}{R}} \cdot dt \quad (B.8)$$

The coefficient  $K$  is expressed by the following equation.

$$K = P_0 \cdot \frac{S \sqrt{2C}}{V \sqrt{\rho}} \quad (B.9)$$

Note that the coefficient  $K$  is proportional to the air-gap area and inversely proportional to the volume of the cavity. Considering equation (8), because can be measured in real-time, the barometric pressure change  $\Delta P$  is determinable.

## Appendix C : Electrical apparatus using in experimental setups

---

Apparatuses used for experiments in this study are presented here. The usage, specification and image of each apparatus are shown in details.

### Network Analyzer

---

Network analyzer was used to measure the frequency response of the piezo-resistive cantilever.

**Table C. 1 Specification of Network Analyzer**

Type	4395A
Manufacturing company	Agilent
Frequency range	1 [Hz] - 500 [MHz]
Frequency resolution	1 [mHz]
Gain resolution	0.1 [dB]
Measurement error	< $\pm 5$ [ppm]
Output range	-50 [dBm] ~ 15 [dBm]
Impedance	50 [W]

### Speaker

---

Dome-type speaker was used as a sound source in the experiment measuring the frequency characteristic of the cantilever. The sound radiated from speaker produces pressure on the piezo-resistive cantilever and causes the cantilever bend.

**Table C. 2 Speaker specification**

Type	FT28D
Manufacturing Company	FOSTEX
Aperture	7 [cm]
Impedance	8 [W]
Output Sound Level	90 [dB/W]
Cross over frequency	> 2 [kHz]



## Microphone

---

Brüel & Kjaer(B&K) microphone was used to calibrate the sound pressure in the experiment measuring the frequency characteristic of the cantilever.

**Table C. 3 B&K Microphone**

Type	4138
Manufacturing Company	Brüel & Kjaer
Aperture	1/8 [inch]
Sensitivity	1 [mV/Pa]
Frequency Range	6.5 [Hz] - 140[kHz]
Capacitance	3.5 [pF]

**Table C. 4 Pre-amplifier for B&K Microphone**

Type	2670
Manufacturing Company	Brüel & Kjaer
Frequency Range	15 [Hz] - 200[kHz]
Impedance	15 [GW], 0.25 [pF]

**Table C. 5 Conditioning Amplifier**

Type	2690-A-0S1
Manufacturing Company	Brüel & Kjaer
Frequency Range	0.1 [Hz] - 100 [kHz]
Input Impedance	1 [MW], 300 [pF]
Gain	-20 [dB] ~ 80 [dB]

## Differential FET Amplifier

---

**Table C. 6 Amplifier specification**

Type	SA-421F5
Application	Voltage Amplifier
Frequency Range	30 [Hz] - 30 [MHz]
Gain	46 [dB]
Input Impedance	1 [MW]

## Pressure generator equipment KAL 100

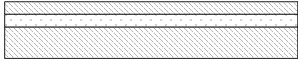

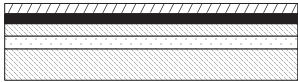
---

This device was used in experiment of evaluating the amount of air leaking through the air gap of the cantilever


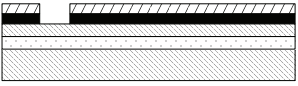
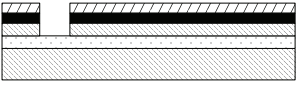
**Table C. 7 Technical data of KAL 100**

Measuring Range	From 0 to 100 kPa
Linearity	up to 100 Pa $\pm$ 0.5%
Internal air compression	Yes
Automatic zero balancing	Yes
Medium	air all non-aggressive gases

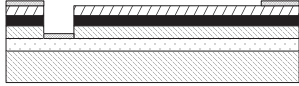


## Appendix D : Fabrication process of a piezo-resistive cantilever

Process Concept	Process content	Comments
1. Clean SOI Wafer 0.3/0.4/300 $\mu\text{m}$ SOI 	Size: 35 mm $\times$ 35 mm Ultrasonic cleaning with acetone Cleaning with ethanol	To remove the dust on the surface of the wafer
2. Form N-type resistor 	Put the wafer into HF solution	To remove the SiO2 layer on the surface of the wafer
	Spin-coating using P-59230 Conditions: - 700 rpm      3 sec - 3000 rpm    30 sec	Doping negative impurity
	Rapidi thermal diffusion using Lamp Heater Machine Conditions: - 935 $^{\circ}\text{C}$ 40 sec - Nitrogen      1.5 l/min	To thermally diffuse the impurity layer
	Put the wafer into HF solution	To remove the SiO2 layer on the surface of the wafer
3. Au deposition 	- Quickly put the wafer in to vacuum deposition element - Using about 3 pieces of Au - Deposite about 50 nm	If the HF solution get dirty, the Au layer becomes fragile and the later processes may fail.

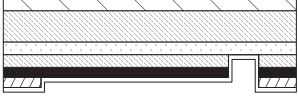
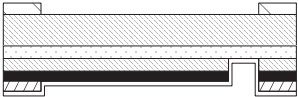
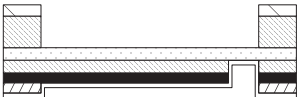

**Fig. D. 1 Fabrication process flow of piezo-resistive cantilever**

Process Concept	Process content	Comments
<p>4. Form cantilever's pattern</p> 	<ul style="list-style-type: none"> <li>- Pre-baking : 110°C 2 min.</li> <li>- Spin-coating using OFPR-23CP <ul style="list-style-type: none"> <li>• 300 rpm 8 sec.</li> <li>• 2000 rpm 30 sec.</li> <li>• 6000 rpm 0.7 sec.</li> </ul> </li> <li>- Main baking: 110°C 2 min.</li> <li>- Exposure 2.5 sec.</li> <li>- Developement using NMD-3 <ul style="list-style-type: none"> <li>• 40 sec. in NMD-3</li> <li>• Wafer cleaning using ultra pure water</li> <li>• O<sub>2</sub> plasma cleaning 10 sec</li> </ul> </li> </ul>	<ul style="list-style-type: none"> <li>- Positive photoregist is used to protect cantilever's pattern</li> <li>- The first mask is shown in Appendix D</li> <li>- Water cleaning is essential. It enhance the yield of device</li> <li>- Pay attention to the intensity of Hg light source of the mask alligner machine.</li> <li>- Should check the pattern after development by microscopes</li> </ul>
<p>5. Etch gold layer</p> 	<ul style="list-style-type: none"> <li>- Etching gold layer using gold etchant ( ~ 20 sec.)</li> <li>- Remove protecting photoregist using acetone and ethanol</li> <li>- O<sub>2</sub> plasma cleaning 1 min.</li> </ul>	<ul style="list-style-type: none"> <li>- 5 min. of acetone cleaning followed by 5 min. of ethanol cleaning is recommended.</li> </ul>
<p>6. Etch device Si layer</p> 	<ul style="list-style-type: none"> <li>- Etching using ICP-RIE machine <ul style="list-style-type: none"> <li>• Program: FAT</li> <li>• Used Gases: He, O<sub>2</sub>, SF<sub>6</sub>, C<sub>4</sub>F<sub>8</sub></li> <li>• Process time: 18 sec</li> </ul> </li> <li>- Cleaning with IPA, acetone and ethanol</li> <li>- O<sub>2</sub> plasma cleaning 1 min.</li> </ul>	<ul style="list-style-type: none"> <li>- Careful cleaning</li> </ul>

**Fig. D. 2 Fabrication process flow of piezo-resistive cantilever**

Process Concept	Process content	Comments
<p>7. Form Au electrodes</p> 	<ul style="list-style-type: none"> <li>- Pre-baking : 110°C 2 min.</li> <li>- Spin-coating with OFPR-100CP <ul style="list-style-type: none"> <li>• 300 rpm 8 sec.</li> <li>• 2000 rpm 30 sec.</li> <li>• 6000 rpm 0.7 sec.</li> </ul> </li> <li>- Main baking: 110°C 2 min.</li> <li>- Exposure 7.5 sec.</li> <li>- Developement using NMD-3 <ul style="list-style-type: none"> <li>• 40 sec. in NMD-3</li> <li>• Wafer cleaning using ultra pure water (twice)</li> <li>• O<sub>2</sub> plasma cleaning 15 sec</li> </ul> </li> </ul>	<ul style="list-style-type: none"> <li>- Positive photoregist is used to protect cantilever's pattern</li> <li>- The second mask for this process is shown in Appendix D</li> </ul>
<p>8. Form Au electrode</p> 	<ul style="list-style-type: none"> <li>- Etching gold layer using gold etchant ( ~ 20 sec.)</li> <li>- Remove protecting photoregist using acetone and ethanol</li> </ul>	<ul style="list-style-type: none"> <li>- Do not clean with O<sub>2</sub> plasma after forming electrode because the O<sub>2</sub> plasma causes damages on the piezo-resistive layer</li> </ul>
<p>9. Deposit Al on the back side</p> 	<ul style="list-style-type: none"> <li>- Deposit 100 nm Al layer on the back side of the wafer using Mini Vacuum Deposition Device (3 big pieces of Al)</li> </ul>	<ul style="list-style-type: none"> <li>- The tungsten wire, which is used to generate heat to liquidified the Al is easy to be broken in this process.</li> </ul>

**Fig. D. 3 Fabrication process flow of piezo-resistive cantilever**

Process Concept	Process content	Comments
<p>10. Etch the handle Si layer</p> 	<ul style="list-style-type: none"> <li>- Pre-baking : 110°C    2 min.</li> <li>- Spin-coating with ZPN 1150 <ul style="list-style-type: none"> <li>• 500 rpm    10 sec.</li> <li>• 3000 rpm    30 sec.</li> </ul> </li> <li>- Main baking: 90°C    90 sec. (using a hot plate to bake)</li> <li>- Exposure    4 sec</li> <li>- Baking again 110°C    1 min. (can use both hot plate or oven)</li> <li>- Developement using NMD-3 <ul style="list-style-type: none"> <li>• 40 sec. in NMD-3</li> <li>• Wafer cleaning using ultra pure water (twice)</li> </ul> </li> </ul>	<ul style="list-style-type: none"> <li>- ZPN 1150 is a negative photo-regist.</li> </ul>
<p>11. Etch Al layer</p> 	<ul style="list-style-type: none"> <li>- Etching Al layer using Al etchant ( ~ 30 sec.)</li> <li>- Remove protecting photoregist using acetone and ethanol</li> </ul>	<ul style="list-style-type: none"> <li>- The mask for this process is the third mask in Appendix D</li> </ul>
<p>12. Etch the handle Si from back side</p> 	<ul style="list-style-type: none"> <li>- Etching using ICP-RIE machine <ul style="list-style-type: none"> <li>• Program: FAT</li> <li>• Used Gases: He, N<sub>2</sub>, SF<sub>6</sub>, C<sub>4</sub>F<sub>8</sub></li> <li>• Process time: about 30 min.</li> </ul> </li> <li>- Cleaning with IPA only</li> </ul>	
<p>13. Remove glass layer by HF</p> 	<ul style="list-style-type: none"> <li>- Vaporization release process with HF 46%</li> <li>- 1 min step</li> </ul>	

**Fig. D. 4 Fabrication process flow of piezo-resistive cantilever**

## Appendix E : Devices and chemicals used in MEMS processes

Table E. 1 Device and Chemical List

Device name	Provider	Type
Mini Vacuum Deposition	SANYU	QUICK MINI VACUUM SYSTEM, SCV-700 TURBO-TM, SCV-700-2
Mask Aligner	UNION KOUKI	PEM-800
ICP-RIE	ALCATEL	A-601E
Lamp Heater	ULVAC-RIKO	SSA-P610CP
Compact Etcher	SAMCO	COMPACT ECHER MODEL FA-1
Ultrasonic Wire Bonder	ULTRASONIC ENGINEERING cCo.	USW- 5Z60K
SEM	JEOL	JSM-6400
Chemical name	Provider	Note
Ethanol	KANTO CHEMICAL Co., Inc	Cica-reagent grade, min 99.5%
Acetone	KANTO CHEMICAL Co., Inc	Cica-reagent grade, min 99.5%
2-Propanol	KANTO CHEMICAL Co., Inc	Cica-reagent grade, min 99.5%
OFPR800-23cp	TOKYO OHKA KOGYO Co.	Positive photoresist, 23cp
OFPR800-100cp	TOKYO OHKA KOGYO Co.	Positive photoresist, 100cp
ZPN1150	NIPPON ZEON	Negative photoresist
OAP	TOKYO OHKA KOGYO Co.	-
NMD-3	TOKYO OHKA KOGYO Co.	Developer, NMD-3 2.38%

**Table E. 1 Device and Chemical List**

HF	MORITA KAGAKU KOGYO	46%
OCD	TOKYO OHKA KOGYO Co.	P-58230, Negative
Conductive Paste	FUJIKURA KASEI Co.	-
KE-113	SHINETSU Co.	Silicone
PDMS	SHINETSU Co.	Silicone
AZP4903	CLARIANT JAPAN K.K	
<b>Material</b>	<b>Company</b>	<b>Note</b>
SOI wafer (G6P-020-01)	Soitec Asia	
EB mask (ST-TLR6-TQZ- 5009(5T)EBR9 HS31)	Toppan Insatsu	
Au wire (AU-171385, 99.95% $\phi = 500 \mu\text{m}$ )	Tanaka Kikinzoku Kogyo	
Al wire (AL-011480, 99.999% $\phi = 1.0 \text{ mm}$ )	The Nilaco Corporation	
W wire (W-461377, 99.95% $\phi = 450 \mu\text{m}$ )	The Nilaco Corporation	
Electric circuit board	Sun-hayato	
<b>IC chip</b>	<b>Company</b>	<b>Note</b>
PIC18F2550	Microchip Technology Inc.	Data communication
AD623	Analog devices	Amplifier
48M025F	TOSHIBA	2.5 V IC
ADR510ARTZ	Analog devices	1 V IC



## Appendix F : Mask design of a piezo-resistive cantilever

---

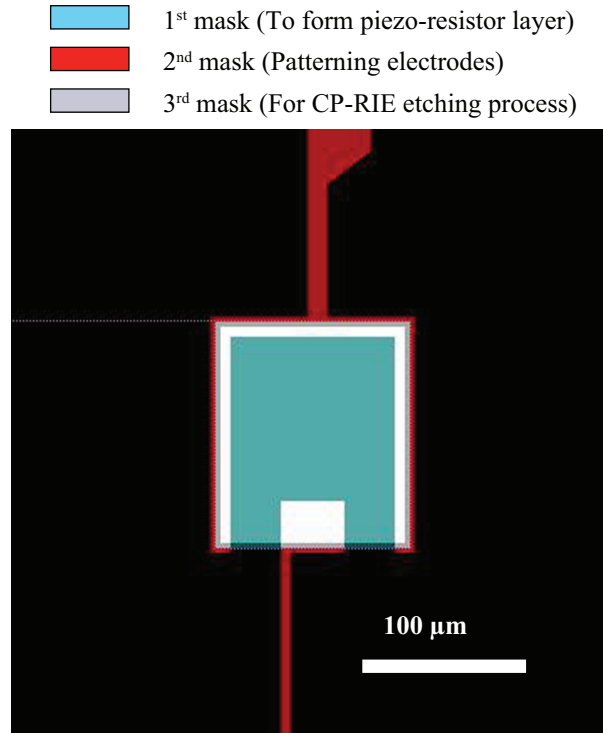


Fig. F. 1 Mask design of a piezo-resistive cantilever.

The piezo-resistive cantilever in this study is fabricated in MEMS fabrication process. There are several steps in this process and each step requires a specific mask design. Photo-masks used in the fabrication process were made by using electron beam (EB) lithography. **Fig. F. 1** shows the design of the photo-masks.

## Publication

### International Journal

- [1] **Nguyen Minh-Dung**, Hidetoshi Takahashi, Takeshi Uchiyama, Kiyoshi Matsumoto, Isao Shimoyama, "A barometric pressure sensor based on the air-gap scale effect in a cantilever," *Applied Physics Letters*, vol. 103, no. 14, article no. 143505, 2013. (Published online on 3 October 2013)
- [2] Hidetoshi Takahashi, **Nguyen Minh-Dung**, Kiyoshi Matsumoto, and Isao Shimoyama, "Differential pressure sensor using a piezo-resistive cantilever," *Journal of Micromechanics and Microengineering*, vol.22, no. 5, article no. 055015, 2012. (published on 16 April 2012)

### International Conference Paper

- [3] **Nguyen Minh-Dung**, Akira Inaba, Akira Suzuki, Hidetoshi Takahashi, Eiji Iwase, Kyoshi Matsumoto, Isao Shimoyama, "Sound Direction Sensor with an Acoustic Channel," *Proceedings of IEEE 23rd International Conference on Micro Electro Mechanical Systems (MEMS2010)*, Hong Kong, pp. 655-658, 2010.
- [4] **Nguyen Minh-Dung**, Hidetoshi Takahashi, Kyoshi Matsumoto, Isao Shimoyama, "Barometric Pressure Change Measurement," *Proceedings of IEEE 16th International Conference on Solid-State Sensors, Actuators and Microsystems (Transducers 2011)*, Beijing, China, pp. 894-897, 2011
- [5] **Nguyen Minh-Dung**, Hidetoshi Takahashi, Kyoshi Matsumoto, Isao Shimoyama, "3D Airflow Velocity Vector Sensor," *Proceedings of IEEE 24th International Conference on Micro Electro Mechanical Systems (MEMS2011)*, Cancun, Mexico, pp. 513-516, 2011.
- [6] **Nguyen Minh-Dung**, Hidetoshi Takahashi, Kyoshi Matsumoto, Isao Shimoyama, "Scale Effect of the Air-Gap in Cantilever and its Application," *IEEE 6th Asia-Pacific Conference on Transducers and Micro/Nano Technologies (APCOT 2012)*, China, 2012
- [7] **Nguyen Minh-Dung**, Hoang Phuong Phan, Kyoshi Matsumoto, Isao Shimoyama, "A Sensitive Liquid-Cantilever Diaphragm for Pressure Sensor," *Proceedings of IEEE 26th International Conference on Micro Electro Mechanical Systems (MEMS2013)*, Taiwan, pp. 617-620, 2013.
- [8] Ken Sato, Hidetoshi Takahashi, **Nguyen Minh-Dung**, Kyoshi Matsumoto, Isao Shimoyama, "Effectiveness of Bristled Wing of Thrips," *Proceedings of IEEE 26th International Conference on Micro Electro Mechanical Systems (MEMS2013)*, Taiwan, pp. 21-24, 2013.
- [9] **Nguyen Minh-Dung**, Hoang Phuong Phan, Kyoshi Matsumoto, Isao Shimoyama, "A Hydrophone Using Liquid to Bridge the Gap of a Piezo-resistive Cantilever," *IEEE 17th International Conference on Solid-State Sensors, Actuators and Microsystems (Transducers 2013)*, Barcelona, Spain, June 16-20, 2013.
- [10] Pham Quang-Khang, **Nguyen Minh-Dung**, Hoang Phuong Phan, Nguyen Binh-Khiem, Kiyoshi Matsumoto, Isao Shimoyama, "Multi-axis force sensor with dynamic covering ultrasonic range," *IEEE 27th International Conference on Micro Electro Mechanical Systems (MEMS2014)*, San Francisco, USA, Jan. 26-30, 2014.)
- [11] Tomonori Kaneko, **Nguyen Minh-Dung**, Kiyoshi Matsumoto, Isao Shimoyama, "Measurement of Mechanomyogram," *IEEE 27th International Conference on Micro Electro Mechanical Systems*

(MEMS2014), San Francisco, USA, Jan. 26-30, 2014.(Accepted)

[12]

### Domestic Conference Paper

- [13] ○稲葉亮, ゲンミンジュン, 高橋英俊, 岩瀬英治, 松本潔, 下山勲, " 単一センサによる音源定位のためのキリギリス規範音響センサ," 第27回日本ロボット学会学術講演会, 2I1-03, 横浜国立大学, 神奈川, Sep. 15-17, 2009.
- [14] ○ Tomonori Kaneko, Nguyen Minh-Dung, Tomoyuki Takahata, Kiyoshi Matsumoto, Isao Shimoyama, "Piezoresistive Cantilever Based Pressure Sensor for Mechanomyogram Measurement," ROBOMECH 2013, Tsukuba, Japan, May 2013.

### Articles and Press Release

- [15] Article on Nikkei Newspaper, "Ultra-sensitive Barometric Pressure Sensor", pp. 11, published on 20th June 2011.
- [16] Article Nikkei Newspaper, "2011 the 3rd technical trend investigation: Leading Edge Researches", Over-all judgment 10th rank, published on 21st October 2011.
- [17] Press Released by The University of Tokyo: [http://www.u-tokyo.ac.jp/public/public01\\_250122\\_j.html](http://www.u-tokyo.ac.jp/public/public01_250122_j.html)
- [18] Article on Tech-on Article: <http://techon.nikkeibp.co.jp/article/EVENT/20130207/264736/>
- [19] Article on Mynabi News <http://news.mynabi.jp/news/2013/01/25/142/index.html>
- [20] Press Released by The University of Tokyo, "An atmospheric pressure sensor which can measure the altitude change of 1 centimeter", 3rd June 2011.([http://www.u-tokyo.ac.jp/public/public01\\_230603\\_j.html](http://www.u-tokyo.ac.jp/public/public01_230603_j.html))

### Patent

- [21] Isao Shimoyama, Kiyoshi Matsumoto, Eiji Iwase, Akira Inaba, ○ **Nguyen Minh-Dung**, Translated Title: "Sound Localization Device and Localizing Method", No. JP 2009-211683.
- [22] Isao Shimoyama, Kiyoshi Matsumoto, Tomoyuki Takahata, Kenta Kuwana, Hidetoshi Takahashi, ○ **Nguyen Minh-Dung** Translated Title: "Flow Sensor", No. JP 2011-001917.
- [23] Isao Shimoyama, Kiyoshi Matsumoto, Tomoyuki Takahata, Kenta Kuwana, Hidetoshi Takahashi, ○ **Nguyen Minh-Dung**, Translated Title: "Flow Sensor", No. JP 2011-001918.
- [24] Isao Shimoyama, Kiyoshi Matsumoto, Tomoyuki Takahata, Kenta Kuwana, Hidetoshi Takahashi, ○ **Nguyen Minh-Dung**, Translated Title: "Barometric Pressure Sensor", No. JP 2011-017168.
- [25] Isao Shimoyama, Kiyoshi Matsumoto, Hidetoshi Takahashi, ○ **Nguyen Minh-Dung**, Translated Title: "Pressure Sensor", No. JP2012-105306.
- [26] Isao Shimoyama, Kiyoshi Matsumoto, Tomoyuki Takahata, Kenta Kuwana, Hidetoshi Takahashi,

- **Nguyen Minh-Dung**, “Differential pressure sensor”, International Patent, PCT/JP2012/05032, Published No. WO/2012/102073.
- [27] Isao Shimoyama, Kiyoshi Matsumoto, Hidetoshi Takahashi, ○ **Nguyen Minh-Dung**, Youko Shinozuka, Takeshi Uchiyama, Manabu Oumi, Translated Title: “Differential pressure measurement”, No. JP 2012-105306 (Colaborated with SII company).
- [28] Isao Shimoyama, Kiyoshi Matsumoto, Binh-Khiem Nguyen, ○ **Nguyen Minh-Dung**, Hoang-Phuong Phan, Translated Title: “Pressure Sensor with Liquid on Cantilever structure”, No. JP 2012-286757.
- [29] Isao Shimoyama, Kiyoshi Matsumoto, Hidetoshi Takahashi, ○ **Nguyen Minh-Dung**, Youko Shinozuka, Takeshi Uchiyama, Manabu Oumi, Translated Title: “Pressure Sensor”, No. JP 2012-286758 (Colaborated with SII company).
- [30] Isao Shimoyama, Kiyoshi Matsumoto, Hidetoshi Takahashi, ○ **Nguyen Minh-Dung**, Youko Shinozuka, Takeshi Uchiyama, Manabu Oumi, Translated Title, “ Touch sensor and touch-input device”, No. JP 2013-043430 (Colaborated with SII company).
- [31] Isao Shimoyama, Kiyoshi Matsumoto, Hidetoshi Takahashi, ○ **Nguyen Minh-Dung**, Youko Shinozuka, Takeshi Uchiyama, Manabu Oumi, Translated Title: “Pressure Sensor”, No. JP 2013-046586 (Colaborated with SII company).
- [32] Isao Shimoyama, Kiyoshi Matsumoto, Hidetoshi Takahashi, ○ **Nguyen Minh-Dung**, Youko Shinozuka, Takeshi Uchiyama, Manabu Oumi, International Patent “Pressure Sensor”, No. PCT/JP2013/057765 (Colaborated with SII company).
- [33] Isao Shimoyama, Kiyoshi Matsumoto, Hidetoshi Takahashi, ○ **Nguyen Minh-Dung**, Youko Shinozuka, Takeshi Uchiyama, Manabu Oumi, Translated Title: “Pressure Sensor”, No. JP 2013-200077 (Colaborated with SII company).

## Acknowledgement

I am very thankful to everyone who all kindly helped and supported me on the road to my PhD thesis.

I would like to express my deepest gratitude to my supervisor, Professor Isao Shimoyama. It is my great honour to get a PhD degree under his supervision. Without his guidance, I could not have completed the thesis effectively and moreover on time. Since I came and started studying at his laboratory, Prof. Shimoyama has taught me many things from moral supports to invaluable technical advice. His guidance, inspiration and professional attitude toward science have provided a precious experience that will help me through all of my career.

I am equally grateful to Professor Kiyoshi Matsumoto, whose encouragement, guidance and support enabled me to develop my knowledge on the study. He had been very kind and patient while listening to my questions and correcting all my doubts with his helpful comments. With his experience of working as a researcher in a leading Japanese company, he gave me a lot of advice that helped me make up my mind to devote myself to Academy. I thank him for his overall supports.

It is my honour to have Professor Hirose, Professor Suzuki, Professor Takagi and Associate Prof. Takeuchi as the judges for my PhD defense. The discussion with them help me significantly in improving the quality as well as the originality of the research.

My sincere appreciation is extended to other lab memers who were always nice and friendly with me. Especially, I would like to thank Khiem-san and Takahashi-san for their support in improving the quality of my thesis. It was my great pleasure to study and research with all the members at Shimoyama lab. Special thanks to Oumi-san, Uchiyama-san, Shinohara-san from Seiko Instruments Inc., who colaborated with me in this study and helped me so much in the rotating experiments. And I would like to thank Japan Society for the Promotion of Science (JSPS) for providing a budget for my research.

Finally, I would like to thank my friends, my family and especially my wife for their emotional support over the three years in my pursuit of completing my PhD degree.

Thanking you